


2005

Characterization of ionic, dipolar and molecular mobility in polymer systems

Zhenrong Guo

College of William & Mary - Arts & Sciences

Follow this and additional works at: <https://scholarworks.wm.edu/etd>

 Part of the [Analytical Chemistry Commons](#), [Materials Science and Engineering Commons](#), and the [Polymer Chemistry Commons](#)

Recommended Citation

Guo, Zhenrong, "Characterization of ionic, dipolar and molecular mobility in polymer systems" (2005). *Dissertations, Theses, and Masters Projects*. William & Mary. Paper 1539623474.
<https://dx.doi.org/doi:10.21220/s2-p36q-nw09>

This Dissertation is brought to you for free and open access by the Theses, Dissertations, & Master Projects at W&M ScholarWorks. It has been accepted for inclusion in Dissertations, Theses, and Masters Projects by an authorized administrator of W&M ScholarWorks. For more information, please contact scholarworks@wm.edu.

**CHARACTERIZATION OF IONIC, DIPOLAR AND
MOLECULAR MOBILITY IN POLYMER SYSTEMS**

A Dissertation

Presented to

The Faculty of the Department of Applied Science

The College of William and Mary in Virginia

In Partial Fulfillment

Of the Requirements for the Degree of

Doctor of Philosophy

by

Zhenrong Guo

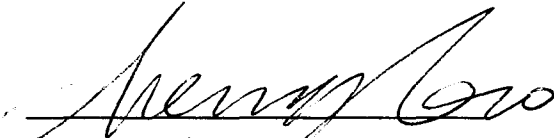
2005

APPROVAL SHEET

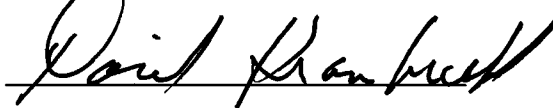
This dissertation is submitted in partial fulfillment of

The requirements for the degree of

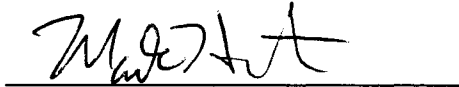
Doctor of Philosophy


Zhenrong Guo

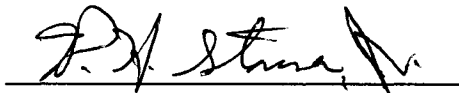
Approved by the Committee, July 2005



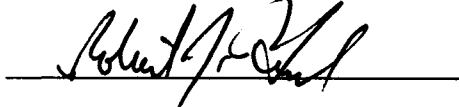
Dr. David Kranbuehl, Chair



Dr. Mark Hinders



Dr. William H. Starnes, Jr.



Dr. Robert J. Hinkle

TABLE OF CONTENTS

	Page
Acknowledgements	viii
List of Figures	ix
List of Tables	xiii
Abstract	xiv
CHAPTER 1. INTRODUCTION	2
1.1. General introduction to polymer dielectric properties	3
1.2. Theories of dielectric relaxation in a polymer	4
1.2.1. Equilibrium molecular theory	6
1.2.2. Dynamic behavior: phenomenological theory	8
1.3. Dielectric relaxation process in an amorphous polymer	11
1.3.1. α -relaxation in amorphous polymers	13
1.3.2. β -relaxation in amorphous polymers	15
1.3.4. Dielectric normal-mode relaxation	16
1.4. Objective of dissertation	17
REFERENCES	19
CHAPTER 2. DIELECTRIC TECHNIQUES AND APPLICATIONS IN POLYMER SYSTEM	22
2.1. Dielectric spectroscopy	22
2.1.1. Principles of measurement	24
2.1.2. Instrumentation and data collection	25
2.1.3. Applications	27

	Page
2.1.3.1. Cure monitoring	27
2.1.3.2. Phase separation	32
2.1.3.3. Aging and degradation of polymeric materials	33
2.1.3.4. Characterization of film formation	34
2.2. Ion time of flight (ITOF)	35
2.2.1. Background/theories	36
2.2.2. Equipment	42
REFERENCES	45
CHAPTER 3. APPLICATION OF ION TIME-OF-FLIGHT MEASUREMENT DURING AN EPOXY-AMINE REACTION	49
3.1. Introduction	49
3.1.1. Problem statement	49
3.1.2. Background for epoxy-amine reaction and its conductivity	50
3.2. Experimental	53
3.2.1. Materials	53
3.2.2. ITOF measurement	53
3.2.3. Rheology	54
3.2.4. Dielectric impedance measurement	54
3.2.5. Reaction kinetics	55
3.3. Results and discussion	55
3.3.1. Kinetics and gelation	55
3.3.2. Source of charge carriers	60

	Page
3.3.3. Dielectric relaxation	61
3.3.4. Ion mobility measurement	63
3.3.4.1. Pulse length, voltage	63
3.3.4.2. Geometry	63
3.3.4.3. Temperature effect on ion mobility and the number of charge carriers for an unreacted epoxy/amine system	65
3.3.4.4. Viscosity dependence of conductance during the reaction	68
3.3.4.5. Ion mobility, charge carrier concentration changes during the reaction	69
3.3.4.6. A comparison between an unreacted and a reacted system	72
3.4. Summary	76
REFERENCES	78
CHAPTER 4. MONITORING STRUCTURAL EVOLUTION DURING VINYL/DIMETHACRYLATE COPOLYMERIZATION WITH FREQUENCY DEPENDENT DIELECTRIC MEASUREMENT	81
4.1. Introduction	81
4.2. Experimental	83
4.2.1. Materials	83
4.2.2. Dielectric impedance measurement	84
4.2.3. DSC measurement	85
4.2.3.1. Kinetics	85
4.2.3.2. Glass transition (T _g) measurement	86
4.2.4. Rheology	86
4.2.5. Transmission electron microscopy (TEM) measurement	87

	Page
4.3. Results and discussion	87
4.3.1. D121/St system	87
4.3.1.1. Dielectric measurement during isothermal cure	87
4.3.1.2. Dielectric relaxation and the DSC profile during a temperature ramp	91
4.3.1.3. WLF equation fitting for the relaxation peaks	98
4.3.1.4. Width of the relaxation peaks	100
4.3.1.5. Network, monomer heterogeneity	103
4.3.2. Influence of the comonomer structure on the network buildup	104
4.3.2.1. Isothermal polymerization	104
4.3.2.2. Structural evolution and network heterogeneity during cure	107
4.3.2.2.1. Dielectric spectroscopy	107
4.3.2.2.2. DSC profile	112
4.3.2.2.3. Dynamic mechanical properties	112
4.3.2.2.4. Morphology from TEM images	119
4.3.2.3. Summary of the influence of the comonomer structure on the network buildup	121
4.4. Conclusion	121
REFERENCES	123
CHAPTER 5. DYE DIFFUSION – A VISUALLY COLOR CHANGING (VCP) SYSTEM	127
5.1. Introduction	127
5.2. Dye migration mechanism	128
5.2.1. Simple diffusion process	128

	Page
5.2.2. Chemical reaction controlled timing process	129
5.3. Stability and migration tests	131
5.4. Dye synthesis and modification	135
5.5. Experimental tests on the VCP system	138
5.5.1. System design	138
5.5.2. Polymer films	139
5.5.3. Acid	141
5.5.4. Base	144
5.6. Issues to be examined	149
5.6.1. New ionamine synthesis	149
5.6.2. Good dispersion for the dye	149
5.6.3. Migration issues	150
REFERENCES	151
CHAPTER 6. SUMMARY AND CONCLUSIONS	152
APPENDIX	154
VITA	156

ACKNOWLEDGEMENTS

The author would like to express his sincere appreciation to his advisor Dr. David E. Kranbuehl for his invaluable guidance and understanding during this research. He invested so much time discussing and providing his wise insight into both research and life as a mentor and a friend. The author is also indebted to Dr. William H. Starnes, Jr., Dr. Robert J. Hinkle and Dr. Mark Hinders for their contributions to this manuscript and careful instructions during this endeavor.

The author wishes to acknowledge the exceptional support of the departments of applied science and chemistry and the entire Kranbuehl group without which this research experience would not have been completed.

In addition, the author is very grateful to all his friends from all over the world for their friendship, care and support.

Finally, the author wishes to thank his wife and parents for their very generous unending support, encouragement and love.

LIST OF FIGURES

	Page
Figure 1.1. The different geometric possibilities for a location of a dipole with respect to the polymer chain.	7
Figure 1.2. Dielectric relaxation dependence on the frequency for a single relaxation.	10
Figure 1.3. Dielectric loss spectra of polymethylacrylate.	12
Figure 1.4. Value of ϵ'' versus T at a frequency of 104 Hz for cis-1,4-polyisoprene samples of Mw 1400 (●), 3830 (■), and 8400 (▲).	17
Figure 2.1. FDEMS experimental setup.	27
Figure 2.2. Classification for the dipolar groups during cure.	28
Figure 2.3. MCDEA/DGEBA isothermal cure at 120 ⁰ C.	31
Figure 2.4. Ion transportation in electric fields.	36
Figure 2.5. Square-wave voltage applied in ITOF measurement.	36
Figure 2.6. Current curve in ITOF measurement.	37
Figure 2.7. Diffusion and migration current curves.	42
Figure 2.8. ITOF experimental equipment.	44
Figure 3.1. Chemical reaction for an epoxy amine system.	51
Figure 3.2. Some types of hydrogen bonds in an epoxide-amine network.	52
Figure 3.3. Chemical structure of epoxy and amine.	53
Figure 3.4. Conversion during isothermal cure at three different temperatures.	56
Figure 3.5a. Viscosity change during 120 ⁰ C isothermal cure.	57
Figure 3.5b. Viscosity change during 140 ⁰ C isothermal cure.	57
Figure 3.5c. Viscosity change during 140 ⁰ C isothermal cure.	58

	Page
Figure 3.6a. $\tan \delta$ changes at different frequencies during 120 ⁰ C cure.	58
Figure 3.6b. $\tan \delta$ changes at different frequencies during 140 ⁰ C cure.	59
Figure 3.6c. $\tan \delta$ changes at different frequencies during 160 ⁰ C cure.	59
Figure 3.7a. Dielectric loss change at different frequencies during 120 ⁰ C cure.	61
Figure 3.7b. Dielectric loss change at different frequencies during 140 ⁰ C cure.	62
Figure 3.7c. Dielectric loss change at different frequencies during 160 ⁰ C cure.	62
Figure 3.8. MCDEA/DGEBA isothermal cure at 140 °C: ion mobility $\log(\mu)$ ($d^2/TOF \cdot V$) against the reaction time (■) small capacitor; (▲) index sensor	65
Figure 3.9. The product of the ion mobility (μ) and the viscosity (η) against the temperature for the unreacted DGEBA/MCDEA mixture	66
Figure 3.10. Unreacted DGEBA/MCDEA heated from 60 °C to 120 °C: (▲) charge carriers concentration calculated from ITOF (■) the product of conductivity and viscosity	67
Figure 3.11. Conductivity versus Viscosity during the reaction at 120 °C	68
Figure 3.12a. Number of Charge Carriers (◆), Conductivity (■) and ion mobility (▲) changes for DGEBA/MCDEA isothermal at 120 ⁰ C	70
Figure 3.12b. Number of Charge Carriers (◆), Conductivity (■) and ion mobility (▲) changes for DGEBA/MCDEA isothermal at 140 ⁰ C	71
Figure 3.12c. Number of Charge Carriers (◆), Conductivity (■) and ion mobility (▲) changes for DGEBA/MCDEA isothermal at 160 ⁰ C	71
Figure 3.13. The change in conductivity for the unreacted epoxy amine system versus viscosity during a temperature ramp and of the conductivity versus viscosity during polymerization as the reaction approaches gel	73
Figure 3.14. The ion mobility measured by ion time of flight versus viscosity for the unreacted epoxy amine system and during polymerization as the system approaches gel over the same range of viscosities as in Figure 3.13	74

	Page
Figure 3.15. The change in the concentration of mobile charge versus viscosity in the unreacted epoxy amine and during the approach to gel in the reacting system	75
Figure 4.1a. $\epsilon''^*\omega$ versus time during 60 ⁰ C isothermal cure of D121/St.	88
Figure 4.1b. $\epsilon''^*\omega$ versus time during 70 ⁰ C isothermal cure of D121/St	88
Figure 4.1c. $\epsilon''^*\omega$ versus time during 80 ⁰ C isothermal cure of D121/St	89
Figure 4.2. Temperature –time procedure used to measure dielectric properties and Tgs at different degrees of cure.	91
Figure 4.3a. $\epsilon''^*\omega$ versus temperature before cure.	93
Figure 4.3b. $\epsilon''^*\omega$ versus temperature after 15 mins cure at 70 ⁰ C	93
Figure 4.3c. $\epsilon''^*\omega$ versus temperature after 30 mins cure at 70 ⁰ C	94
Figure 4.3d. $\epsilon''^*\omega$ versus temperature after 50 mins cure at 70 ⁰ C	94
Figure 4.3e. $\epsilon''^*\omega$ versus temperature after 70 mins cure at 70 ⁰ C	95
Figure 4.4. Tg evolution during 70 ⁰ C isothermal polymerization of D121/St (The Tg mark () is determined by TA instrument software)	96
Figure 4.5a. $\epsilon''^*\omega$ versus time during isothermal polymerization of D121/DVB	105
Figure 4.5b. $\epsilon''^*\omega$ versus time during isothermal polymerization of D121/St	106
Figure 4.6. Monomers conversion during cure for D121/DVB and D121/St	106
Figure 4.7a. ϵ'' versus temperature at different degrees of conversion for D121/DVB	108
Figure 4.7b. ϵ'' versus temperature at different degrees of conversion for D121/St	108
Figure 4.8a. Tg evolution during 70 ⁰ C isothermal polymerization of D121/DVB	111
Figure 4.8b. Tg evolution during 70 ⁰ C isothermal polymerization of D121/St	111

	Page
Figure 4.9a. Evolution of the storage modulus G' and $\tan\delta$ as a function of temperature for D121/St	115
Figure 4.9b. Evolution of the storage modulus G' and $\tan\delta$ as a function of temperature for D121/DVB	116
Figure 4.9c. Evolution of the storage modulus G' and $\tan\delta$ as a function of temperature for D121/St and D121/DVB at low conversion	117
Figure 4.9d. Evolution of the storage modulus G' and $\tan\delta$ as a function of temperature for D121/St and D121/DVB at high conversion	118
Figure 4.10a. TEM morphology for 54% conversion D121/DVB	120
Figure 4.10b. TEM morphology for 55% conversion D121/St	120
Figure 5.1. Simple diffusion system	129
Figure 5.2. Design of long-term VCP system	130
Figure 5.3. Scheme of Banana Yellow preparation	135
Figure 5.4. Scheme of Chloride substituted Banana Yellow preparation	136
Figure 5.5. Scheme of aldehyde bisulfite salts preparation	137
Figure 5.6. Scheme of ionamines preparation	138
Figure 5.7. Fast triggered, long-term VCP system	139

LIST OF TABLES

	Page
Table 3.1. Gel times of the epoxy-amine during isothermal cure.	60
Table 4.1. Chemical products used in polymerization.	84
Table 4.2. Gel times (min) in the dielectric loss spectra (at 0.1KHz) during isothermal cure for D121/St.	90
Table 4.3. Total conversion, Tg temperatures determined by MDSC and Tg temperatures determined by dielectric measurement (2.5 KHz) at different curing cycles for D121/St shown in Figure 4.2.	96
Table 4.4. D121/St monomer/oligomer WLF fitting parameters	100
Table 4.5. Shape parameter (β) determined by half height width of relaxation peak (Δ) of D121/St monomer-oligomer region.	101
Table 4.6. Total conversions at different curing cycles for D121/St and D121/DVB.	107
Table 5.1. Structures of unmodified non-polar dyes.	131
Table 5.2. Structures of modified polar state dyes (ionamines)	132
Table 5.3. Ionamines and their stability	134
Table 5.4. Structures of acids	141
Table 5.5. Acid (benzoic acid) and Base (AEPD)* ratio effects	142
Table 5.6. Color-changing test with different acids*	143
Table 5.7. Structures of bases	145
Table 5.8. Color-changing test with base in PMMA films, glycol as releasing agent*	145
Table 5.9. Color-changing test with base in PMMA films, glycerol as releasing agent*	146
Table 5.10. The composition of acid and base films*	147
Table 5.11. Color-changing test with acid and base films*	148

ABSTRACT

Changes in the ionic and dipolar molecular mobility in a polymer system are the basis for the changes in the dielectric mechanical properties of polymer materials. Frequency Dependent Dielectric Measurements (FDEMS) and Ion Time-of-Flight (ITOF) are two important techniques to investigate ionic and dipolar molecular mobility in polymer systems. Their results can be related to the macro- and molecular dielectric, electrical and dynamic properties of polymeric materials. The combination of these two methods provides a full view of electric, dielectric and dynamic behavior for the systems as they undergo chemical and/or physical changes during polymerization, crystallization, vitrification, and/or phase separation.

The research on microscopic mass mobility in polymer systems was done on three aspects: 1) ion mobility in an epoxy-amine reaction system; 2) dipolar mobility and relaxation during dimethacrylate resin cure and 3) dye molecule migration and diffusion in polymer films.

In the ion mobility study, we separately monitor the changes in the ion mobility and the number of charge carriers during the epoxy-amine polymerization with FDEMS and ITOF measurements. The isolation of the number of carriers and their mobility allows significant improvement in monitoring changes in the state and structure of a material as it cures. It is essential for those systems where the number of charge carriers cannot be assumed constant.

For the dipolar mobility and relaxation study, FDEMS measurements were used to detect structural evolution and spatial heterogeneity formation during the polymerization process of dimethacrylate resins. The changes in molecular dipolar mobility are related to the development of the heterogeneity. The dielectric spectra, glass transition (T_g) profiles and dynamic mechanical measurements were used to investigate the existence of two cooperative regions of sufficient size to create two α -relaxation processes representing oligomer rich and polymer microgel regions during the polymerization.

For the dye migration research, we tried to develop a visually color changing paper (VCP) due to dye molecule migration in polymer films. The mobility of dye molecules in polyvinyl films was controlled by the acidity of the environment. Ionamine derivatives of dyes were stable when mixed with acid. Their diffusion in polymer films can be quickly triggered as the result of an acid/base neutralization reaction. The effect of the type of base, acid and the compatibility of polymer films on the diffusion rate is discussed.

**CHARACTERIZATION OF IONIC, DIPOLAR AND
MOLECULAR MOBILITY IN POLYMER SYSTEMS**

CHAPTER 1. INTRODUCTION

Interest in dielectric properties and spectroscopy of polymeric materials flourished and developed with our fundamental understanding of polymer structure and properties. Several monographs¹⁻³ of polymer dielectric properties and applications were published for a comprehensive description of the fundamental and new progress in this research area. Based on a literature search, the area seems to have developed very quickly in the past decade. This is at least partly the result of the power that the dielectric properties of polymeric materials bring to the understanding of dynamics of complex polymer systems such as liquid crystals, blends, polymer solutions, and polymerization. Advances in instrumentation, as well as in theory and modeling, have also helped to stimulate renewed interest.

Today, polymer dielectric measurements have become popular with commercially available equipment for laboratory tests and monitoring polymer material fabrication. Polymer dielectric analysis is widely used for the characterization of coatings, curing systems and thermoplastics. It has many advantages over thermal and mechanical analysis, and it also can be used as a supplement to many standard analysis methods.

1.1. General introduction to polymer dielectric properties

When an electric field is applied across a dielectric polymer material, the charges in the material are displaced from their equilibrium position and the material is said to be polarized. There are two major polarization mechanisms in polymeric materials that are studied by dielectric methods:

1. polarization due to charge migration
2. polarization due to orientation of permanent dipoles

Migration of charges results in conductivity. The measured conductivity is due to contributions from extrinsic migrating charges (e.g., ionic impurities) and intrinsic migrating charges such as proton transfer along hydrogen bonds. Extrinsic conductivity is commonly assumed to be inversely proportional to viscosity according to the viscous model for charge transfer (Stokes law):

$$v = \frac{2gr^2(\rho - \rho_0)}{9\eta} \quad (1-1)$$

Where v is the velocity of a spherical particle in a viscous medium, r is the radius of the particle, ρ and ρ_0 are the densities of the particle and the medium, η is the coefficient of the medium.

The Equation (1-1) implies that highly viscous materials should exhibit a very low conductivity, which is not the case under all conditions. This is because intrinsic charge migration contributes more to the conductivity of the highly crosslinked polymer networks or polymers in the solid state. While the extrinsic conductivity decreases during

reaction as a result of the increase in viscosity, intrinsic conductivity can follow a more complex pattern, and hence the trend exhibited by the overall measured conductivity will depend on which mechanism dominates the dielectric response. As a direct consequence of this interplay between extrinsic and intrinsic contribution, the measured value can display different trends, as will be discussed in chapter 3.

The other polarization mechanism is the orientation of dipoles in polymeric materials. When materials that contain permanent dipoles are placed in the electric field, dipole orientation or dipole polarization is produced as a result of the alignment of dipoles in the direction of the applied electric field. The orientation of the dipoles involves cooperative motions of polymer chains and localized motions of molecular segments. These effects can be measured by dielectric methods with different time scales. The time-dependent loss due to re-orientation of dipoles upon removal of the electric field is called dipole relaxation. In chapter 4, we shall discuss the effect of cross-linking and network formation on the dynamic dipolar motions.

1.2. Theories of dielectric relaxation in a polymer

Experimental studies of the dielectric properties of materials have been made over a range of frequencies and temperature for over 100 years. The first systemic interpretation for such a kind of conduction and polarization in terms of molecular processes was proposed by the work of Debye⁴ – for which he was awarded the Nobel Prize in Chemistry in 1936. In dielectric spectroscopy, reorientational motions of dipolar

molecules were shown to give rise to dielectric dispersion behavior with accompanying dielectric absorption. The connection between dielectric permittivity and molecular dipole moments provided a method to determine molecular structure and dynamic properties.

In polymer dielectric research, dielectric relaxation spectroscopy broadly breaks into studies below and above 10^7 Hz. Microwave region (10^8 - 10^{11} Hz) dielectric spectroscopy is used to monitor the dielectric dispersion and absorption features for highly fluid polymer solutions. The dielectric features for most viscous, amorphous, crystalline, or liquid-crystalline polymers and the glass formation process commonly occur at frequencies less than 10^7 Hz. Such studies yield three essential items of information for the materials in which we are interested:

1. The magnitude of each of the dielectric relaxation processes $\Delta\epsilon_\alpha$, $\Delta\epsilon_\beta$, etc.
2. Their frequency dependence on temperature (T) , pressure (P) and conversion (α). These are defined by average relaxation (correlation) times $\tau_i = (2\pi f_{mi})^{-1}$ and where f_{mi} is the frequency of maximum loss for each process.
3. Band-shape or dielectric absorption contour for each dielectric relaxation process.

The above information is accumulated, reviewed and analyzed to relate to behavior of amorphous, crystalline, liquid crystal (LC) and glass forming polymers. These dielectric studies give information on: 1) the dipolar reorientation processes involving chain segments, polymer regions or whole molecules; 2) how these processes

vary with temperature, pressure and degree of cure; 3) characterization of phase changes in the materials.

Much experimental dielectric data has become available in the past 50 years, and numerous corresponding theories were proposed for explanation and prediction.^{3,5-9} The molecular equilibrium theory and phenomenological theory of dielectric permittivity as they relate to the dipolar mobility and polymer structures are the most widely accepted.^{7,10-14}

1.2.1 Equilibrium molecular theory

Dielectric spectroscopy deals with the influence of an alternating electric field $E(\omega)$ on polymer materials. Application of E results in a polarization P of the medium. The equilibrium theory explores the problem from a microscopic point of view. The macroscopic observable polarization P is related to the dipole density of N permanent molecular dipoles μ_i in a volume V . This is in contrast to low molecular weight molecules, where the dipole moment can be well represented by a single rigid vector. For long chain molecules there are different geometric possibilities for the orientation of molecular dipole vectors with respect to the polymer backbone (Figure 1.1).

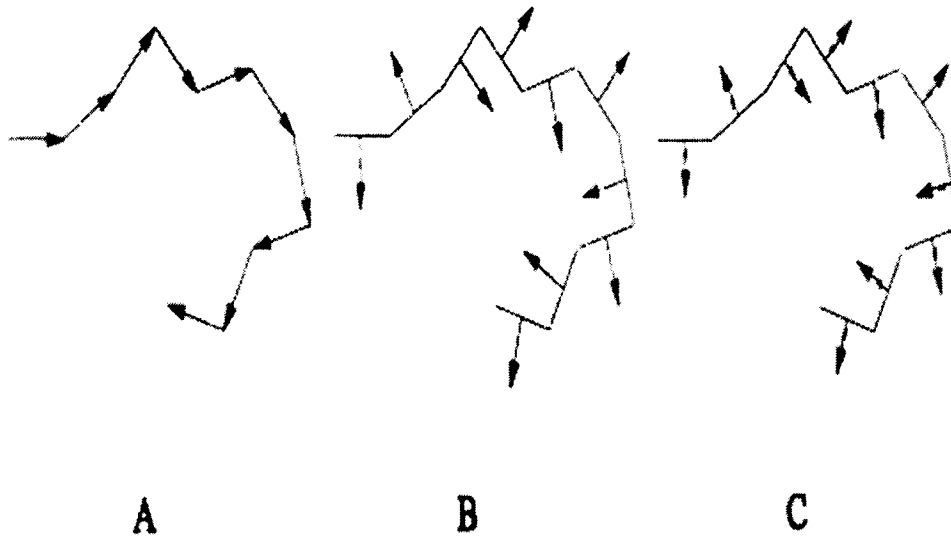


Figure 1.1. The different geometric possibilities for a location of a dipole with respect to the polymer chain

Type A polymer: polymer with the dipoles fixed parallel to the main chain;

Type B polymer: polymer with a dipole moment rigidly attached to the main chain;

Type C polymer: polymer with a flexible dipolar side group.

The net dipole moment per unit volume (polarization) of a polymer system is given as a vector summation over all molecular dipole types in the repeating unit, the polymer chain, and over all chains in the system:

$$P = \frac{1}{V} \sum_{\text{all chains}} \sum_{\text{chain}} \sum_{\text{repeating unit}} \mu_i \quad (1-2)$$

For small electric-field strengths a linear relationship holds between E and P.

$$P(\omega) = (\varepsilon^*(\omega) - 1)\varepsilon_{vac} E(\omega) \quad \text{with} \quad \varepsilon^*(\omega) = \varepsilon'(\omega) - i\varepsilon''(\omega) \quad (1-3)$$

where ε_{vac} is the permittivity in vacuum. The complex dielectric permittivity ε^* is related by the theory of dielectric relaxation to the correlation function $\Phi(t)$ of the polarization fluctuations:¹⁵

$$\frac{\varepsilon^*(\omega) - \varepsilon_\infty}{\varepsilon_0 - \varepsilon_\infty} = \int_0^\infty \left[\frac{-d\Phi(t)}{dt} \right] \exp(-i\omega t) dt \quad \text{with} \quad \Phi(t) = \frac{\langle \Delta P(t) \Delta P(0) \rangle}{\langle \Delta P(0)^2 \rangle} \quad (1-4)$$

where ΔP is a fluctuation of the polarization around its equilibrium value, the brackets mean the averaging over time t , ε_∞ and ε_0 are the permittivities at very high frequency and static state, respectively. The relative dielectric permittivity $\varepsilon_0 - \varepsilon_\infty$ is a frequency independent value. For an isotropic amorphous polymer system with N equivalent molecules each having a dipole moment, μ , and contained in a spherical volume, V , the quantity of $\varepsilon_0 - \varepsilon_\infty$ can be expressed as:^{4,11-13,15}

$$\varepsilon_0 - \varepsilon_\infty = \left\{ \frac{4\pi}{3kT} \frac{3\varepsilon_0(2\varepsilon_0 + \varepsilon_\infty)}{(2\varepsilon_0 + 1)^2} \right\} \frac{\langle M(0) \bullet M(0) \rangle}{V} \quad (1-5)$$

where $M(0)$ is the instantaneous dipole moment of the macroscopic sphere at the arbitrary time $t=0$. The equilibrium average of the scalar product $\langle M(0) \bullet M(0) \rangle$ will be independent of time for a stationary thermodynamics system. Equation (1-5) is the essential starting equation for understanding the static dielectric permittivity for a polymer system with dipolar molecules. The subsequent modifications and improvements of Equation (1-5) are made with respect to the special cases of the applied electric field and the local field experienced by the molecules.^{5,6} The subject of polymer dielectric study based on molecular theory has not been active for many years because most dielectric studies of polymer system have been concerned with relaxation dependence on frequency and related material property information rather than the static dielectric properties.

1.2.2 Dynamic behavior: phenomenological theory

The phenomenological theory of dielectric relaxation in a polymer system is generally summarized in a series of functions to describe the strength of the dielectric response, the shape of the relaxation peak or the distribution of the relaxation times, and the temperature and pressure effect on the dielectric relaxation.

In general the complex relative permittivity $\epsilon(\omega)$ is:

$$\epsilon(\omega) = \epsilon'(\omega) - i\epsilon''(\omega) + i(\sigma/\omega)\epsilon_{vac} \quad (1-6)$$

where $\omega = 2\pi f$ is the angular frequency of the measuring electric field; ϵ' and ϵ'' are the real permittivity and dielectric loss factor, respectively, measured at ω ; and σ is the frequency-independent dc conductivity of the sample that arises from the motion of charge carriers (ionic or electronic). The relaxation component of the complex permittivity is given by:

$$\frac{\epsilon(\omega) - \epsilon_{\infty}}{\epsilon_0 - \epsilon_{\infty}} = 1 - i\omega\xi[\Phi(t)] \quad (1-7)$$

where $\epsilon_0 - \epsilon_{\infty}$ is the total relaxation strength, ξ indicates a Fourier transform, and $\Phi(t)$ is a macroscopic relaxation function that can be measured as the transient charge decay function following the step withdrawal of a steady applied electric field from a sample.

For the single relaxation time model

$$\Phi(t) = \exp(-t/\tau) \quad (1-8)$$

where τ is a single macroscopic relaxation time. On insertion of Equation(1-8) into Equation (1-7), The familiar single relaxation time equations are obtained:

$$\epsilon'(\omega) = \epsilon_{\infty} + \frac{\epsilon_0 - \epsilon_{\infty}}{1 + \omega^2\tau^2} \quad (1-9)$$

$$\epsilon''(\omega) = (\epsilon_0 - \epsilon_{\infty}) \frac{\omega\tau}{1 + \omega^2\tau^2} \quad (1-10)$$

As shown in Figure 1.2, $\epsilon'(\omega)$ exhibits dispersion in the frequency domain, falling from ϵ_0 to ϵ_∞ with increasing frequency, and $\epsilon''(\omega)$ exhibits a “bell-shaped” absorption curve whose maximum value occurs at $\omega_m\tau = 1$, hence τ is determined.

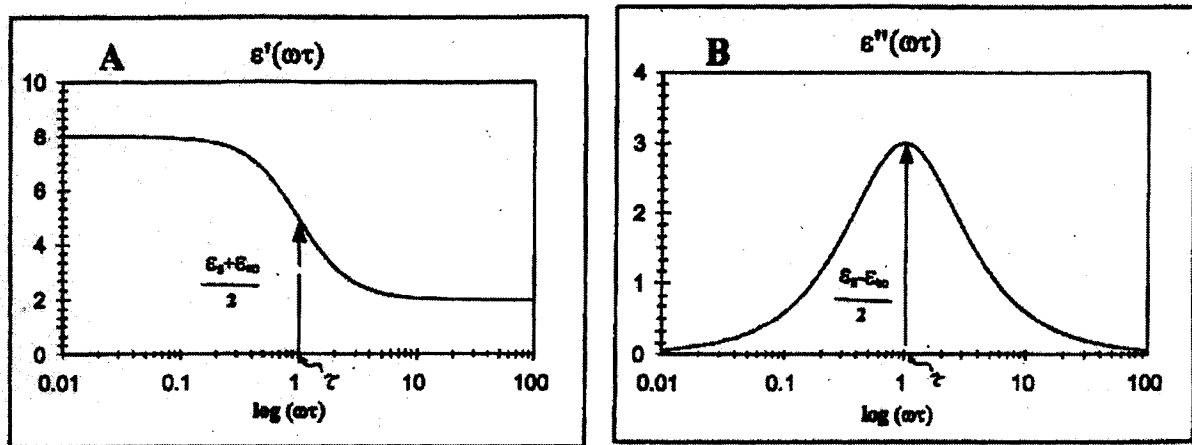


Figure 1.2. Dielectric relaxation dependence on the frequency for a single relaxation

For polymer materials, different types of dipolar orientations from side groups, chain segments and whole molecules create different relaxation peaks in dielectric spectroscopy. Even the same type of relaxation can have different distributions due to the heterogeneity of polymer system.¹⁶⁻²¹ All these factors make the dielectric spectroscopy of polymers rich and complicated. Compared with a single relaxation process, we can express this combined relaxation process with a discrete distribution of relaxation processes.

$$\frac{\epsilon(\omega) - \epsilon_\infty}{\epsilon_0 - \epsilon_\infty} = R(\omega) = \sum_j a_j R_j(i\omega) = \sum_j a_j \{1 - i\omega\zeta[\Phi_j(t)]\} \quad (1-11)$$

where α_j is the fraction of the total relaxation magnitude that is relaxed by process i and $R_j(\omega) = (1+i\omega\tau_j)^{-1}$ is the relaxation function for process j , and $\Phi_j(t)$ is the corresponding relaxation function for process j , $\sum\alpha_j = 1$.

1.3 Dielectric relaxation process in an amorphous polymer

Dielectric spectroscopy deals with the influence of an alternating electric field $E(\omega)$ on polymer materials. When the molecular dipole reorientation movement in polymers is on the same time scale as the alternating polarization produced by the electric field at a certain frequency, a relaxation process is observed. The molecular dipolar motions in dense amorphous polymer systems are controlled by different time and length scales. Further, different types of dipole movement can be reoriented by different motional processes. Thus, the dielectric spectrum of an amorphous polymer generally shows multiple relaxation behavior where each process is indicated by a peak in ϵ'' versus frequency plot or a step-like decrease in ϵ' versus frequency plot.

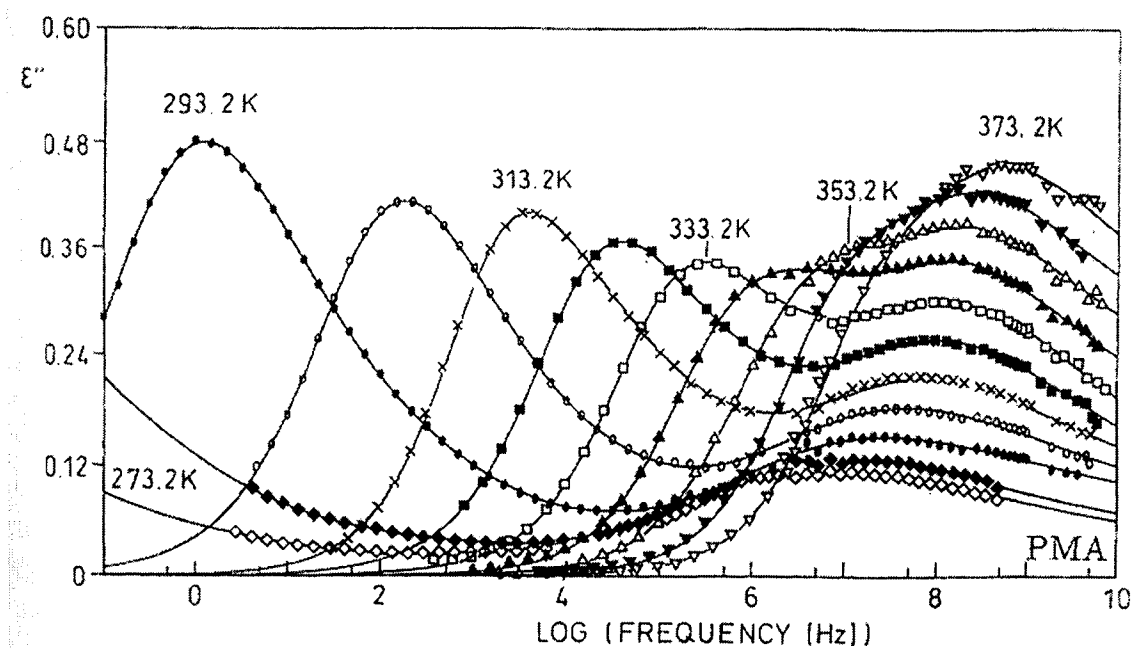


Figure 1.3. Dielectric loss spectra of polymethylacrylate²²

Most amorphous polymers exhibit a secondary, or β -process, and a principle, or α -relaxation, located at lower frequencies or a higher temperature than the β -relaxation. As a typical example, Figure 1.3 shows the dielectric loss spectrum for polymethylacrylate in the frequency range from 10^{-1} Hz to 10^{10} Hz displaying the high frequency, β , and the low frequency, α -processes.²² For the polymer with the dipoles fixed parallel to the main chain (Type A polymer in Figure 1.1), a further process called α' - or normal-mode relaxation can be observed at frequencies below the α -relaxation. The α' -process corresponds to the molecular motion due to the vibrational modes of the whole polymer chain.²³

Dielectric spectroscopy becomes more complicated in a polymer blend or a polymerizing system. One or multiple α , β -relaxations can be observed to indicate

miscibility, phase separation and network formation. This will be discussed in detail in chapter 2.1.2.

The geometric forms of non-linear chains like combs, stars, rings, or networks will clearly influence the relaxation and dielectric behavior. Apart from the α -, β - and the vibrational normal-mode processes, many amorphous polymers also exhibit further relaxation process that can be detected dielectrically, provided that the relaxation process involves a reorientation of a type of dipole moment vector.²⁴⁻²⁶

1.3.1 α -relaxation in amorphous polymers

The α -relaxation in the polymer system is related to cooperative dipolar motion of a region. The understanding of the α -process during the dynamic glass transition at low frequencies (around 10^{-3} Hz) is related to the calorimetric glass transition. Most workers agree that the calorimetric glass transition corresponds to the cooperative segmental motions, such as the dipolar rotation fluctuations caused by gauche-trans transition about C-C bonds. All these segmental motions are restricted by the environment of surrounding segments of other chains. The time scale of these segmental motions reflect the properties of the local region about each mobile segment and macroscopic properties such as density, colligation and crystallization, which present peaks in dielectric spectroscopy.

The empirical temperature dependence of the α -relaxation rate (f_α) can be determined by Vogel/Fulcher/Tammann/Hesse (VFT) Equation:²⁷⁻²⁹

$$\log(f_\alpha) = \log f_{\infty\alpha} - A/(T - T_0) \quad (1-12)$$

where $\log f_{\infty\alpha}$ ($f_{\infty\alpha} = 10^{10}$ - 10^{12} Hz) and A are constants. T_0 is the so-called ideal glass transition or Vogel temperature which is found 30-70K below T_g . Several models, such

as the free volume model, lattice theory and kinetic processes, have been proposed to understand the physical origin of the VFT equation and T_0 .^{30,31} The physical meaning of T_0 can be explained as the temperature for fractional free volume becomes zero, or the second order phase transition temperature. Although the meaning of T_0 is not yet clear, the universality of the VFT equation suggests that T_0 is a significant temperature for the dynamics of a glass transition. The cooperativity of molecular motion sets in well above T_g and increases with decreasing temperature.

The most widely used model is the Williams/Lander/Ferry (WLF) equation:³²

$$\log \frac{f_\alpha(T)}{f_\alpha(T_{ref})} = -\frac{C_1(T - T_{ref})}{C_2 + T - T_{ref}} \quad (1-13)$$

where T_{ref} is a reference temperature and $f_\alpha(T_{ref})$ is the relaxation rate at this temperature. C_1 and $C_2 = T_{ref} - T_0$ are so called WLF parameters. The physical origin is that C_1 is inversely proportional to the fractional free volume (v_0) in the materials at the temperature of interest ($C_1 = 1/v_0$) and C_2 equals to the fractional free volume (v_0) over thermal expansion coefficient (α_f) ($C_2 = v_0 / \alpha_f$). Empirically it was shown that the glass transition temperature corresponds to relaxation rates of 10^{-3} to 10^{-2} . When the T_{ref} has been set as T_g , the parameters C_1 and C_2 should have universal values ($C_1 = 17.44$, $C_2 = 51.5$) for polymer systems.

The temperature affects the relaxation strength as well as relaxation rate in the α -relaxation process.

$$\Delta\varepsilon = \varepsilon_{stat,i} - \varepsilon_{\infty,i} = \frac{\varepsilon_{stat,i}(\varepsilon_{\infty,i} + 2)^2}{3 \times (2\varepsilon_{stat,i} + \varepsilon_{\infty,i})} \times \frac{gN\mu^2}{3kT} \quad (1-14)$$

where μ is the dipole moment of the moving unit, T is the temperature, and k is the Boltzmann constant. The Kirkwood correction factor g was introduced to describe local, static correlation of dipoles. As indicated by Equation (1-14), the dielectric relaxation strength of the α -relaxation decreases with increasing temperature. This is understood from the point of a cooperative process in that the re-orientation of dipoles is influenced increasingly by its environment with decreasing temperature.

In general the α -process shows in the frequency domain a broad (2-6 decades), asymmetric peak. The width of the α -relaxation peak for polymers depends on various factors such as temperature, structure of the chain and crosslinking density. It becomes narrower with increasing temperature and broadens dramatically with crosslinking.

1.3.2 β -relaxation in amorphous polymers

It is well agreed that the dielectric β -relaxation of polymers arises from localized rotational fluctuations of the dipole vector. The rotational of fluctuations of localized parts of the main chain and side groups or parts of them contribute to the formation of β -relaxation peaks.^{26,33-38}

Compared with the cooperative dipolar motion in an α -relaxation, the localized dipolar motion of the β -relaxation is located at a higher frequency (as seen in Figure 1.2) and a lower temperature. For most polymers, the β -relaxation has been studied below the glass transition temperature. The temperature dependence of the β -relaxation rate is found to follow the Arrhenius equation:

$$f_{\beta} = f_{\infty\beta} \exp\left[-\frac{E_{\beta}}{kT}\right] \quad (1-14)$$

where $f_{\infty\beta}$ is the preexponential factor, and E_{α} is activation energy. In general, $f_{\infty\beta}$ should be of the order of magnitude 10^{12} to 10^{13} Hz. The activation energy E_{α} , related to the slope of $f_{\infty\beta}$ versus $1/T$, depends on both the internal rotation barriers and the environment of the moving unit.^{34,39-41}

The relaxation strength for an α -relaxation is stronger than a β -relaxation for amorphous polymers. When the main dipole moment is located in the side group, small fluctuations of the side group can contribute significantly to the dielectric loss of chain segments or the whole molecular chain. Unlike the α -relaxation process, $\Delta\epsilon_{\beta}$ increases with temperature. Although the net dipole moment is nearly independent of temperature, this temperature dependence can be understood as an increase of the fluctuation angle of the dipole vector or by the number of moving dipoles increasing with temperature.

1.3.3 Dielectric normal-mode relaxation

For polymers having a dipole component parallel to the chain backbone, a normal-mode process can be observed at frequencies below the α -relaxation.^{16,23} The molecular dipole vectors that are parallel to the repeating unit are summed over the chain, and therefore the normal-mode relaxation is related to both the geometry and the dynamics of the polymer. Compared to α , β -relaxation, the normal mode relaxation is more restricted with the polymer chain length, because it is the result of molecular motion of the whole polymer chain. As seen in Figure 1.4, the normal-mode relaxation has obvious molecular weight dependence.

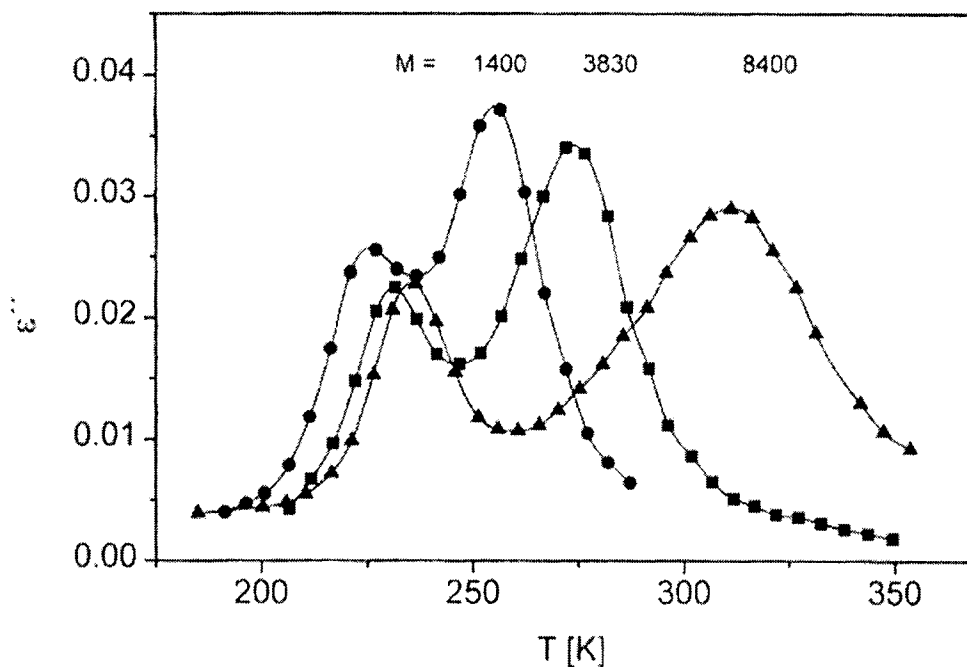


Figure 1.4. Value of ϵ'' versus T at a frequency of 104 Hz for cis-1,4-polyisoprene samples of Mw 1400 (●), 3830 (■), and 8400 (▲)⁴²

For the polymer with dipoles parallel to the chain skeleton, the whole dipole moment can be obtained by integration over the chain length. Therefore the relaxation strength of the normal mode relaxation $\Delta\epsilon_n$ is proportional to the mean end to end vector of the chain $\langle r^2 \rangle$. And in the other way, if $\Delta\epsilon_n$ is known for this type of polymer, the mean end to end vector of the chain can be estimated.⁴³

1.4. Objective of dissertation

The primary purpose of this dissertation is to monitor the ionic mobility and dipolar relaxation on a molecular level, and to relate these properties to the macroscopic property changes and structural evolution during polymerization. This research is presented in four chapters:

Chapter 2 is dedicated to discussing the two measurement techniques, the ion time-of-flight measurement (ITOF) and frequency dependent dielectric sensing measurement (FDEMS). The theoretical background and applications are introduced for these two techniques.

Chapter 3 explores the application of the ITOF measurement in an epoxy-amine curing system. With FDEMS measurements, we can separately monitor the changes in the ion mobility and the number of charge carriers during the epoxy-amine polymerization. The combination of ITOF and FDEMS measurements that isolates both the number of carriers and their mobility allows significant improvement in monitoring changes in the state and structure of a material as it cures. It is essential for those systems where the number of charge carriers cannot be assumed constant.

Chapter 4 focuses on measurements of dielectric properties using FDEMS to detect structural evolution and spatial heterogeneity formation during the polymerization process of dimethacrylate resins. The changes in molecular dipolar mobility are related to the development of the heterogeneity. The dielectric spectra and glass transition (T_g) profiles are used to investigate the existence of two cooperative regions of sufficient size to create two α -relaxation processes representing oligomer rich and polymer microgel regions during the polymerization.

Chapter 5 describes the migration of dye molecule in polymer films. With the chemical modification of dye molecular structures, selection of polymer films and design of the migration process, we tried to develop a series of visual color changing papers with different timing effects.

REFERENCE

- (1) Runt, J. P.; Fitzgerald, J. J. *Dielectric Spectroscopy of Polymeric Materials: Fundamentals and Applications*; Oxford Univ Pr, 1997.
- (2) Schonhals, A.; Kremer, F. *Broadband Dielectric Spectroscopy*; Springer Verlag, 2002.
- (3) McCrum, N. G.; Read, B. E.; Williams, G. *Anelastic and Dielectric Effects in Polymer Solids*; Wiley: New York, 1967.
- (4) Debye, P. W. *Polar Molecules*; Chemical Catalog Co.: New York, 1927.
- (5) Hill, N.; Vaghan, W. E.; Price, A. H.; Davies, M. M. *Dielectric properties and molecular behaviour*; Van Nostrand Reinhold: New York, 1969.
- (6) Bottcher, C. J. F.; Bordwijn, P. *Theory of electric polarization*, 2nd ed.; Elsevier: Amsterdam, 1978; Vol. 2.
- (7) Williams, G.; Pethrick, R.; Richards, R. W., Eds.: Dordrecht, Holland, 1982; Vol. Dynamic Properties of Solid Polymers, pp 213-239.
- (8) Von Hippel, A. *Dielectris and Waves*; Wiley: New York, 1959.
- (9) Von Hippel, A. *Dielectric Materials and Applications*; Wiley: New York, 1954.
- (10) Williams, G. In *Comprehensive Polymer Science*; Allen, G.; Bevington, J. C.; Booth, C.; Price, C., Eds.; Pergamon: Oxford, England, 1989; Vol. 2, p 601.
- (11) Williams, G. *Chem. Rev.* **1972**, 72, 55.
- (12) Williams, G. *Chem. Soc. Rev.* **1978**, 7, 89.
- (13) Williams, G. *Adv. Polym. Sci.* **1979**, 60.
- (14) Williams, G.; Edwards, D. A. *Trans. Fara. Soc.* **1966**, 62, 1329.
- (15) Cook, M.; Watt, D. C.; Williams, G. *Trans. Fara. Soc.* **1970**, 66, 2503.
- (16) Riande, E.; Saiz, E. *Dipole moments and Birefringence of polymers*; Prentice Hall: Englewood Cliffs, NJ, 1992.
- (17) Wu, L. *Phys. Rev.* **1991**, 43, 9906.
- (18) Cole, K. S.; Cole, R. H. *J. Chem. Phys.* **1941**, 9, 341.

- (19) Davidson, D. W.; Cole, R. H. *J. Chem. Phys.* **1951**, *19*, 1484.
- (20) Schonhals, A.; Schlosser, J. *J. Non-cryst. Solids* **1991**, *132*, 161.
- (21) Havriliak, S.; Havriliak, J. *J. Non-cryst. Solids* **1994**, *173*, 297.
- (22) Kremer, F.; Hofmann, A.; Fischer, E. W. *Am. Chem. Soc. Polym. Prepr.* **1992**, *33*, 96.
- (23) Adachi, K.; Kotaka, T. *Prog. Polym. Sci.* **1993**, *18*, 585.
- (24) Pathmanathan, K.; Johari, G. P. *J. Polym. Sci.* **1987**, *25*, 379.
- (25) Johari, G. P. *Polymer* **1986**, *27*, 866.
- (26) Buerger, D. E.; Boyd, R. H. *Macromolecules* **1989**, *22*, 2649.
- (27) Vogel, H. *Phys. Z.* **1921**, *22*, 645.
- (28) Fulcher, G. S. *J. Am. Chem. Soc.* **1925**, *8*, 339.
- (29) Tammann, G.; Hesse, W. *Z. Anorg. Allg. Chem.* **1926**, *156*, 245.
- (30) Gres, G. S.; Cohen, M. H. *Adv. Chem. Pys.* **1981**, *48*, 455.
- (31) Donth, F. *Relaxation and Thermodynamics in Polymer: Glass Transition*; Hkademie-verlog: Berlin, Germany, 1992.
- (32) Ferry, J. D. *Viscoelastic Properties of polymers*, 3rd ed.; J. Wiley and Sons: New York, 1980.
- (33) Garwe, F.; A.Schonhals; M.Beiner; K.Schroter; E.Donth. *Macromolecules* **1996**, *29*, 247.
- (34) Katana, G.; Kremer, F.; Fischer, E. W.; Plaetscke, R. *Macromolecules* **1993**, *26*, 3075.
- (35) Gomes Ribelles, J. L.; Diaz Calleja, R. J. *J. Polym. Sci. Part B Polym. Phys.* **1985**, *23*, 1297.
- (36) Tetsutani, T.; Kakizaki, M.; Hideshima, T. *Polymer J* **1982**, *14*, 305.
- (37) Tetsutani, T.; Kakizaki, M.; T., H. *Polymer J* **1982**, *14*, 471.
- (38) Zeeb, S.; Horing, S.; Garwe, F.; Beiner, M.; Schonhals, A.; Schroter, K.; Donth, E. *Polymer* **1997**, *38*, 4011.

- (39) Havriliak, S. *Polymer* **1992**, *33*, 938.
- (40) Colmeno, J.; Arbe, A.; Alegia, A. *Physica A*. **1993**, *201*, 447.
- (41) Hofmann, A.; Kremer, F.; Fischer, E. W. *Physica A*. **1993**, *201*, 106.
- (42) Schonhals, A. *Macromolecules* **1993**, *26*, 1309.
- (43) Adachi, K.; Nishi, I.; Itoh, S.; Kotaka, T. *Macromolecules* **1990**, *23*, 2550.

CHAPTER 2. DIELECTRIC TECHNIQUES AND APPLICATIONS IN POLYMER SYSTEM

Dielectric spectroscopy and ion time-of-flight measurements are two important techniques to investigate the macro- and molecular dielectric and electrical properties of polymeric materials. The combination of these two methods will provide a full view of electric and dielectric behavior for the systems as they undergo chemical and/or physical changes during polymerization, crystallization, vitrification, phase separation, etc. In this chapter we shall focus on the background, equipment and applications of these two techniques.

2.1. Dielectric spectroscopy

There are very good reasons for the interest in fundamental and applied aspects of dielectric spectroscopy in material characterization. Fundamental investigations of the dielectric response yield a wealth of information about different molecular motions and relaxation processes. A unique characteristic of dielectric measurement is the wide frequency range, from 10^{-5} Hz to 10^{11} Hz, over which molecules respond to an applied electric field. This information is the key feature that enables one to relate the observed dielectric response to slow and/or fast molecular events. Complementary information to dielectric spectroscopy studies can be obtained from nuclear magnetic resonance (NMR), dynamic mechanic analysis (DMA), light scattering (LS), neutron scattering, transient

fluorescence depolarization, and ultrasonic measurements, but none of those techniques can cover as wide a frequency range as dielectric spectroscopy. A strong interest in dielectric measurement reflects the growth of its application in materials characterization and processing in laboratory and industrial environments.

Dielectric spectroscopy measurements in the frequency region from hertz to megahertz are normally used for the study of chain or segment motions on the molecular level and provide a sensitive, convenient automated means for characterizing the physical properties of polymeric materials as well. Dielectric sensing techniques have the advantage that the measurement can be made both in the laboratory and *in situ* in the manufacturing environment. This frequency domain can be effective for monitoring a variety of resin-cure processing properties such as reaction onset, viscosity, point of maximum flow, degree of cure, buildup in glass transition temperature, and reaction completion, as well as detecting the variability in processing properties due to resin age and degradation. At the heart of dielectric sensing is the ability to monitor the changes in the transitional mobility of ions and changes in the rotational mobility of dipoles in the presence of a force created by an electric field. These variations in molecular position due to an electric field force are a very sensitive means of monitoring changes in macroscopic mechanical properties.

The general practice of dielectric measurements is to sweep the frequencies during the chemical/physical processes. The variation in the magnitude of the complex permittivity $\epsilon''(\omega)$ with frequency and with time and temperature provide molecular-level information on parameters such as relaxation time, relaxation amplitude, and distribution of relaxation times. From this we draw conclusions on the state of material. Some new

experimental techniques, such as temperature modulated dielectric analysis (TMDA)¹ and ambient pressure dielectric measurement,² were developed to separate the combined effects on the dielectric properties during a reaction or to collect the data in an extreme experimental condition.

2.1.1 Principles of measurement

Dielectric measurements are conducted by applying voltage to the electrode interface and measuring the amplitude and the phase shift of the resulting current. If the input signal is the current and the output signal is the voltage, the transfer function is the system impedance (Z), which is the sum of the contributions from resistance (R) and capacitance (C):

$$\vec{Z} = \frac{1}{\vec{Y}} = \frac{1}{\frac{1}{R} + i\omega C} = Z' + iZ'' \quad (2-1)$$

where Y is the admittance, which equal to the reciprocal overall impedance, Z . i is $(-1)^{1/2}$ and ω is the angular frequency, $\omega = 2\pi f$. The real and imaginary components of impedance are given by:

$$Z' = \frac{R}{1 + (\omega CR)^2} \quad (2-2)$$

$$Z'' = -i \frac{\omega CR^2}{1 + (\omega CR)^2} \quad (2-3)$$

The relation between the impedance and complex permittivity is $Z^* = 1/(\epsilon^* i\omega\epsilon_0)$, then impedance can be expressed by permittivity:

$$Z' = -\frac{\epsilon''}{\omega\epsilon_0(\epsilon'^2 + \epsilon''^2)}$$

$$Z'' = -\frac{\varepsilon'}{\omega\varepsilon_0(\varepsilon'^2 + \varepsilon''^2)} \quad (2-4)$$

when R^*C is equal to τ , the relaxation time of the system. This complex permittivity expression is often reported in terms of the complex dielectric constant

$$\varepsilon^* = \varepsilon'_\infty + \frac{(\varepsilon'_0 - \varepsilon'_\infty)}{1 + i\omega\tau} \quad (2-5)$$

By separating equation (2-5) into its real and imaginary components, we get the following equations:

$$\begin{aligned} \varepsilon'(\omega) &= \varepsilon_\infty + \frac{\varepsilon_0 - \varepsilon_\infty}{1 + \omega^2\tau^2} \\ \varepsilon''(\omega) &= (\varepsilon_0 - \varepsilon_\infty) \frac{\omega\tau}{1 + \omega^2\tau^2} \end{aligned} \quad (2-6)$$

Several derived quantities can be obtained from dielectric spectroscopy. These include conductance, dielectric modulus and complex dielectric constant.

2.1.2 Instrumentation and data collection

Prior to the 1980s, frequency dependent measurements of the dielectric properties of molecular materials were performed using a range of manually balanced resistance-capacitance and capacitance-bridge. It was difficult to make measurements covering broad frequency range, or monitor the dielectric properties changes *in-situ* during a temperature ramp or cure. With the development of the impedance analyzer, computer-controlled instruments can be designed to measure dielectric quantities over a large frequency range. Most recently, an excellent review of the instrumentation for dielectric spectroscopy was written by Kremer and Schonhals.³ Based on their literature survey, the following impedance analyzers are widely used by research community.

1) Solartron 1260 gain phase impedance analyzer (operable in the frequency from 10^{-5} Hz to 32MHz).

2) HP 4000 series impedance analyzers provide the affordable solutions for different frequency requirements. For example, HP4192A works in the frequency range from 5Hz to 13MHz, HP4263 can make the measurements at 0.1, 0.12, 1, 10, 100 kHz and HP4291 can operate from 1MHz to 1.8GHz.

3) Genrad 1600 series bridges also provide an inexpensive solution for multi-frequency dielectric measurement.

At present, some leading technology companies offer complete setups for dielectric measurements for different purposes. NETZSCH, NOVOCONTROL, Scientifica Inc., Microwave Properties North (MPN), Stain Measurement Device Inc. (SMD) provide dielectric measurement solutions for laboratory and manufacturing applications. The following is the equipment and experimental apparatus used in our experiments

- Impedance analyzer

HP 4192A impedance analyzer with the frequency rang of 5Kz-13MHz and HP4263B impedance analyzer with five fixed frequencies at 100Hz, 120Hz, 1KHz, 10KHz and 100KHz.

- Sensors

Two microsensors designed and patented by Prof. Kranbuehl were purchased from Century Circuit&Electronics. The kapton sensor consisted of inter-digitated copper electrodes (50 microns in width) on an area of 2.5×1.2 cm flexible polyimide substrate with an air gap of 86 microns. A glass sensor consisted of inter-digitated gold electrodes

(30 microns in width) on an area of 2.0×1.1 cm glass substrate with an air gap of 30 microns.

- Software

Several programs were developed to collect and analyze the data through a GPIB interface. FDEMSRUN.EXE and FASTDATA.EXE were developed with basic for DOS operation system. FDEMS DATA ACQUISITION.EXE (version 1.0) was developed with Visual C++ for WINDOWS operation system.

- Diagram

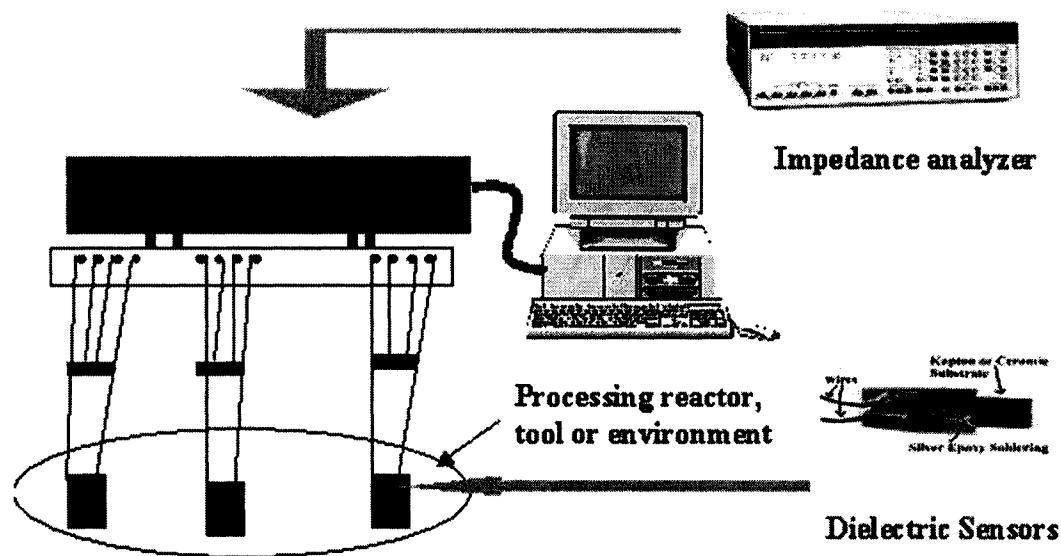


Figure 2.1. FDEMS experimental setup

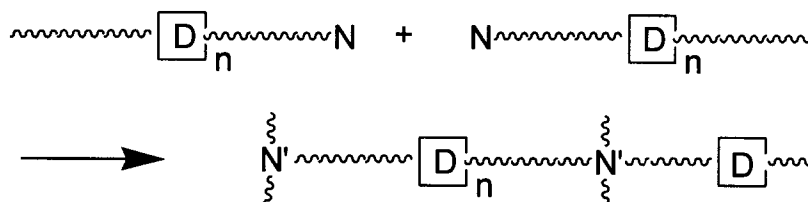
2.1.3 Applications

2.1.3.1 Cure monitoring

A reason for the use of dielectric spectroscopy in the study of polymerization is that the materials (reactants and/or products) contain a permanent dipole. In a

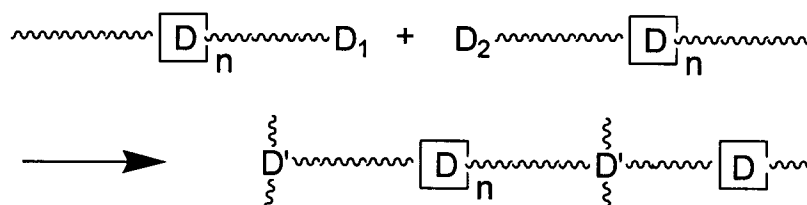
polymerization process, the type and the concentration of dipoles can vary during the reaction. Figure 2.2 illustrates two classes of reactions that are widely studied by dielectric measurement.

Class 1: Dipoles Not Involved In Reaction



N = reactive non-polar group
 D = non-reactive polar group
 N' = non-polar group formed
 Example: Polymerization of vinyl terminated monomers

Class 2: Dipoles Reacting To Form New Dipoles



D₁, D₂ = reactive polar group
 D = non-reactive polar group
 D' = a new polar group formed
 Example: Epoxy-amine reactions

Figure 2.2. Classification for the dipolar groups during cure

Class 1: dipoles present in the reactants are not involved in the chemical reaction so that the product contains the same concentration and type of dipolar groups (e.g., the polymerization of vinyl ended monomers, terminally functional linear polymers with low polarity reactive end groups)

Class 2: dipoles present in the reactants (though not necessarily all of them) are involved in the reaction and a new type of dipoles is formed. (e.g., the reaction of epoxide- and amine- containing monomers)

Fundamental studies in this area correlate dipolar dynamics with the kinetics of structure formation. Dielectric permittivity, loss factor and electrical conductivity have been related to the glass transition, appearance of secondary transitions and various rheological phenomena. From the mid-eighties, the dielectric analysis of thermoset cure was made by Seferis,⁴⁻⁶ Bidstrup, Senturia, Sheppard⁷⁻⁹ and Kranbuehl,¹⁰⁻²⁴ who wrote many papers on the dielectric monitoring of polymerization and cure, in which they showed a number of examples of the use of sensors to monitor the dielectric response for various applications. The essential contribution of their work is the correlation between dielectric functions (dielectric permittivity and loss) and the curing parameters (viscosity and degree of cure). They were joined in the early 1990s by Johari and coworkers,^{25,26} who also initiated a series of comprehensive dielectric studies of curing kinetics. All of these groups used the complex electrical modulus to describe electric conductivity and dipolar relaxation.

Johari and co-workers suggested a decrease in conductivity obeyed a power law form which could be used to determine the critical phenomenon during cure –gel point. The conclusion about the gelation determined by dielectric measurement is still being debated.²⁷ Recently, additional substantial contributions to the development of a molecular understanding of the cure process have been made by Mijovic and his coworkers.^{28,29}

In dielectric measurements during cure, the dielectric impedance of a material characterized by its equivalent capacitance, C , and conductance, G are used to calculate the complex permittivity by the following equation:

$$\varepsilon^* = \varepsilon' - i\varepsilon'' \quad (2-7)$$

$$\varepsilon'(\omega) = \frac{C(\omega)_{material}}{C_0}$$

$$\varepsilon''(\omega) = \frac{G(\omega)_{material}}{\omega * C_0}$$

where $\omega = 2\pi f$, is the measurement frequency and C_0 is the air replacement capacitance of the sensor. This calculation is possible when using a sensor whose geometry is invariant over all measurement conditions. Both the real and the imaginary parts of ε^* can have dipolar (d) and ionic (i) charge components.

$$\varepsilon' = \varepsilon_d' + \varepsilon_i' \quad (2-8)$$

$$\varepsilon'' = \varepsilon_d'' + \varepsilon_i'' \quad (2-9)$$

Kranbuehl and co-workers showed that plots of the product of frequency (ω) multiplied by the imaginary component of the complex permittivity $\varepsilon''(\omega)$ make it relatively easy to visually determine when the low-frequency magnitude of ε'' is dominated by the mobility of ions and when at higher frequencies the rotational mobility of bound charge dominates ε'' .²¹ Generally, the magnitude of the low-frequency overlapping values of $\omega\varepsilon''(\omega)$ can be used to measure the change with time of the ionic mobility through the parameter σ where

$$\sigma(\text{ohm}^{-1}\text{cm}^{-1}) = \varepsilon_0 \omega \varepsilon_i'' \quad (2-10)$$

$$\varepsilon_0 = 8.8554 \times 10^{-14} \text{C}^2 \text{J}^{-1} \text{cm}^{-1}$$

The changing value of the ionic mobility is a molecular probe, which can be used to monitor changes in the viscosity during cure. The dipolar component of the loss at higher frequencies can then be determined by subtracting the ionic component.

$$\varepsilon_d'' = \varepsilon'' - \frac{\sigma}{\varepsilon_0 \omega} \quad (2-11)$$

The peaks in ε_d'' (which are usually close to the peaks in ε'') can be used to determine the time or point in the cure process when the “mean” dipolar relaxation time has attained a specific value:

$$\tau = \frac{1}{\omega} \quad (2-12)$$

The dipolar mobility, as measured by the mean relaxation time τ , can monitor the α -relaxation process associated with vitrification, and it can be used as a molecular probe of the buildup in T_g .

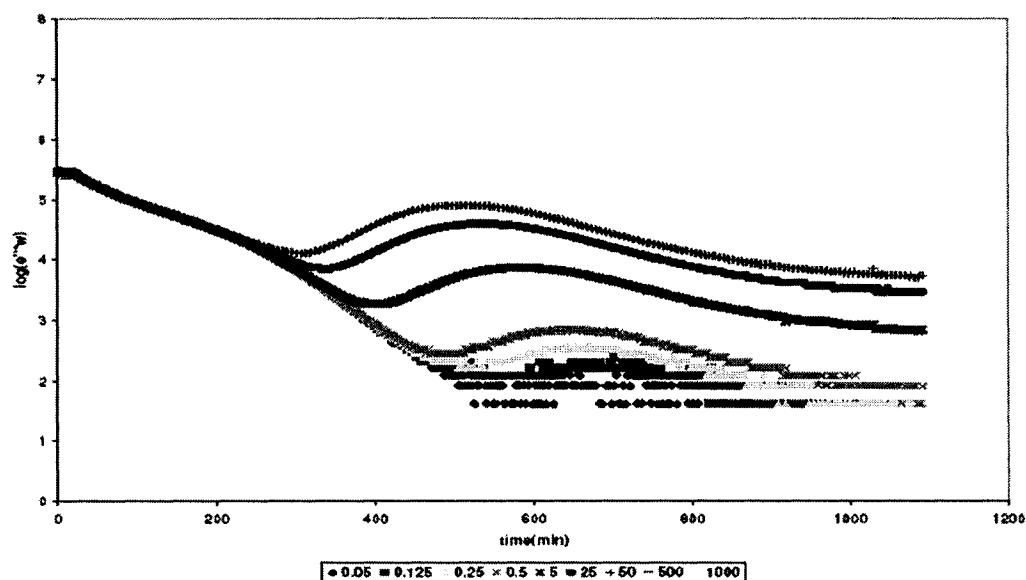


Figure 2.3. MCDEA/DGEBA isothermal cure at 120°C

Figure 2.3 is a typical plot of the frequency dependent measurement during the cure of an epoxy/amine mixture. At low frequency, the motion of ionic species will be over large distances and reflect the macroscopic viscosity to some extent. At higher frequencies, the motion of ionic species will be over small distances and the microscopic viscosity is sensed. In the initial stages of the cure process, the microscopic and macroscopic viscosity will be essentially identical and it is only as the micro regions with different sizes are formed that the differences in size-time scale become important. The decrease of the low frequency dependence of ϵ'' indicates an increase in the viscosity of the medium. Then the dipolar motion of the matrix becomes active and is the dominant feature as the viscosity continues to build up and the glass transition temperature increases with reaction advancement. Careful inspection of the plots indicates that the relaxation frequency moves to lower frequencies as cure proceeds and is an indication of the loss of free volume and the increasing T_g of the matrix.

2.1.3.2 Phase separation

The viscosity and onset of phase separation of thermoset/thermoplastic blends are critical processing properties and affect the final morphology. Frequency dependent dielectric measurements have the particular advantage to monitor these processes in both laboratory and the industrial fabrication environment.

Normally, the initial dielectric constant of these blends (e.g., amine cured epoxy with rubber) are relatively low, however, as cure proceeds, the dielectric constant rises and a related event can be observed in dielectric spectroscopy. This feature is associated with the phase separation in the system and often can create a Maxwell-Wagner-Sillars loss process.^{30,31} This process is caused by the generation of an occluded phase that has a

higher ionic mobility than the matrix phase in which it is dispersed. In the presence of an applied electric field the ion will move to an appropriate phase boundary and will then become temporarily trapped at this point. Reversal of the field will cause the ions to flow to the opposite phase boundary and therefore the magnitude of the effective dipole change reflects the projection of the occluded volume dimension in the electric field direction. The conductivity of the matrix will determine the time it takes for these ions to move between the extremes of the phase and hence dictate the effective relaxation time of the media. Analysis of this feature provides information of the shape and volume fraction of this occluded phase. The dielectric studies on these thermoplastic/thermoset phase separation systems have been made by Kranbuehl and Pethrick.³²⁻³⁶

2.1.3.3 Aging and degradation of polymeric materials

Hydrothermal aging which is caused by the diffusion of moisture into thermoset materials (PA-11, epoxy resin, etc.) has been extensively investigated. Since water has a large dipole and strong dielectric response, it is ideally suited for study with dielectric measurements.³⁷ Studies of the dielectric relaxation of water in various polymeric materials have shown that three distinct regions can be detected in materials.³⁸⁻⁴⁰ At high water absorption region, proton transfer occurs rapidly and the dielectric relaxation is dominated by dc conductivity. In a lower water absorption region, aggregated water can be detected in a frozen state at approximately 0°C. At temperatures below 0°C, a further relaxation related to the third water absorption state can be observed and associated with water dispersed as either single molecules or small clusters. For the resin systems which are toughened with thermoplastics components, it is difficult to predict water absorption behavior. But in these blend systems, the rate and extent of water absorption can have a

profound effect on the mechanical properties of the matrix and the stability of the interface that is formed between the thermoset resin and the thermoplastic substrate.

The physical aging process of thermoplastics also can be followed by dielectric analysis.⁴¹⁻⁴³ In these aging study, the time dependent dielectric spectra were compared to the variation in the positron annihilation and the dynamical mechanical thermal analysis for a molecular interpretation of the processes that are occurring during physical aging.^{44,45} Normally, as the aging occurs the dipolar process associated with the T_g appears sharper. This relaxation process is associated with the reorientation of cooperative dipolar motions and requires free volume. The positron annihilation studies indicate that the physical aging process is associated with the reduction of the free volume and correlates well with the changes in the dielectric spectrum. The changes in the distribution of relaxation processes are a consequence of the effects of the loss of free volume in the system,

2.1.3.4 Characterization of film formation

The real time dielectric technique can also be applied to the study of the coalescence of polymer latexes during the film formation.^{46,47} Water is the usual solvent for latex emulsion preparation and its polarity is ideal for dielectric investigation. By monitoring the water relaxation process in free, bonding and limited state, this technique provides the information of the various stages of the overall latex film formation process.

Dielectric spectroscopy also can be used to monitor film formation with polymerization and cure processes.⁴⁸⁻⁵¹ Measurements have been made on neat thermoset resins, thermoset resin with nano-size metal particles and solution polymerization reactions. In addition to the extent of polymerization and the dielectric and physical

nature of polymer network, the results indicate that this technique can be used to separate the effect of the nano-particle formation^{48,49} and to investigate gravitational effects^{50,51}.

The technique is able to distinguish between surface and solution polymerizations during formation of thin films. Furthermore, it is capable of monitoring convection effects during solution polymerization.

2.2. Ion time of flight (ITOF)

The concept of time-of-flight is familiar to most scientists in the context of mass spectroscopy, which measures the time for ions to travel through a fixed distance in a vacuum with a uniform electric field. Thereby the chemical properties of ions can be identified by measuring the travelling time. Here, the same concept is introduced into polymeric materials or diluted polymer solutions.

Compared with the frequency dependent dielectric measurement, ion time-of-flight (ITOF) measurement is more like a dielectric measurement made at very low frequency (10^{-1} to 10^{-3} Hz). A square wave electric field is alternated with a time scale of several seconds to several minutes. The current change in each cycle is investigated to directly determine the mobility of the charge carriers of interest in a liquid dielectric material. It is an accurate and efficient method to separate the ion mobility from the dipolar effect on the conductivity of the materials.

The time-of-flight technique, coupled with the dielectric measurement of conductivity σ , allows one to determine separately changes in the number of charge carriers, along with changes in mobility of a charge carrier due to cure or temperature. It can help to characterize and monitor the advancement of a polymerization process and

the corresponding changes in chemical/physical properties. In particular, ITOF provides additional useful knowledge regarding the relationship of viscosity to changes in electrical and material properties throughout the reaction.^{52,53}

2.1.1 Background/Theories

Ion time-of-flight (ITOF) is a measure of the length of time an ion takes to travel across a fixed distance between two electrodes with a given potential. Starting from an equilibrium ion distribution (Figure 2.4a), the electrodes are oppositely charged (Figure 2.4b), and the attraction of unlike charges causes the anions to move towards the positively charged plate, while the cations migrate to the negative plate (Figure 2.4c).

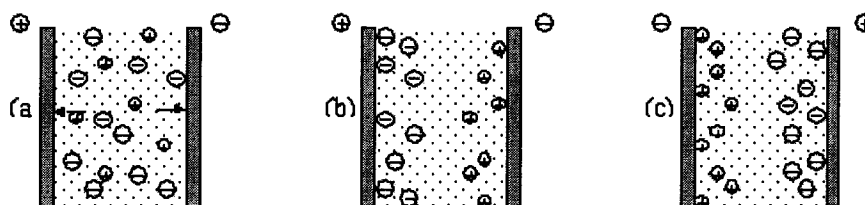


Figure 2.4. Ions transportation in electric fields

A square-wave voltage pulse is applied to the system for a fixed length of time.

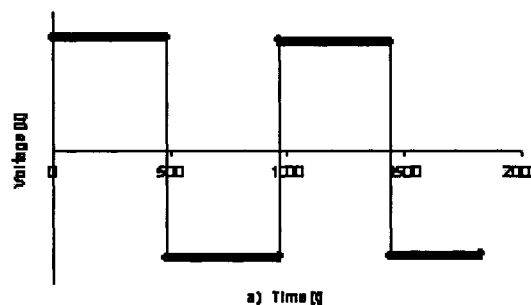


Figure 2.5. Square-wave voltage applied in ITOF measurement

At a particular time after the initial pulse, a peak is observed in the measured current, $I(t)$, in each subsequent pulse. This peak represents the point in time when the highest rate of ions is arriving at the electrode, resulting in a peak in the measured current, I .⁵⁴⁻⁵⁶

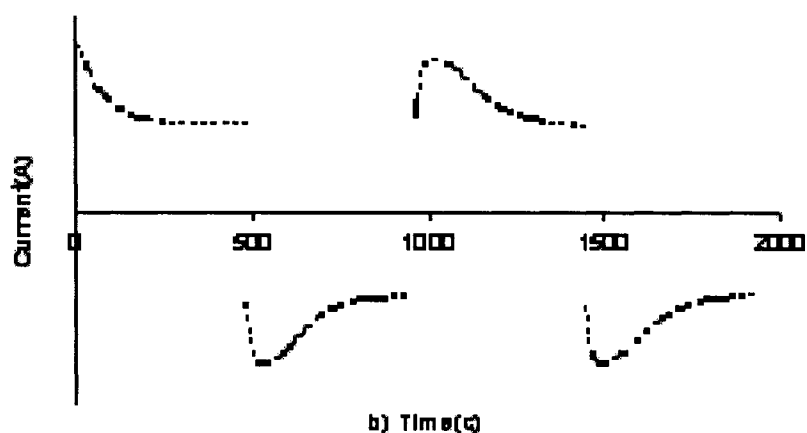


Figure 2.6. Current curve in ITOF measurement

Reversing the charges on the plates creates the pulse sequence, and the ions are then drawn to the opposite plate. Here (Figure 2.6) the measurement pulse sequence involved four sets of equal length pulses. The time-of-flight flight time occurs at the peak in the output current versus time after a reversal of voltage polarity. This time marks the time of maximum number of mobile species arriving at the electrodes and characterizes the ion transit time. These measurements are repeated while conditions within the experiment are changing. The ITOF is dependent on these changing variables including: changes in the viscosity of the medium due to a change in temperature or a chemical reaction, the measurement parameters such as the fixed distance between electrodes (sensor material and geometry), the possibility of a charge polarization effect on the

plates after a given time, the length of time allowed before the pulse is switched, and the magnitude of the applied voltage.

The effect of these variables on the ion mobility can be described mathematically. The ionic mobility, μ , is defined as the ratio of the velocity, v , and the magnitude of the electric field, E

$$\mu = \frac{v}{E} \quad (2-13)$$

Neglecting internal field effects, the electric field acting on the ions is:

$$E = \frac{V}{d} \quad (2-14)$$

where V is the applied voltage, and d is the distance between plates. We can substitute Equation (2-13) into Equation (2-14) to yield

$$v = \mu \times \frac{V}{d} \quad (2-15)$$

Substitution of $v = d/t$ gives

$$\mu \times \frac{V}{d} = \frac{d}{t} \quad (2-16)$$

Rearranging to solve for t gives us an expression for the ion mobility time of flight.

$$t = \frac{d^2}{\mu \times V} = ITOF \quad (2-17)$$

From this equation, we can see that ion mobility, time of flight, ITOF, is dependent upon the distance between the electrodes in the sensor, the mobility, and the applied voltage. Since mobility is observed experimentally to be inversely proportional to viscosity to a power a , where a is ≤ 1 , we can rewrite the above equation as

$$ITOF = K \frac{\eta^\alpha}{V} \quad (2-18)$$

where K is a constant.

From Equation (2-17), we also can get the charge carrier mean mobility:

$$\mu = \frac{d^2}{ITOF \times V} \quad (2-19)$$

The ionic conductivity of a material on a molecular level can be expressed as a sum of the product of the number of ions present and their respective average mobility:

$$\sigma = \sum N_i \times \mu \quad (2-20)$$

Combining the Equation (2-10), (2-19) and (2-20), we can calculate the concentration of charge carriers in the system.

$$N_i = \frac{\sigma \times V \times ITOF}{d^2} \quad (2-21)$$

In general, the ionic conductivity (σ) for a viscous system can be obtained with low frequency dielectric measurements as described in *Section 2.1.2.1* and is expressed with following equation:

$$\sigma(\text{ohm}^{-1}\text{cm}^{-1}) = \varepsilon_0 \omega \varepsilon_i'' \quad (2-22)$$

A combination of both measurement techniques isolates the number of charge carriers and their mobility. This allows significant improvement in monitoring changes in the state and structure of a material as it cures and is essential in systems where N_i cannot be assumed constant.

In the measurement, the voltage setting and sensor geometry are two important factors determining the reliability of the results.

In an ITOF measurement, the magnitude of the current is dictated by the charge collected on the electrode surface and the action of an electric double layer. To get a good result, we want to minimize any electrode double layer effects to monitor the current contribution of the ion movement in the solution. A low voltage setting (e.g., less than 10V for pure water with gold electrode) was applied in the ITOF measurements to prevent reactions and a double layer effect on the electrodes. The barrier voltage for electrode double layers varies greatly with each system and different electrode materials. Thus the voltage setting needs to be selected carefully to avoid reactions and double charge layers on electrodes in each system.

For the ion transport, three rate processes need to be considered to decide what is the process determining the current during the measurements:⁵⁷

1) Movement of electrons within the electrode, either to or from the interface

The movement of electrons through an electrode will usually be extremely fast since the materials from which the vast majority of electrodes are made will have been chosen because of their superior electronic conductivity. Gold, copper and stainless steel sensors are all used in our experiment for this reason. The inert metals, such as Au, Pd are the best sensor materials for ITOF measurements due to less likelihood of reactions on the electrode surface

2) Movement of electrons across the electrode/solution interface.

This step is usually very fast for a viscous liquid system.

3) Movement through the solution.

This movement is termed mass transport, and proceeds via three mechanisms: migration, convection and diffusion. ITOF technique is based on the charge migration

between electrodes, so we need to minimize the convection and diffusion effects. The large area parallel plate electrodes with small distance can decrease the convection effect for a low viscous system. As for a highly viscous system, the mass transportation rate is slow, so we need to minimize the distance between electrodes to get a fast response of the ITOF signal. Due to the high concentration of ions on the electrode surface, the diffusion effect is dominant when the voltage is reversed. In some circumstances, the diffusion effect is dominant so that the migration current peak (ITOF peak) is indiscernible due to the diffusion current (Figure 2.7). The ITOF technique is not useful for these situations.

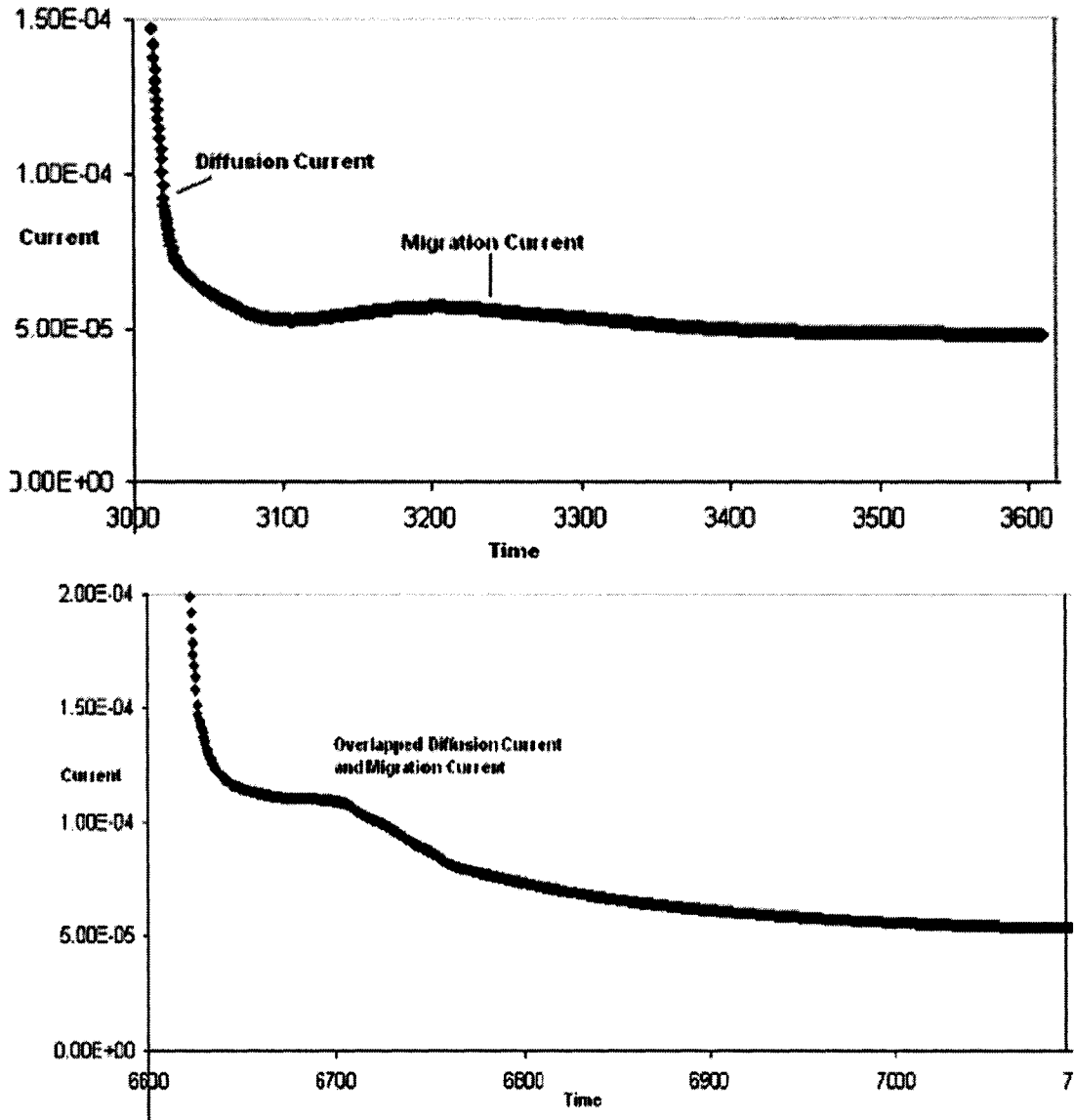


Figure 2.7. Diffusion and migration current curves

2.2.2 Equipment

- Voltage source

Keithley 237 high voltage source measurement unit is used to generate square-wave voltage pulse in the system for a fixed length of time

- *Sensors*

The distance between electrodes plays an important role in ITOF measurements. When a large electrode distance sensor is used, a longer pulse length and a higher voltage are needed to pull the ions to an ideal level for accurate ITOF measurement. As described in Equation (2-17), the distance d has a power two effect on the ITOF time. Considering the voltage requirement discussed above and the fast signal collecting, we need to choose a sensor with proper electrode distance to get optimized results for each system. The following sensors are used for ITOF measurement for different systems.

Glass sensor: consists of inter-digitated gold electrodes (30 microns in width) on an area of 2.0×1.1cm glass substrate with a spacing of 30 microns. Patented by Kranbuehl.^{58,59}

Index sensor: consists of inter-digitated nickle electrodes (200 microns in width) on an area of 2.5×1.5cm flexible polyimide substrate with a spacing of 115 microns. Purchased from Micromet, Inc.

Small air capacitor (160-110-1): has a large beryllium copper compressed rotor contact, and nickle-plated-steatite ($\text{Mg}_3\text{Si}_4\text{O}_{10}(\text{OH})_2$) metal parallel plates with a 432 microns spacing. Purchased from Cardwell Condenser Corp.

Large air capacitor: has the same design as small air capacitor and with a 762 microns air gap. Purchased from Cardwell Condenser Corp.

All these geometries produced no measurable current when tested alone in air, and were able to provide good measurements of the ion mobility for suitable systems.

- *Software*

TOF.EXE was developed for WINDOWS operation system to collect and analysis the data through GPIB interface.

- *Diagram*

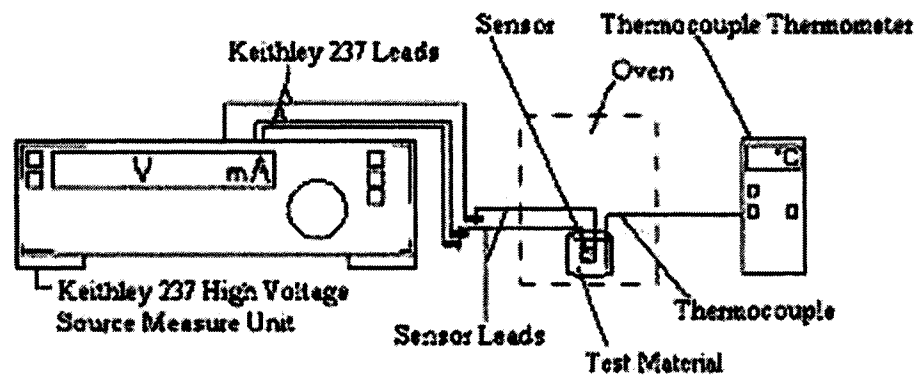


Figure 2.8. ITOF experimental equipment

REFERENCES

- (1) Kazilas, M. C.; Partridge, I. K. *Meas.Sci.Technol.* **2004**, *15*, L1.
- (2) Hilal, N. A.; Wickcted, J. P. *Proc. Okla. Acad. Sci.* **1991**, *71*, 21.
- (3) Kremer, F.; Schonhals, A. In *Broadband dielectric spectroscopy*, 1st ed.; Schonhals, A., Ed.; Springer-Verlag: New York, 2002; pp 35-57.
- (4) Lane, J. W.; Seferis, J. C.; Bachmann, M. A. *Polym, Eng. Sci.* **1986**, *26*, 346.
- (5) Nass, K. A.; Seferis, J. C. *Polym Eng Sci* **1989**, *29*, 315.
- (6) Dusi, M. R.; May, C.; Seferis, J. C. In *Chemrheology of thermosetting polymers*: CA, 1983; Vol. 227, p 301.
- (7) Bidstrup, S. A.; Sheppard, N. F., Jr.; Senturia, S. D. *Polym. Eng. Sci.* **1989**, *29*, 325.
- (8) Bidstrup, S. A.; Simpson, J. O. *J. Polym. Sci., Part B: Polym. Phys.* **1995**, *33*, 43.
- (9) Senturia, S. D.; Sheppard, N. F., Jr. *Adv. Polym. Sci.* **1986**, *80*, 1.
- (10) Kranbuehl, D.; Delos, S.; Yi, E.; Mayer, J.; Jarvie, T.; Winfree, W.; Hou, T. *Polym. Eng. Sci.* **1986**, *26*, 338.
- (11) Kranbuehl, D.; Delos, S.; Hoff, M.; Haverty, P.; Freeman, W.; Hoffman, R. D.; Godfrey, J. J. *Polym. Eng. Sci.* **1989**, *29*, 285.
- (12) Hoffman, R. D.; Godfrey, J. J.; Kranbuehl, D.; Weller, L.; Hoff, M. *J Reinforced Plast Compos* **1987**, *6*, 223.
- (13) Kranbuehl, D.; Haverty, P.; Hoff, M.; Hoffman, R. D. *Polym. Eng. Sci.* **1989**, *29*, 988.
- (14) Kranbuehl, D.; Eichinger, D.; Hamilton, T.; Clark, R. *Polym. Eng. Sci.* **1991**, *31*, 56.
- (15) Kranbuehl, D. *Plast Rubber Compos Process Appl* **1991**, *16*, 213.
- (16) Kranbuehl, D. *J. Non-Cryst. Solids* **1991**, *132*, 930.
- (17) Kranbuehl, D.; Kingsley, P.; Hart, S.; Hasko, G.; Dexter, B.; Loos, A. *Polym. Compos.* **1994**, *15*, 297.

- (18) Kranbuehl, D.; Hood, D.; Wang, Y.; Boiteux, G.; Stephan, F.; Mathieu, C.; Seytre, G.; Loos, A.; McRae, D. *Polym. Adv. Technol.* **1997**, *8*, 93.
- (19) Kranbuehl, D.; Delos, S.; Jue, P. K. *Polymer* **1986**, *27*, 11.
- (20) Kranbuehl, D.; Hoff, M.; Haverty, P.; Loos, A.; Freeman, W. In *Proceeding of the 33rd Int. SAMPE Symposium Ser.*, 1988; p 1276.
- (21) Kranbuehl, D. In *Dielectric Spectroscopy of polymeric materials*; Fitzgerald, J. R. a. J., Ed., 1997; pp 303-328.
- (22) Kranbuehl, D. In *Processing of Composites*; Loos, A., Ed., 2000; pp 137-157.
- (23) Kranbuehl, D.; Rogozinski, J. *Polym. Mater. Sci. Eng.* **1999**, *81*, 197.
- (24) Kranbuehl, D. In *J. Coating Tech.*, 2004; pp 48-55.
- (25) Mangion, M.; Johari, G. P. *J. Polym. Sci. Part B: Polym. Phys.* **1990**, *29*, 1127.
- (26) Parthum, M. G.; Johari, G. P. *Macromolecules* **1992**, *25*, 3254.
- (27) Zukas, W. *Macromolecules* **1992**, *26*, 2390.
- (28) Fitz, B. D.; Mijovic, J. *J. Phys. Chem.B* **2000**, *104*, 12215.
- (29) Andjelic, S.; Fitz, B. D.; Mijovic, J.; etc. *J. Polym. Sci. Part B: Polym. Phys.* **1996**, *34*, 379.
- (30) Vanbeek, L. H. K. *Prog. Dielectr.* **1967**, *7*, 69.
- (31) Sillers, R. W. *Inst. Wlwctr. Engrs.* **1937**, *80*, 378.
- (32) Poncet, S.; Pascault, J. P.; Sautereau, H.; Boiteux, G.; Seytre, G.; Rogozinski, J.; Kranbuehl, D. *polymer* **1999**, *40*, 6811.
- (33) Bonnet, A.; Pascault, J. P.; Sautereau, H.; Rogozinski, J.; Kranbuehl, D. *Macromolecules* **2000**, *33*, 3833.
- (34) Delides, C. G.; Hayward, D.; Pethrick, R. A.; Vatalis, A. S. *Eur. Polym. J.* **1992**, *28*, 505.
- (35) Delides, C. G.; Hayward, D.; Pethrick, R. A. *J. Appl. Polym. Sci.* **1993**, *47*, 2037.
- (36) Machinnon, A.; Jenkins, S.; McGrail, P.; Pethrick, R. A. *Macromolecules* **1992**, *25*, 3492.

- (37) Hasted, J. B. *Aqueous dielectrics*; Chapman&Hall: London, 1973.
- (38) Pethrick, R. A.; Crofton, D. *Polymer* **1981**, *22*, 1048.
- (39) Pethrick, R. A.; Maxwell, I. D. *J. Appl. Polym. Sci.* **1983**, *28*, 2363.
- (40) Pethrick, R. A.; Hollins, E. A.; etc. *Polym. Int.* **1996**, *39*, 275.
- (41) Hodge. *J. Non-crystl. Solids* **1994**, *169*, 211.
- (42) Mijovic, J. *Polym. Eng. Sci.* **1994**, *34*, 381.
- (43) Hutchinson, J. M. *Prog. Polym. Sci.* **1995**, *20*, 703.
- (44) Davis, W. J.; Pethrick, R. A. *Polymer* **1998**, *39*, 255.
- (45) Pethrick, R. A.; Davis, W. J. *Polym. Int.* **1998**, *47*, 65.
- (46) Cannon, L. A.; Pethrick, R. A. *Macromolecules* **1999**, *32*, 7617.
- (47) Cannon, L. A.; Hayward, D.; Pethrick, R. A. *Polymer* **2002**, *43*, 1223.
- (48) Warner, J. D.; Kranbuehl, D. E.; Thompson, D. W.; Espuche, E.; David, L. *Polymer Preprints (American Chemical Society, Division of Polymer Chemistry)* **2003**, *44*, 254.
- (49) Espuche, E.; David, L.; Afeld, J. L.; Compton, J. M.; Kranbuehl, D. E. *PMSE Preprints* **2005**, *92*, 58.
- (50) Kennedy, A. P.; Tadesse, S. *Ann. N.Y. Acad. Sci.* **2002**, *974*, 87.
- (51) Kennedy, A. P.; McLendon, J. *Book of Abstracts, 219th ACS National Meeting, San Francisco, CA, March 26-30, 2000* **2000**, POLY-623.
- (52) Warner, J.; Guo, J.; Khoshbin, M.; Raheem, S.; Kranbuehl, D. E.; Seytre, G.; Boiteux, G. *Polymer* **2003**, *44*, 3537.
- (53) Guo, Z.; Warner, J.; Christy, P.; Kranbuehl, D. E.; Boiteux, G.; Seytre, G. *Polymer* **2004**, *45*, 8825.
- (54) Friedrich, K.; Vinh-Tung, C.; Boiteux, G.; Seytre, G.; Ulanski, J. *J. Appl. Polym. Sci.* **1997**, *65*, 2529.
- (55) Friedrich, K.; Ulanski, J.; Boiteux, G.; Seytre, G. *IEEE Trena. Dielec. Elec.Insul.* **2001**, *8*, 572.

- (56) Ulanski, J.; Friedrich, K.; Boiteux, G.; Seytre, G. *J. Appl. Polym. Sci.* **1997**, *65*, 1143.
- (57) Monk, P. M. S. *Fundamentals of Electroanalytical Chemistry*; Wiley&Sons: New York, 2001.
- (58) Kranbuehl, D. E. In *U.S.*; (USA). Us, 1987; pp 7 pp. Division of U.S. Ser. No. 729,459.
- (59) Kranbuehl, D. E.; Fox, R. L. In *U.S.*; (Center for Innovative Technology, USA). Us, 1992; p 5 pp.

CHAPTER 3. APPLICATION OF ION MOBILITY TIME-OF-FLIGHT MEASUREMENT DURING AN EPOXY-AMINE REACTION

3.1. Introduction

3.1.1. Problem statement

The relationship of viscosity, electric properties and bonding structure to the changes of material properties during a reaction have been studied for many years using a variety of techniques including those of dynamic mechanical, dielectric relaxation and FTIR. The use of conductivity due to migration of charges to monitor the advancement of reaction has been widely reported¹⁻²⁵. In a majority of these published reports, the charge carriers in the reaction system are seldom identified. It is commonly assumed that a correlation should exist between the decrease in conductivity, and the increasing viscosity and/or extent of reaction. This is based on the assumption that the number of charge carriers in the polymer-forming system is constant. Unfortunately, this assumption is not correct in an epoxy/amine system where the number of OH groups and NH groups changes as the reaction advances. A method to measure the number of charge carriers directly during the reaction is desired.

Typically, the electrical conductivity, σ , is obtained through dielectric measurements using an *in-situ* micro-sensor and a multi-frequency impedance analyzer.

In general, at low viscosities and low frequencies, the ionic conductivity dominates the impedance of materials. The ionic conductivity of a polymerizing material on a molecular level is a sum of the product of the number of ions present and their mobility μ ($\sigma = \sum Ni * \mu_i$). A combination of measurement techniques that isolates both the number of carriers (Ni) and their mobility (μ_i) allows significant improvement in monitoring changes in the state and structure of a material as it cures. It is essential in those systems where the number of charge carriers cannot be assumed constant.

With the ion time-of-flight (ITOF) technique, coupled with the dielectric measurement of σ , it is possible to monitor the number of charge carriers (Ni) and their mobility (μ) separately²⁶ during polymerization of an epoxy such as a diglycidyl ether of bisphenol-A (DGEBA) /4,4'-methylene bis [3-chloro-2,6-diethylaniline] (MCDEA) reaction system. In an epoxy/amine reaction, the primary charge carrier source is proton transfer along with intermolecular hydrogen bonding²⁷⁻³⁰. The hydrogen bonding changes with the conversion of the monomers and the temperature. Both can cause changes in the number of the charge carriers in this system. The relationship between the changes in the number of charge carriers, their mobility and the properties and bonding structure changes of an epoxy material are discussed in this chapter. The results are compared with FTIR results reported previously³¹⁻³⁴.

3.1.2. Background for an epoxy-amine reaction and its conductivity

For an epoxy-amine reaction system, the ionic impurity presents a small contribution to the overall or apparent conductivity. The measured conductivity encompasses the contributions from both extrinsic and intrinsic mechanisms, which are

discussed in chapter 1.1. As a result of the interplay between extrinsic and intrinsic contributions to the overall conductivity during reaction³⁵, an increase in viscosity can be accompanied by an increase in the measured conductivity³⁶. The chemical bonds/structure changes during cure need to be described to understand these phenomena.

Normally, an epoxy-amine reaction proceeds according to the sequence shown in Figure 3.1.

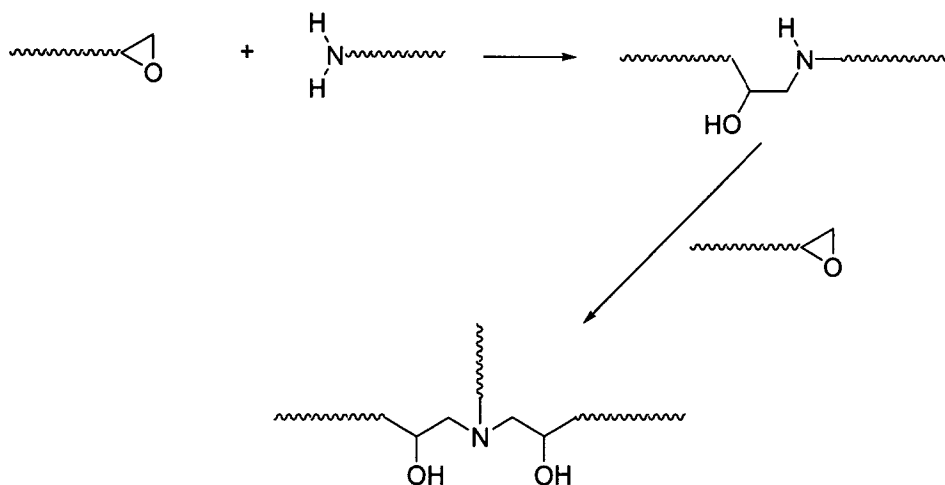
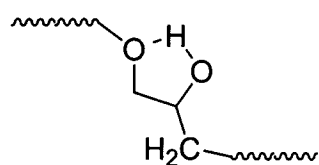


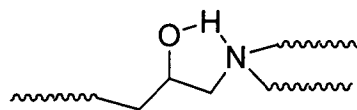
Figure 3.1. Chemical reaction for an epoxy amine system

As a result, many hydrogen-bonded species co-exist in amine-crosslinked epoxy network systems (Figure 3.2). Based on the bonding structure, they can be divided into categories: intramolecular and intermolecular hydrogen bonding. The ratio of the different types of hydrogen bonds in the system varies with temperature, curing degree as well as the type of epoxy and amine and they contribute differently to the overall conductivity of material.

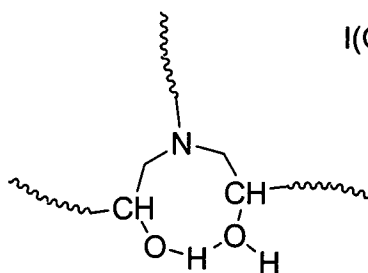
Intramolecular Hydrogen Bonds



I(OH----O)

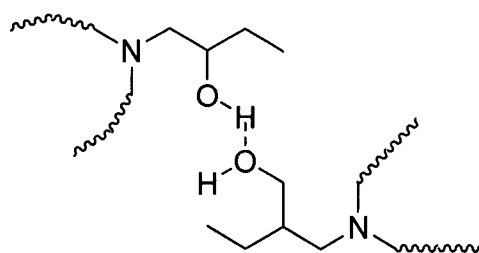


I(OH----N)

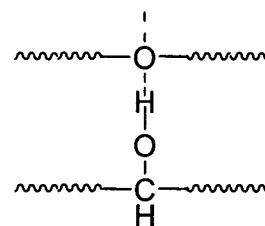


I(OH----OH)

Intermolecular Hydrogen Bonds



E(OH----OH)



E(OH----O)

Figure 3.2. Some types of hydrogen bonds in an epoxide-amine network

3.2. Experimental

3.2.1. Materials

Diglycidyl ether of Bisphenol-A (DGEBA) (Figure 3.3) with $n = 0.15$ received from Dow Chemical as LY556 is a relatively viscous epoxy at room temperature and readily polymerizes with the bi-functional amine 4,4'-methylene bis [3-chloro-2,6-diethylaniline] (MCDEA) (Figure 3.3) supplied by Air Products and labeled as LONZACURE.

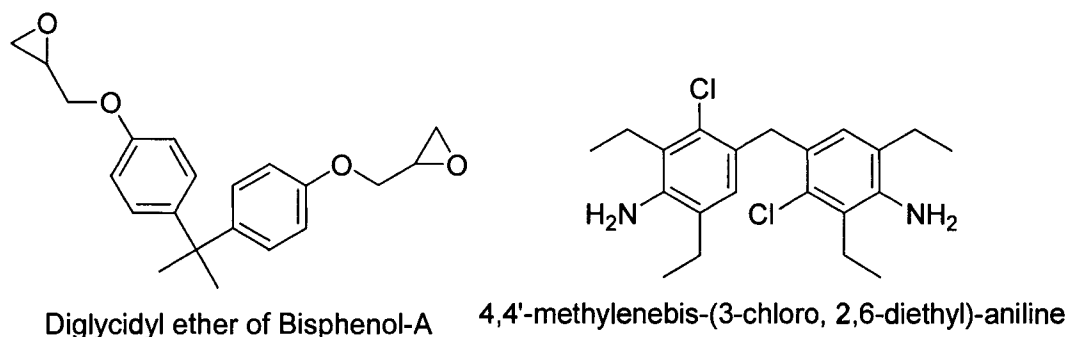


Figure 3.3. Chemical structure of the epoxy and amine

In an effort to verify the primary charge carrier in our system, the epoxy resin was loaded with additional chlorine ions (using sodium chloride from Aldrich, 99+% pure) to observe the conductivity change of the system.

3.2.2. ITOF measurement

A current/voltage source-measurement unit, Keithley 237, was used to control the voltage and to measure the output current. Data was stored with an IBM/PS2 computer and collected with software developed specifically for this application. Current

measurements were taken every 0.33 seconds and plotted versus time in seconds. The temperature was controlled by a Delta Design 9015 forced air oven. A thermocouple monitored the temperature of the sample during the time of the measurements.

Two commercial products index sensor (036S) and small air capacitor (160-110-1) were chosen as *in-situ* sensors.

3.2.3. Rheology

A TA instrument AR 1000 rheometer was used to measure the viscosity changes and detect the gelation during the isothermal cure: 40mm diameter aluminum parallel plates were used in measurements, housed inside an environmental test chamber. The complex viscosity (η) was measured at regular intervals, from 0.1 Hz to 1 kHz where it was frequency independent, at zero normal force. The gel point was determined by the method of H. Winter³⁷⁻³⁹, from the time at which $\tan \delta$ became independent of frequency. This is the point in time when the values of $\tan \delta$ measured at different frequencies become equal and crossover each other.

3.2.4. Dielectric impedance measurement

The liquid epoxy-amine mixture was introduced into a cell made of two glass plates separated by a 4mm-rubber gasket. An index sensor with inter-digitized copper electrodes on a flexible polyimide substrate was enclosed in the cell and electrodes were linked to a HP 4192A-impedance analyzer by wires to measure the conductance and subsequent capacitance of the materials over a range of temperature and frequency.

The enclosed cell was placed in an isothermal oven during the experiment. The dielectric permittivity and dielectric loss were measured at 10 frequencies in the range from 50Hz to 500KHz. The measurement was taken every 2 seconds across all these

frequencies. A computer acquired the dielectric data automatically, the frequency dependent of data were used to create plots of conductance vs. time.

3.2.5. Reaction kinetics

A TA 2920 modulated DSC was used for the thermokinetic studies. The thermal analysis consisted of an isothermal DSC run to determine Q_i at that temperature and then followed by a dynamic ramp to a suitable high temperature to determine the residual heat of polymerization Q_r for all the samples. The extent of the reaction at a given time was calculated from:

$$\alpha(t) = Q_t / (Q_r + Q_i) \quad (3-1)$$

where $\alpha(t)$ is the extent of the reaction, and Q_t is the heat produced by the reaction at the time t .

3.3. Results and discussion

3.3.1. Kinetics and gelation

Figure 3.4 shows the extent of conversions of reactant as a function of time at three different temperatures. The extent of reaction is determined by the reaction heat measured by MDSC. By increasing the cure temperature, the reactive species have more energy to break the diffusion limitation and reaction energy barrier. Thus, the reaction rate and the total conversion increase with the cure temperature.

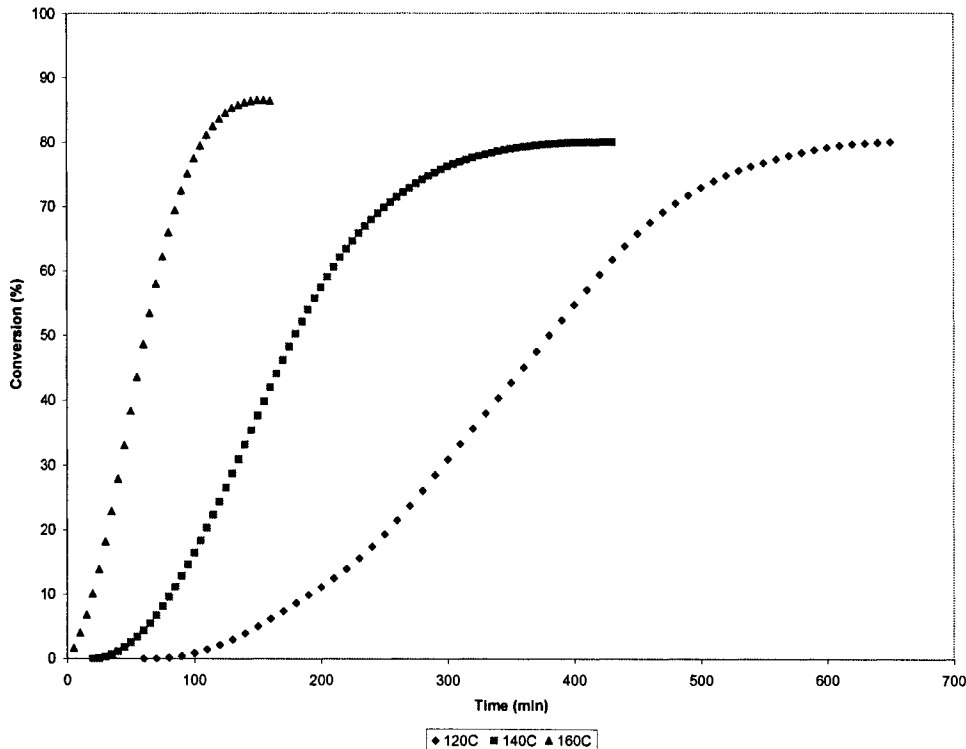


Figure 3.4. Conversion during isothermal cure at three different temperatures

Figure 3.5a-c shows the viscosity change during the reaction at three different temperatures. The gel time is determined from the $\tan\delta$ crossover point where $\tan\delta$ is frequency independent (Figure 3.6a-c). Gel times for curing at three different temperatures are reported in Table 3.1. As the temperature increases, the gel time decreases significantly. The gel time is characterized by a sharp increase in viscosity and signals the existence of a network structure in the material. This point is particularly relevant for ion-time-of-flight experiments since after the gel point, viscosity builds quickly, and therefore the ITOF measurements after the gel point become much longer, less sharp and increasingly more difficult to characterize.

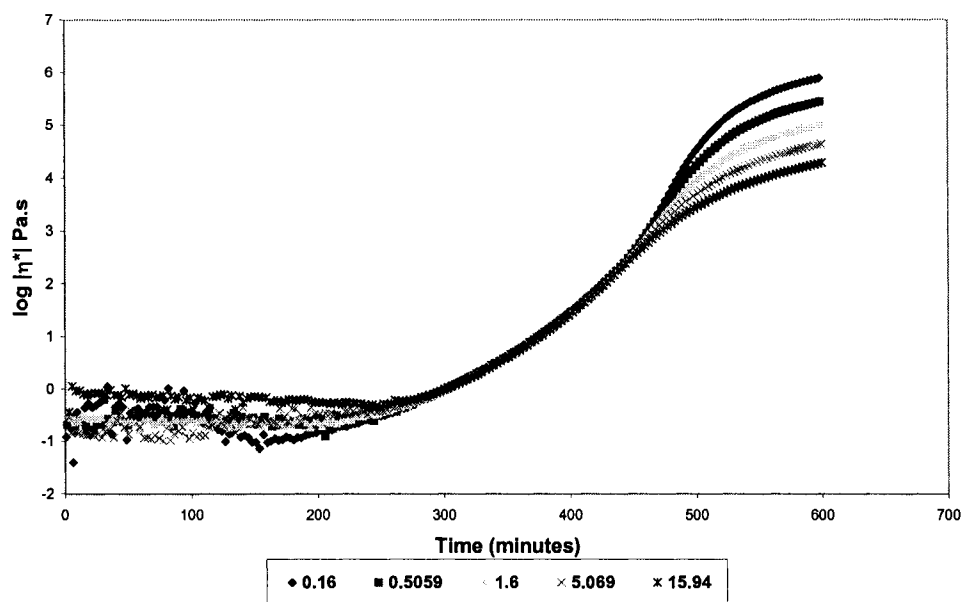


Figure 3.5a. Viscosity change during 120⁰C isothermal cure

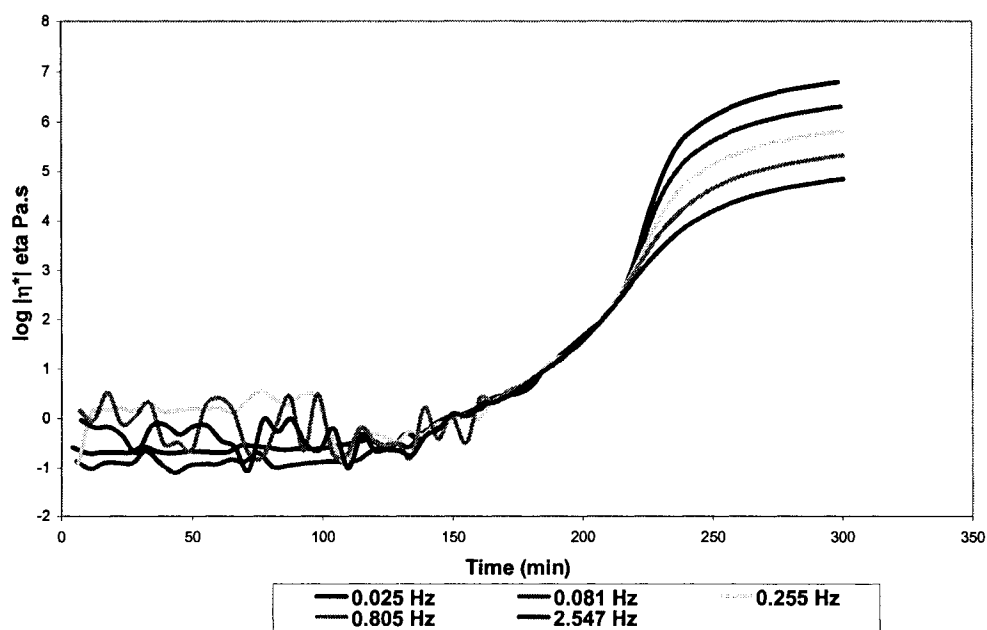


Figure 3.5b. Viscosity change during 140⁰C isothermal cure

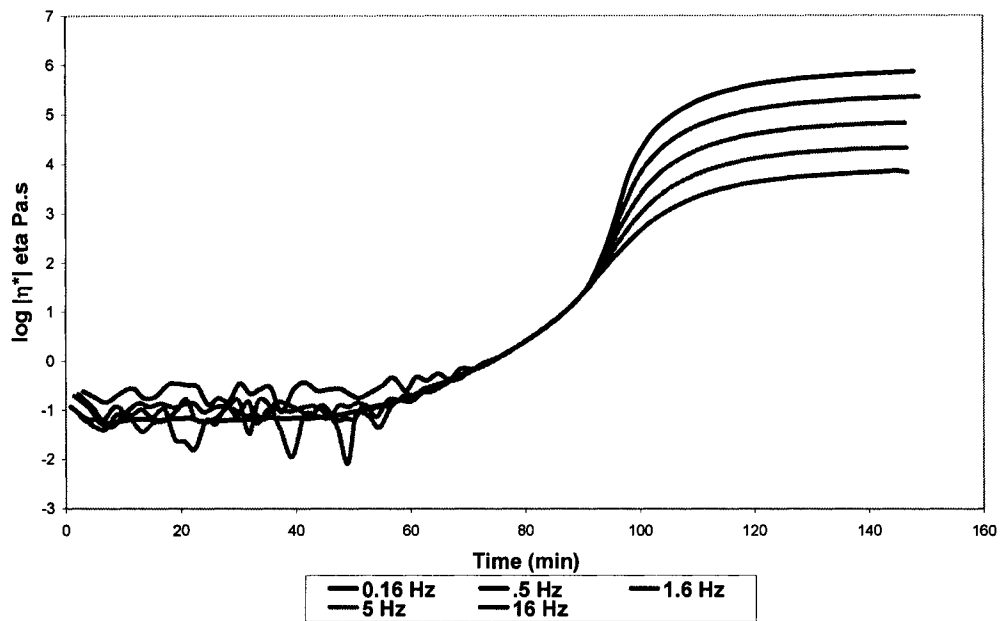


Figure 3.5c. Viscosity change during 140°C isothermal cure

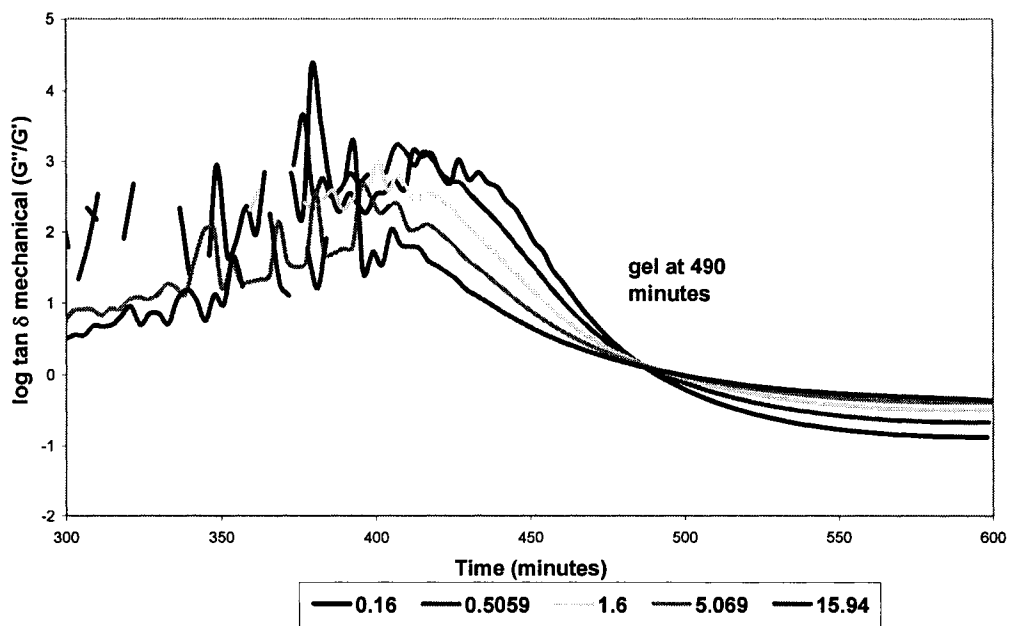


Figure 3.6a. $\tan \delta$ changes at different frequencies during 120°C cure

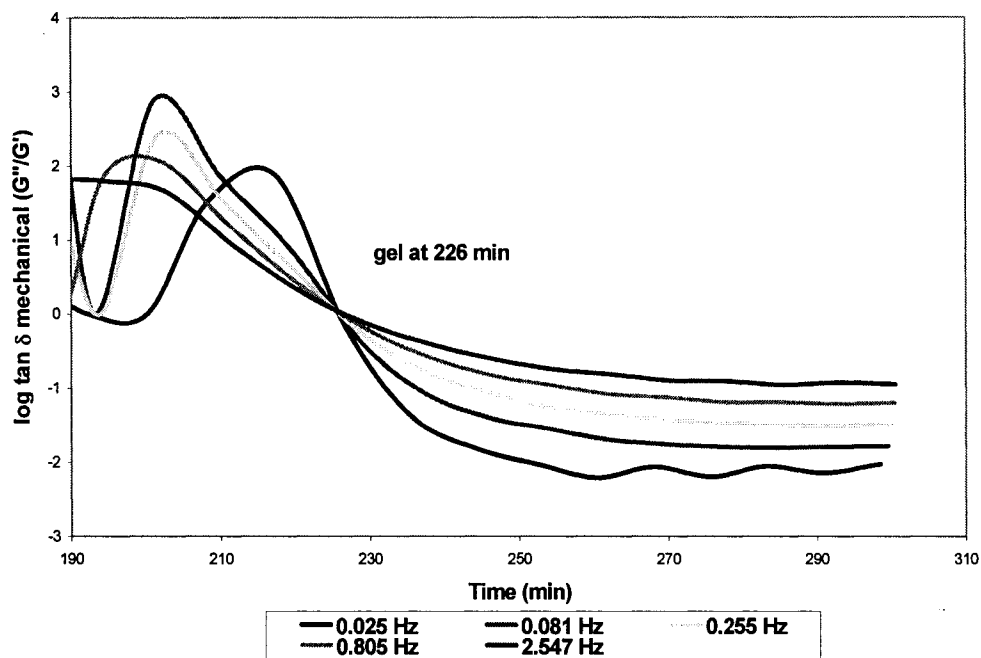


Figure 3.6b. $\tan \delta$ changes at different frequencies during 140°C cure

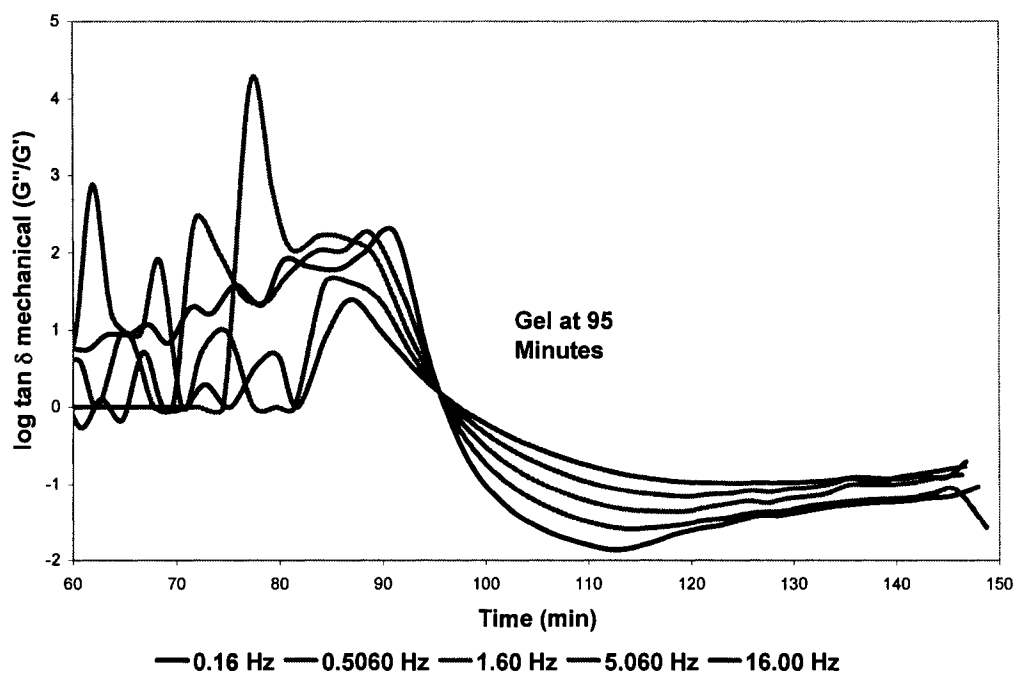


Figure 3.6c. $\tan \delta$ changes at different frequencies during 160°C cure

Table 3.1. Gel times of the epoxy-amine during isothermal cure

Isothermal Temp (°C)	gel time (min)
120	490
140	226
160	95

3.3.2. Source of charge carriers

Based on work by Bidstrup and Simpson²⁰, the source of the charge carriers is reported to be the DGEBA resin, and not the amine. A primary charge carrier is hydrogen ions due to proton transfer. Chlorine ions are also another potential source of charge transfer left over from the synthesis of DGEBA from epichlorohydrin. In an effort to verify the identity of the primary charge carrier in our system, the epoxy resin was loaded with additional chlorine ions to a concentration of approximately 3000 ppm (by addition of NaCl to the neat resin). According to supplier standards, the DGEBA epoxy resin is highly pure and contains a nominal amount of chlorine ions, at less than 300 ppm. The addition of the salt did not increase the conductivity of the system within the experimental error. This indicates that the chlorine ions are not the source of charge transport in the system.

The conductivities of pure MCDEA and the DGEBA/MCDEA mixture were measured. The results showed that the MCDEA has low conductivity and can be ignored compared with the conductivity of DGEBA. When MCDEA is mixed with DGEBA, it dilutes the concentration of the proton charge carriers resulting from [OH] groups in the $n=0.15$ epoxy resin in the system, and causes a decrease in the conductivity. The

conductivity decrease is proportional to the weight fraction of the MCDEA added into DGEBA.

3.3.3. Dielectric relaxation

Figure 3.7a-c shows the dielectric spectrum for the epoxy/amine cured at different temperatures. At high frequencies, the rotational mobility of bound charge dipole orientation contributes to the conductivity of the material and in particular is monitoring the α -relaxation vitrification process. According to Equation (2-4), the conductivity of the material is dominated by ion mobility at the lowest frequencies,

The conductivity drop is due in part to the decrease of ion mobility μ which is caused by the increase of the viscosity of the resin, and also to the possibility of changes in the number or concentration of mobile charge carriers N_i , which can be determined by the Equation (2-14).

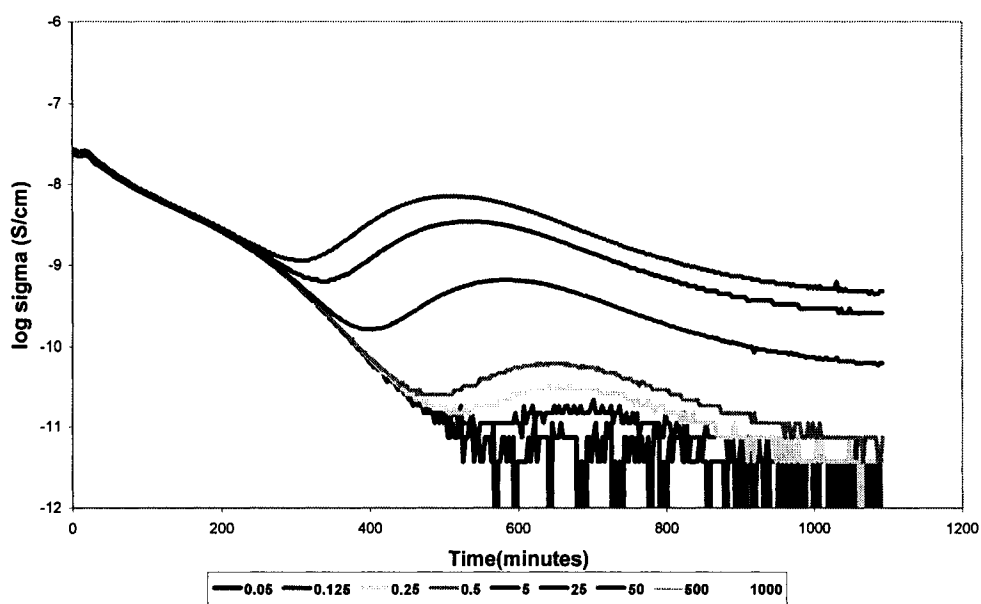


Figure 3.7a. Dielectric loss change at different frequencies during 120°C cure

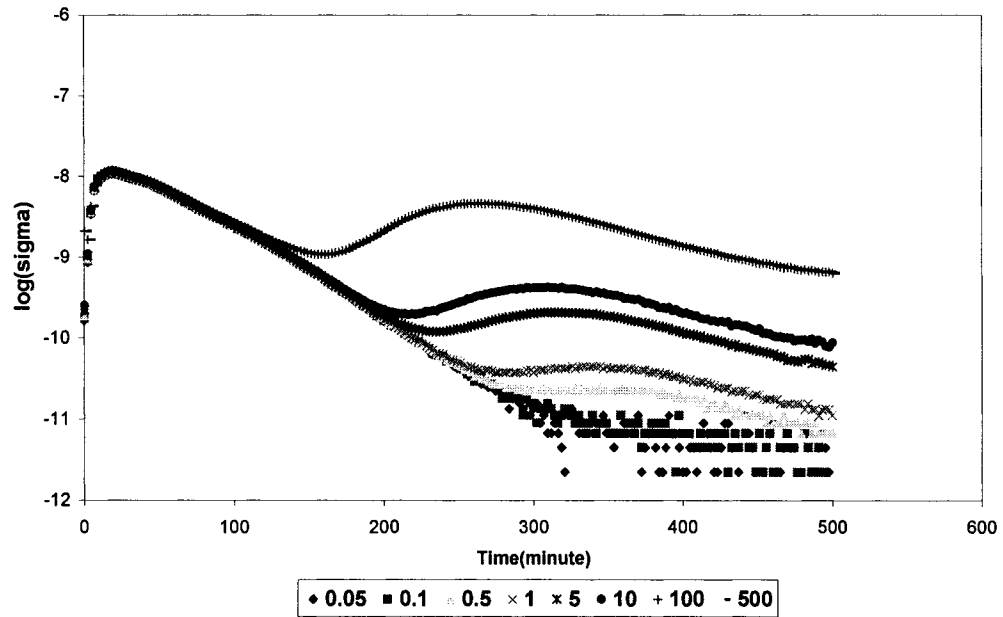


Figure 3.7b. Dielectric loss change at different frequencies during 140⁰C cure

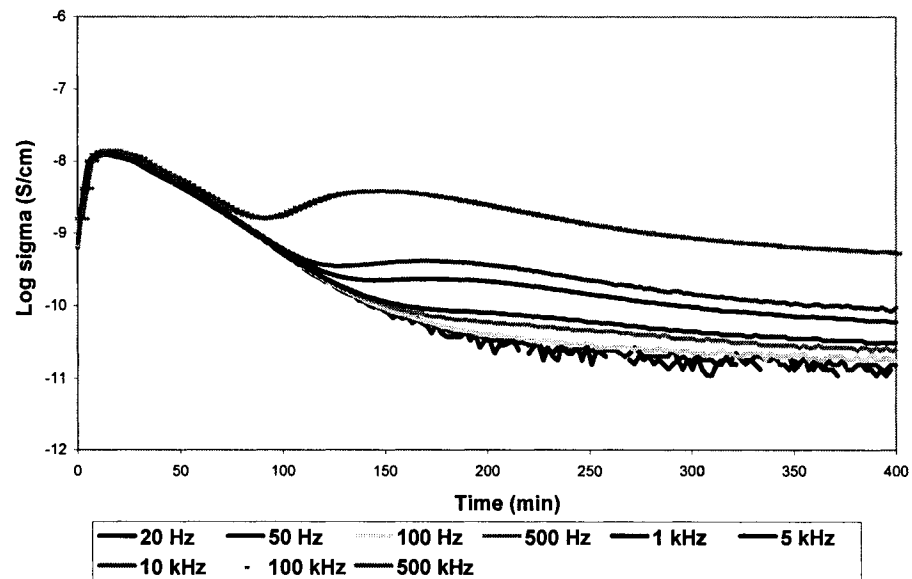


Figure 3.7c. Dielectric loss change at different frequencies during 160⁰C cure

3.3.4. Ion mobility measurement

3.3.4.1. Pulse length and voltage

According to the Equation (2-12), the product of ITOF and voltage is the quantity which monitors the ion mobility μ , for a fixed distance d between the plates of the measurement capacitor. The pulse lengths, together with magnitude of the applied voltage are two critical parameters to obtain good ITOF data. If the pulse length is too small and/or the voltage is too weak, ions migrate only partially to the opposite plate. That is, the major concentration of charge is between the two plates and not at the electrode surfaces. When the voltage is reversed on the electrodes, the shorter distance for the major concentration of ions to travel produces a smaller value for the ITOF. On the other hand, if the voltage is too strong, and/or the pulse length is too long, a polarizing and discharging process at the electrode can be created⁴⁰⁻⁴². When the voltage is reversed on the electrodes, an additional time is needed to reverse this excess effect at the electrodes and pull the ions from plates. As a result, one observes a longer than expected ITOF.

In order to determine the proper pulse length and voltage, the voltage applied to the plates is alternated from low to high during the cure. The experimental data which fit the relationship of pulse length and voltage as described by Equation (2-10) are used.

3.3.4.2. Geometry

As the system polymerizes, the mobility of the charge carriers drops as mobility is hindered by the developing thermosetting network structure. At a high curing temperature,

the viscosity increases in a relatively short period of time. The viscosity, which is related directly to the mobility, causes the time it takes for an ion to cross the distance between electrodes to increase. Consequently, single sensor geometry was unable to monitor the ions' progress throughout the duration of the curing reaction. Early in the cure, when the material is relatively fluid and mobility high, a larger spaced sensor is appropriate to measure the ITOF. However, the same sensor will fail to accurately measure the ITOF at a later time in the cure, as a shorter distance is necessary to allow an accurate measure of ITOF. Voltages were increased accordingly to compensate for the loss of mobility, but increasing the voltage alone wasn't enough to accommodate the decreasing mobility. The distance between electrodes, or d , is related to mobility by a squared factor and is therefore a more significant control of the mobility than voltage alone. The overlap for these two sensors was checked. According to Equation (2-10), no matter which sensor was used, the ion mobility was the same in the overlapping region. This is an additional check of the reliability of the ITOF data. Figure 3.8 shows the first 150 minutes of cure at 140°C as it is monitored by the small capacitor geometry, followed by the smaller spacing of the idex sensor for the remainder of the cure. It is interesting to note that at the point of gel (for example, 226 minutes at 140°C), there is no change in the gradual decrease in mobility with reaction advancement. This provides further evidence that dielectric measurements do not detect gel.

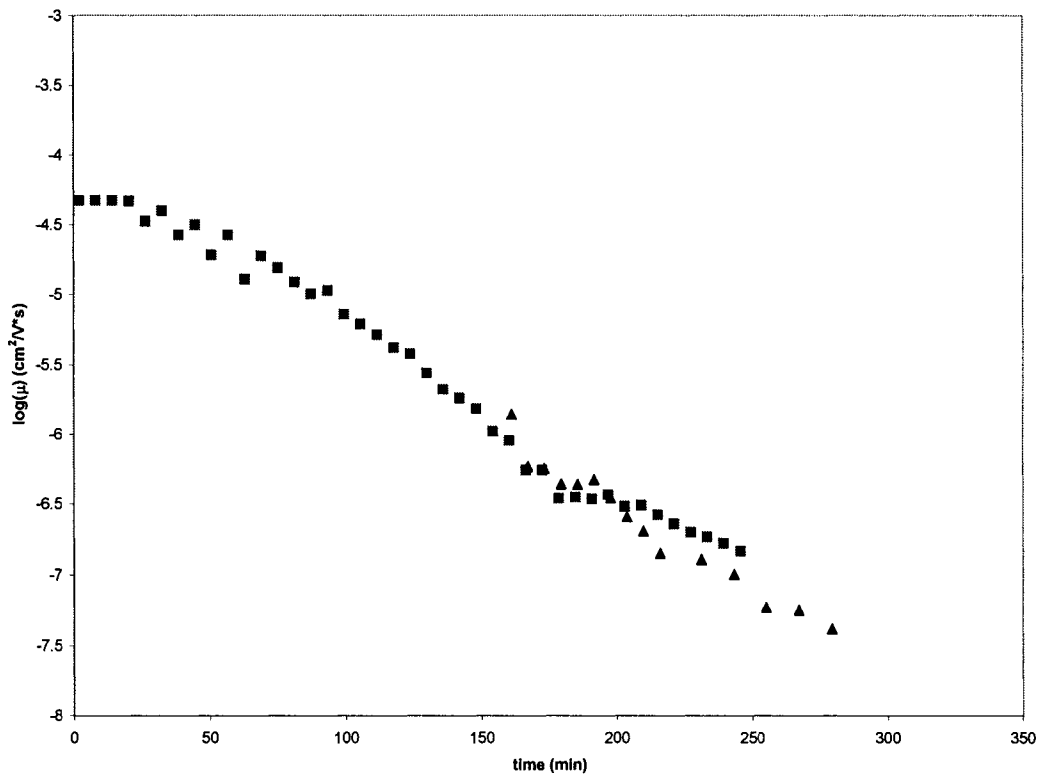


Figure 3.8. MCDEA/DGEBA isothermal cure at 140 °C: ion mobility $\log(\mu)$ ($d^2/TOF \cdot V$) against the reaction time (■) small capacitor; (▲) index sensor

3.3.4.3. Temperature effect on ion mobility and the number of charge carriers for an unreacted epoxy/amine system

Figure 3.9 shows the product of the ion mobility μ and the viscosity η changes 20% when the temperature ramped from 60 °C to 120 °C for the unreacted, non-curing epoxy/amine system. The relation between μ and η is approximately:

$$\mu \propto 1/\eta \quad (3-2)$$

Substitution of μ in Equation (2-13) gives the following expression:

$$Ni \propto \eta^* \sigma \quad (3-3)$$

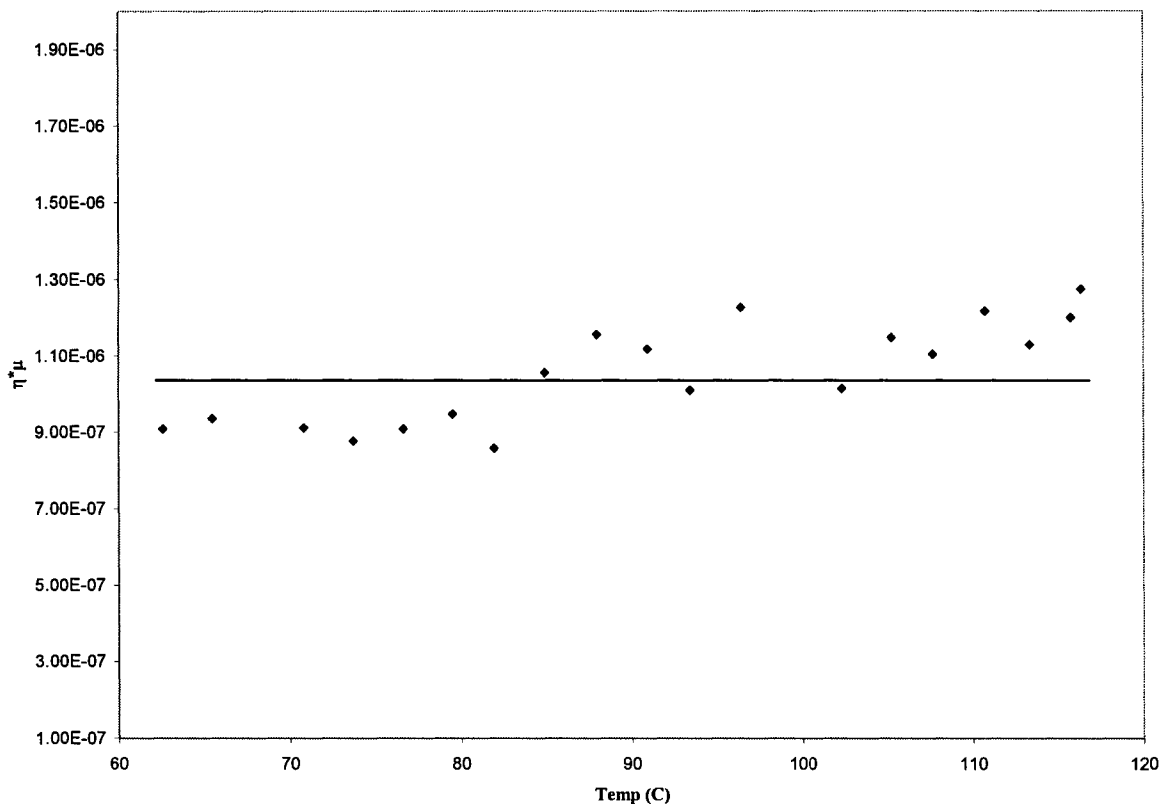


Figure 3.9. The product of the ion mobility (μ) and the viscosity (η) against the temperature for the unreacted DGEBA/MCDEA mixture

Figure 3.10 indicates the change in the charge carrier concentration with temperature for this unreacted epoxy /amine system based on Equation (3-3).

A more direct method is to use the ITOF measurement and Equation (2-21). Also seen in Figure 3.10, the ITOF measurement shows that there is a decrease of the charge carrier concentration when the temperature goes up. It is interesting that both methods for calculating the number of charge carriers indicate the same decrease in N_i with temperature for the unreacted system. The absolute numbers can be obtained only by Equation (2-21) and ITOF method.

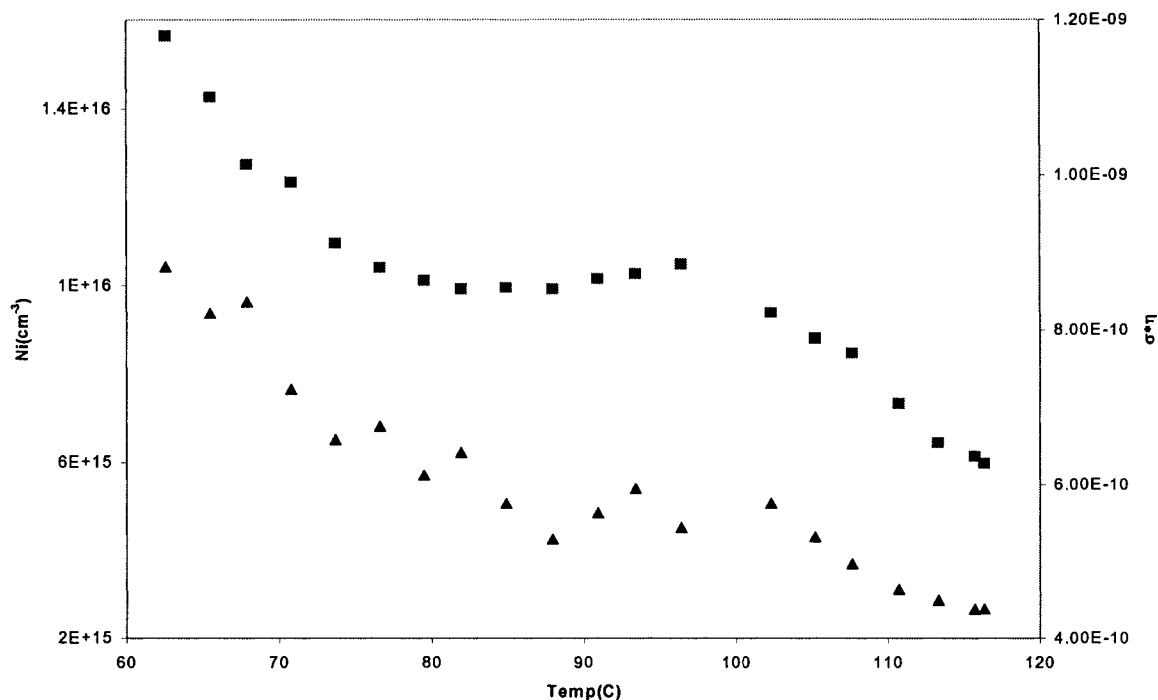


Figure 3.10. Unreacted DGEBA/MCDEA heated from 60 °C to 120 °C: (\blacktriangle) charge carriers concentration calculated from ITOF (\blacksquare) the product of conductivity and viscosity

The varying change in the number of charge carriers with temperature supports a mechanism of charge transportation in this system by the proton transfer involving long range intermolecular hydrogen bonding bridges as previously reported³¹. This temperature effect on hydrogen bonding was also shown in earlier FTIR studies of epoxy/amine kinetics. These studies show that long-range hydrogen bonding occurs at low temperatures, and that this type of hydrogen bonding decreases as the temperature goes up³³. Both results are consisted with our experiment results.

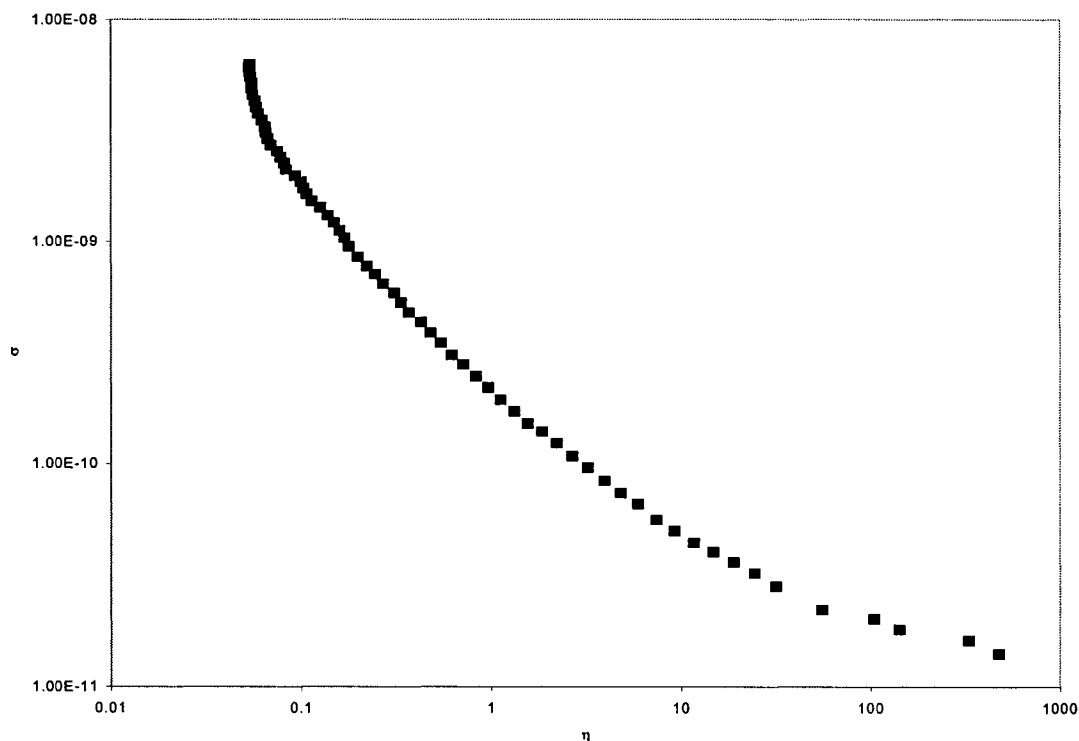


Figure 3.11. Conductivity versus viscosity during the reaction at 120 °C

3.3.4.4 Viscosity dependence of conductance during the reaction

Figure 3.11 shows the conductivity dependence versus the viscosity during the reaction. The conductivity drops faster in the low viscosity region than in the high viscosity region. The viscosity (η) plot (Figure 3.5a) shows that after 200 minutes ($\alpha = 0.2$) the structure build-up causes the viscosity to begin to increase rapidly. A corresponding rapid decrease of conductivity is not observed in Figure 3.7a. During the reaction, the changes in structure affects the conductivity and viscosity of the material at a different rate. There is not an inverse linear relation between the viscosity and the conductivity.

3.3.4.5 Ion mobility, charge carrier concentration changes during the reaction

Figure 3.12a shows the relationship of mobility (μ) and ionic conductivity (σ) during cure at 120 °C. Both decrease, as anticipated by the knowledge that the epoxy is becoming increasingly more viscous and crosslinked as it cures. Figure 3.12a also shows that the number of charge carriers changes little in the early stages of the reaction and begins to decrease after it has reacted for 200 minutes when the conversion α equals 0.20.

This decrease is observed at all three cure temperatures, as seen in Figures 3.12b for 140°C and 3.12c for 160°C. The decrease in the number of charge carriers is observed after 170 minutes ($\alpha = 0.30$) for 140°C and 90 minutes ($\alpha = 0.45$) 160°C. Due to the sensitivity of the HP 4195A impedance analyzer, it is difficult to measure the conductivity lower than 10^{-11} S/cm. Hence, measurements are no longer made at this point.

The initial epoxy/amine reaction produces hydroxyl groups, which have the potential to form more hydrogen bonds in the material^{43,44}. This initial increase in hydroxyl groups does not increase the conductivity. At a later degree of curing, the number of charge carrier species actually starts to decrease. As described in section 3.1.2, the hydrogen bonds in the epoxy/amine system can be divided into two categories: one can be described as intramolecular hydrogen bonding, the other as intermolecular hydrogen bonding. Only the intermolecular hydrogen bonding contributes to the long-range hydrogen bonding which affects the number of charge carriers as described in Equation (2-13), which result in conduction in the system.

During the reaction, the intra-molecular hydrogen bonds varies almost proportionally with the amount of hydroxyl groups, but the number of intermolecular hydrogen bonds varies as the conversion increases, chain branching increases and the polymer chain motions become more restricted³². This makes the formation of long range hydrogen bridges more difficult. Thus, the number of charge carriers varies as in Figure 3.12a most clearly, but also in Figure 3.12b and 3.12c.

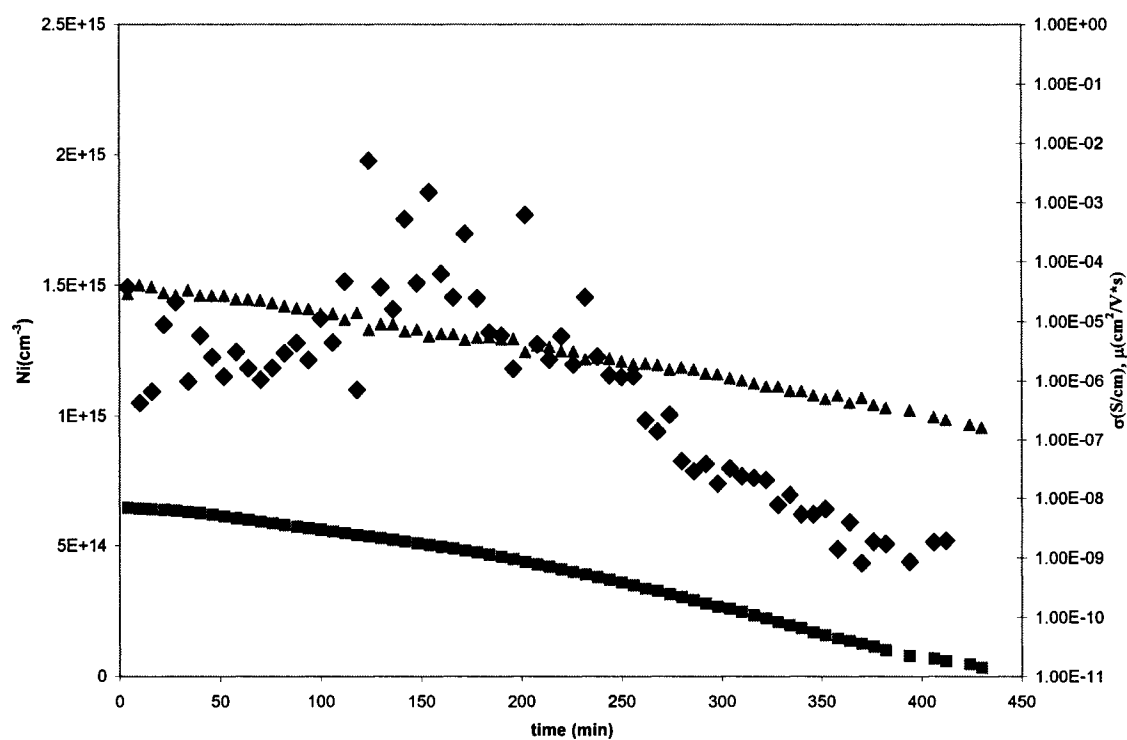


Figure 3.12a. Number of Charge Carriers (♦), Conductivity (■) and ion mobility (▲) changes for DGEBA/MCDEA isothermal at 120C

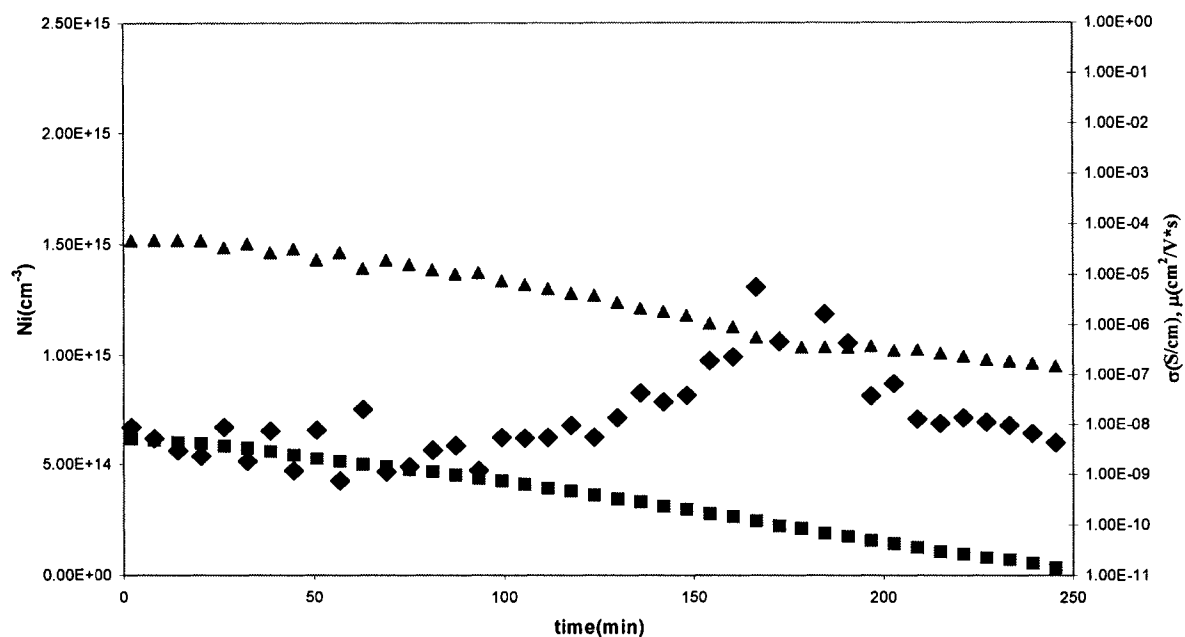


Figure 3.12b. Number of Charge Carriers (♦), Conductivity (■) and ion mobility (▲) changes for DGEBA/MCDEA isothermal at 140C

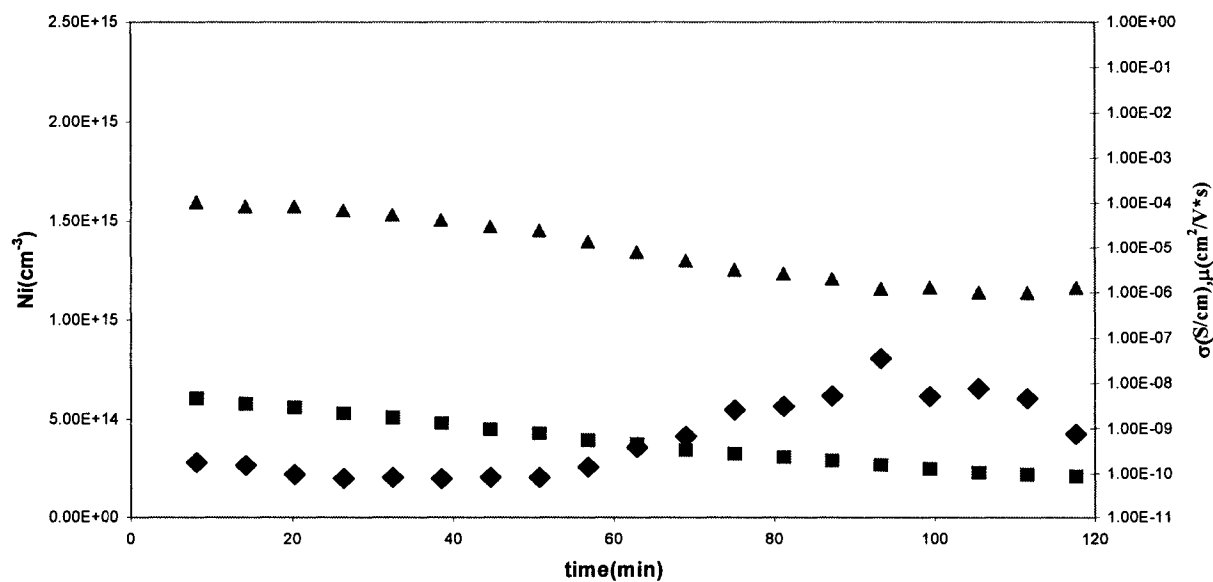


Figure 3.12b. Number of Charge Carriers (♦), Conductivity (■) and ion mobility (▲) changes for DGEBA/MCDEA isothermal at 140C

3.3.4.6. *A comparison between an unreacted and a reacted system*

Here, we would compare the relationships of conductivity (σ), viscosity (η), mobility (μ), and number (N_i) of mobile charge carriers in an unreacted epoxy system to similar viscosity conditions during a polymerization as the crosslinking system approaches gel. Figure 3.13 is a plot of conductivity versus the viscosity during a temperature ramp for the unreacted epoxy amine resin and during cure over a similar range in viscosities of 1 to 10,000 Pa.s. During the period of the reaction there is a large buildup in the crosslink density as the reaction approaches the gel point at 20,000 Pa.s. The gel time was determined from the frequency independence of $\tan\delta$.

From Figure 3.13, the slope of the $\log \sigma$ versus $\log \eta$ data for the unreacted epoxy-amine system is -0.86 and for the reacting epoxy-amine system as it approaches gel is -0.42 . These two differing slopes reflect the often observed changing power law dependence of conductivity on viscosity. Thus, σ can only be used to quantitatively monitor viscosity if a calibration curve has been previously established for that particular epoxy-amine system.

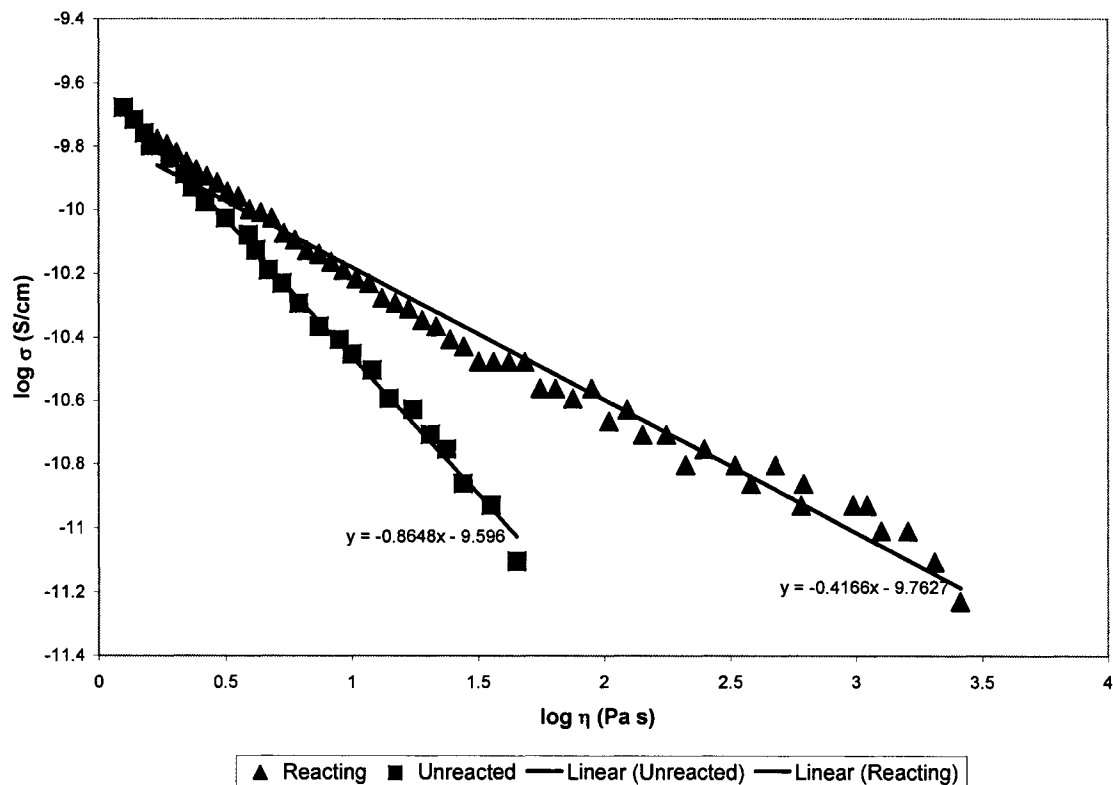


Figure 3.13. The change in conductivity for the unreacted epoxy amine system versus viscosity during a temperature ramp and of the conductivity versus viscosity during polymerization as the reaction approaches gel

Figure 3.14 is a plot of the mobility as determined by ion-time-of-flight measurements for these two differing structures at similar viscosity. The relationship of mobility to viscosity of a monomer mixture of epoxy and amine molecules is compared to that during the buildup in crosslink density as the network structure approaches gel.

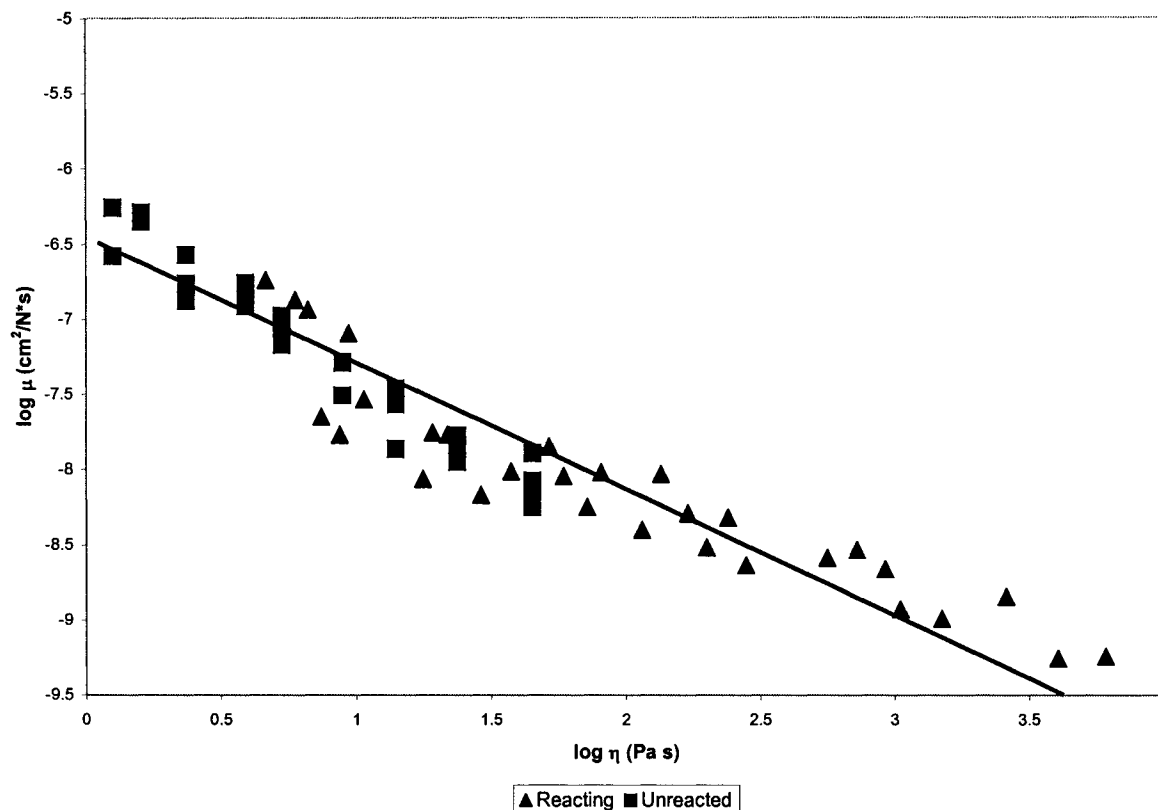


Figure 3.14. The ion mobility measured by ion time of flight versus viscosity for the unreacted epoxy amine system and during polymerization as the system approaches gel over the same range of viscosities as in Figure 3.13

From Figure 3.14 it is clear that the mobility of the ions does track the viscosity with a similar dependence during the buildup in crosslink density as it does in the monomer state. The slope of the $\log(\mu)$ versus $\log(\eta)$ in Figure 3 is -0.84 in close agreement with the slope of conductivity versus viscosity of -0.86 for the unreacted system. Thus, the mobility does track the viscosity when the system consists of small molecules and when it exists as a crosslinked structure. And the power law relationship of mobility to viscosity remains in the generally observed range of -0.8 to -1.0 for small molecules.

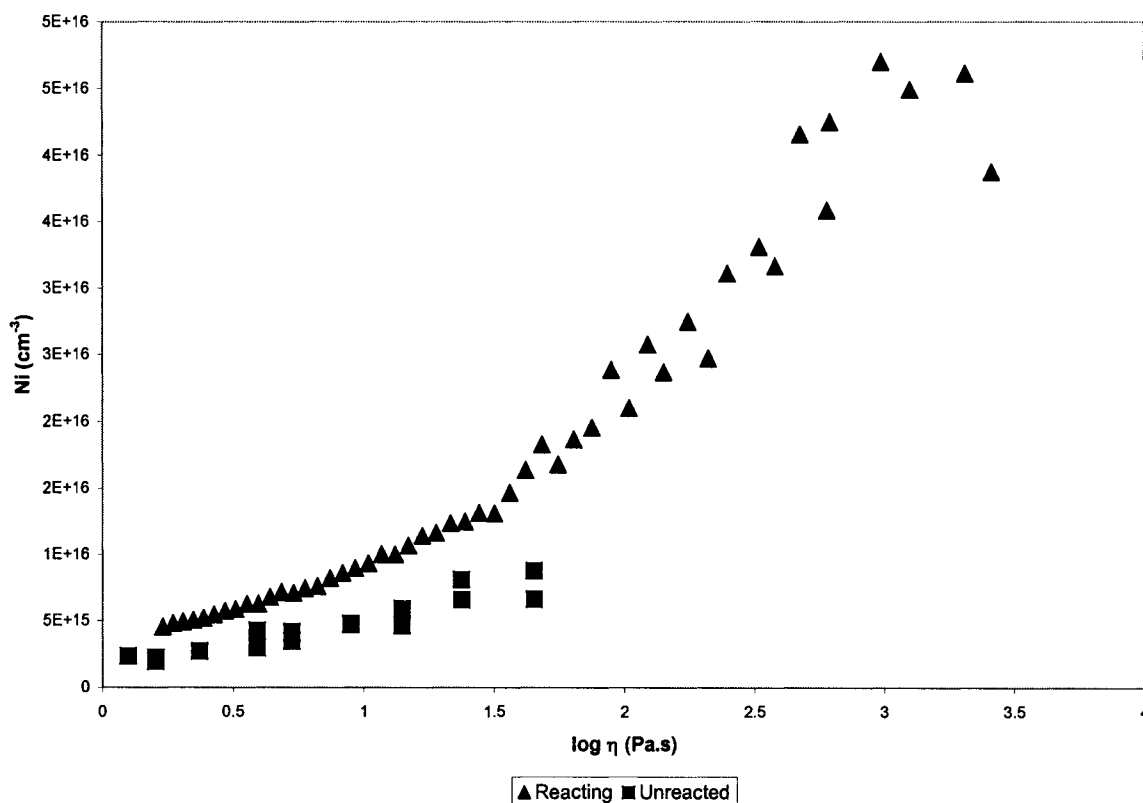


Figure 3.15. The change in the concentration of mobile charge versus viscosity in the unreacted epoxy amine and during the approach to gel in the reacting system

Figure 3.15 is a plot of the number of charge carriers, assuming one unit of charge equivalent to an electron versus viscosity for the two structures. Over the range of 1 to 10,000 Pa.s in the curing system the number of mobile ions experiences a significant increase. Three factors can contribute to this increase; first, an increase in the number of hydrogen bonding groups; second, closer proximity and less mobility of O-H groups relative to each other; and third, a decrease in the volume of the system with reaction advancement. All three of these factors can increase the rate of proton exchange. The first factor is believed to be the dominant term. For the unreacted system, the higher

viscosity shows a small increase in N_i , probably due to the increasing density with decreasing temperature.

3.4. Summary

The ITOF technique, coupled with dielectric measurements of conductivity can be used to monitor separately the number of charge carriers and their mobility. In a DGEBA/MCDEA system, the intermolecular hydrogen bonding is the primary source of the charge carriers. The change in the charge carrier concentration monitored by ITOF with conductivity characterizes the changes in the bonding structure with temperature and reaction advancement. During the reaction, the formation of long range hydrogen bridges becomes more difficult. Thus, the number of charge carriers is dependent on both an increase in the number of hydroxyl groups and that the long-range hydrogen bridge formation becomes more difficult with increasing conversion.

The mobility, not the conductivity, is observed to correlate with the changing viscosity *both* with changes in temperature and buildup in network structure. The generally expected inverse power dependence relating mobility to viscosity of -0.8 to -1.0 is observed and is near -0.84 for this DGEBA-MCDEA epoxy-amine system.

There is a significant increase in the number of mobile charge carriers during the buildup in the crosslink density. Hence the conductivity changes during the epoxy amine polymerization are due to both an increase in viscosity which affects mobility and changes in the number and type of proton transfer groups produced as a result of the elementary epoxy-amine reactions, which occur in this complex polymerization. These

changes in H-bonding proton exchange interactions produce in turn changes in the formation of the long-range hydrogen bridging with the advancement of the reaction and thereby the ease of proton exchange.

REFERENCES

- (1) Kranbuehl, D. In *Dielectric Spectroscopy of polymeric materials*; Fitzgerald, J. R. a. J., Ed., 1997; pp 303-328.
- (2) Bonnet, A.; Pascault, J. P.; Sautereau, H.; Rogozinski, J.; Kranbuehl, D. *Macromolecules* **2000**, *33*, 3833.
- (3) Bidstrup, S. A.; Sheppard, N. F., Jr.; Senturia, S. D. *Polym. Eng. Sci.* **1989**, *29*, 325.
- (4) Day, D. R. *Polym. Eng. Sci.* **1989**, *29*, 334.
- (5) Bellucci, F.; Valentino, M.; Monetta, T.; Nicodemo, L.; Kenny, J.; Nicolais, L.; Mijovic, J. *J. Polym. Sci., Part B: Polym. Phys.* **1995**, *33*, 433.
- (6) Stephan, F.; Fit, A.; Duteurtre, X. *Polym. Eng. Sci.* **1997**, *37*, 436.
- (7) Mangion, M. B. M.; Johari, G. P. *Macromolecules* **1990**, *23*, 3687.
- (8) Mangion, M. B. M.; Johari, G. P. *J. Polym. Sci., Part B: Polym. Phys.* **1991**, *29*, 1117.
- (9) Mangion, M. B. M.; Johari, G. P. *J. Polym. Sci., Part B: Polym. Phys.* **1991**, *29*, 1127.
- (10) Maffezzoli, A.; Trivisano, A.; Opalicki, M.; Mijovic, J.; Kenny, J. M. *J. Mater. Sci.* **1994**, *29*, 800.
- (11) Mijovic, J.; Kenny, J. M.; Maffezzoli, A.; Trivisano, A.; Bellucci, F.; Nicolais, L. *Compos. Sci. Technol.* **1993**, *49*, 277.
- (12) Carrozzino, S.; Levita, G.; Rolla, P.; Tombari, E. *Polym. Eng. Sci.* **1990**, *30*, 366.
- (13) Deng, Y.; Martin, G. C. *Macromolecules* **1994**, *27*, 5141.
- (14) Butta, E.; Livi, A.; Levita, G.; Rolla, P. A. *J. Polym. Sci., Part B: Polym. Phys.* **1995**, *33*, 2253.
- (15) Casalini, R.; Livi, A.; Rolla, P. A.; Levita, G.; Fioretto, D. *Phys. Rev. B: Condens. Matter* **1996**, *53*, 564.
- (16) Senturia, S. D.; Sheppard, N. F., Jr. *Adv. Polym. Sci.* **1986**, *80*, 1.
- (17) Eloundou, J. P.; Gerard, J. F.; Pascault, J. P.; Boiteux, G.; Seytre, G. *Angew. Makromol. Chem.* **1998**, *263*, 57.

- (18) Tajima, Y. A. *Polym. Compos.* **1982**, *3*, 162.
- (19) Johari, G. P.; Wasylyshyn, D. A. *J. Polym. Sci., Part B: Polym. Phys.* **2000**, *38*, 122.
- (20) Bidstrup, S. A.; Simpson, J. O. *J. Polym. Sci., Part B: Polym. Phys.* **1995**, *33*, 43.
- (21) Gotro, J.; Yandrasits, M. *Polym. Eng. Sci.* **1989**, *29*, 278.
- (22) Kaur, I.; Misra, B. N.; Chauhan, M. S.; Chauhan, S.; Gupta, A. *J. Appl. Polym. Sci.* **1996**, *59*, 389.
- (23) Simpson, J. O.; Bidstrup, S. A. *Polym. Mater. Sci. Eng.* **1993**, *69*, 451.
- (24) Kranbuehl, D. E. *J. Non-Cryst. Solids* **1991**, *132*, 930.
- (25) Lane, J. W.; Seferis, J. C.; Bachmann, M. A. *Polym. Eng. Sci.* **1986**, *26*, 346.
- (26) Warner, J.; Guo, J.; Khoshbin, M.; Raheem, S.; Kranbuehl, D. E.; Seytre, G.; Boiteux, G. *Polymer* **2003**, *44*, 3537.
- (27) Gierer, A.; Wirtz, K. *J. Phys. Chem.* **1952**, *56*, 914.
- (28) Bountis, T. *Proton transfer in hydrogen bonded system*; Plenum Press: London, 1992.
- (29) Pang, X.-F.; Feng, Y.-P. *Chem. Phys. Lett.* **2003**, *373*, 392.
- (30) Pissis, P.; Kyritsis, A.; Shilov, V. V. *Solid State Ionics* **1999**, *125*, 203.
- (31) Harrod, J. F. *J. Poly. Sci.* **1963**, 385.
- (32) Bellenger, V.; Verdu, J.; Francillette, J.; Hoarau, P.; Morel, E. *Polymer* **1987**, *28*, 1079.
- (33) Mijovic, J.; Andjelic, S. *Macromolecules* **1995**, *28*, 2787.
- (34) Mijovic, J.; Andjelic, S.; Yee, C. F. W.; Bellucci, F.; Nicolais, L. *Macromolecules* **1995**, *28*, 2797.
- (35) Tombari, E.; Ferrari, C.; Salvetti, G.; Johari, G. P. *J. Phys.: Condens. Matter* **1997**, *9*, 7017.
- (36) Gallone, G.; Levita, J.; Mijovic, J.; Andjelic, S.; Rolla, P. A. *Polymer* **1998**, *39*, 2095.

- (37) Eloundou, J.; Feve, M.; Gerard, J. F.; Harran, D.; Pascault, J. P. *Macromolecules* **1996**, *29*, 6907.
- (38) Holly, E.; Venkataraman, S. K.; Chambon, F.; Winter, H. H. *J. Non-Newtonian Fluid Mech.* **1988**, *27*, 17.
- (39) Lange, J.; Johansson, M.; Kelly, T. C.; Halley, P. J. *Polymer* **1999**, 5699.
- (40) Seanor, D. *Electrical properties of polymers*; Academic Press: New York, 1982.
- (41) Winokur, P. S.; Roush, M. L.; Silverman, J. J. *Chem. Phys.* **1975**, *63*, 3478.
- (42) Vojnovic, B.; Visscher, K. J. *Radiat. Phys. Chem.* **1991**, *38*, 349.
- (43) Girard-Reydet, E.; Riccardi, C. C.; Sautereau, H.; Pascault, J. P. *Macromolecules* **1995**, *28*, 7608.
- (44) Girard-Reydet, E.; Riccardi, C. C.; Sautereau, H.; Pascault, J. P. *Macromolecules* **1995**, *28*, 7599.

CHAPTER 4. MONITORING STRUCTURAL EVOLUTION DURING VINYL/DIMETHACRYLATE COPOLYMERIZATION WITH FREQUENCY DEPENDENT DIELECTRIC MEASUREMENT

4.1. Introduction

Highly cross-linked polymers made by free radical polymerization of multifunctional monomers have desirable properties for a wide variety of applications¹⁻⁹. A particularly interesting property of these materials is their potential to exhibit spatial heterogeneity due to the formation of microgels,¹⁰⁻¹² domains of high crosslinking density, dispersed in a pool of unreacted monomers. Various experimental techniques have been used by others¹³⁻²⁴ to investigate the structural heterogeneous formation process during network evolution.

Frequency dependent dielectric sensing (FDEMS) is a particularly insightful method as it monitors the dipolar reorientational motion of molecules in a polymer.²⁵⁻²⁹ This chapter reports on dielectric relaxation measurements of the molecular mobility and differential scanning calorimetric (DSC) measurements of the buildup in T_g during the polymerization of the dimethacrylate/styrene resin. There are numerous dielectric research publications on epoxy-amine curing systems. Our research is one of only a few

dielectric studies made on the polymerization process of a dimethacrylate resin,^{30,31} although a number of papers focus on an acrylate polymers^{17,32-37} and blends.³⁸⁻⁴⁶

A particular objective of this paper is to explore the existence of spatial heterogeneity during cure of this system. The hypothesis of a spatial heterogeneity during cure of a network was initially proposed by Dusek et al.¹⁰⁻¹². The existence of a spatial heterogeneity in cured dimethacrylate resins has been characterized by Bowman et al.¹³⁻¹⁵ Early experimental results suggesting the existence of a spatial heterogeneity are found in the earlier work by Landin and Macosko,⁴³ Hamilec et al.⁴⁴⁻⁴⁶ and Kloosterboer and co-workers.⁴⁷⁻⁴⁹ These groups observed that the reactivity of pendant functional groups in the crosslinked regions was much less than free active vinyl groups. While a correct observation, it is not the full explanation for the existence of the spatial heterogeneity they proposed. This was explained as due to the fast polymerization at the radicals resulting in localized network formation and thereby producing poor compatibility with the regions containing monomer/oligomer components in the system by Dusek et al.,¹⁰⁻¹² Pascault et al.⁴² and Kloosterboner et al.⁵⁰

This chapter focuses on the evolution of the dipolar dielectric loss $\epsilon_d''(\omega, t, T)$ as the sample cures at different temperatures (T), frequency (ω) and time (t) while achieving different conversions, (α). Our interest is to relate the changes in molecular dipolar mobility to the development of the heterogeneity. Another interest is to characterize the glass transition regions in the DSC profiles. Dielectric spectra and the DSC's Tg profiles are used together to characterize the evolution of the heterogeneity during the buildup of the styrene/dimethacrylate based network. Then the dielectric spectra and DSC Tg profiles are used to investigate the existence of two cooperative

regions of sufficient size to create two α -relaxation processes representing oligomer rich and polymer microgel regions during the polymerization.

We also investigated the polymerization of a dimethacrylate monomer (D121) in the presence of higher functionality comonomer - divinylbenzene (DVB). The results show that the chemical structures of comonomer have a large influence on the polymerization rate, structural evolution, system heterogeneity and final network morphology. In this chapter, first we will introduce the dielectric studies on D121/St crosslinked network formation. Then, we will compare the D121/St system with a more crosslinked dimethacrylate network – D121/DVB system. The comonomer effect on the network structure and dielectric, mechanical properties are discussed.

4.2. Experimental Section

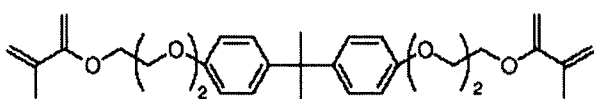
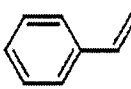
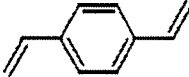
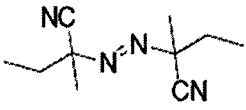
4.2.1 Materials

Two reactive systems were used in this study. Two comonomers (20 wt%) divinylbenzene (DVB) from Fluka and styrene from Adrich were used. Each was mixed with Dimethacrylate of tetraethoxylated bisphenol A (D121) from Akzo-Nobel (80 wt%) separately. 0.5 wt% of chain transfer agent 1-dodecanethiol (Adrich) and 0.2 wt% of thermal initiator azobis(methylbutyronitrile) (Adrich) were added to the reactive ingredients. All products were used as received. Table 4.1 shows the formulas of these reactants.

Mixing was carried out in a glass vial with a magnetic stirrer and Argon bubbling at ambient temperature for 30 min to ensure a homogeneous blend of all components and

to remove oxygen in order to avoid inhibition. Further details of the sample preparation have been previously described in papers by L.Rey et al.^{21,24}

Table 4.1. Chemical products used in polymerization

Name	Chemical formula
Dimethacrylate of tetraethoxylated bisphenol (D121)	
Styrene (St)	
Divinylbenzene	
1-Dodecanethiol	$\text{CH}_3(\text{CH}_2)_{11}\text{SH}$
azobis(methyl-butyronitrile)	

4.2.2. Dielectric Impedance Measurements

The liquid mixture was introduced into a mold made of two glass plates separated by a 4mm rubber gasket. A thin sample was needed to maintain a constant temperature during this exothermic reaction. A microsensor from Century Circuit&Electronics,

consisted of inter-digitated copper electrodes (50 microns in width with a spacing of 86 microns) on an area of 2.5×1.2 cm flexible polyimide substrate was enclosed in the cell. The electrodes were linked to a HP 4192A impedance analyzer by wires to measure the conductance and capacitance of the materials over a range of temperature and frequency.

The enclosed cell was placed in an oven at a constant temperature for cure. The dielectric permittivity and dielectric loss were measured at several frequencies in the range from 50Hz to 500kHz. The measurement was taken every two seconds across all ten frequencies. A computer acquired the dielectric data automatically. The frequency dependence of the dielectric data was used to monitor changes in the dielectric properties versus time during cure and then versus temperature for samples at various degrees of conversion. The frequency dependence of the dielectric loss was used to characterize changes in the alpha-relaxation processes of the glass transition during the polymerization and to investigate the existence of two distinct dynamic regions in the system at certain extents of the cure.

4.2.3. DSC Measurement

4.2.3.1. Kinetics

A TA 2920 modulated DSC was used for the thermo kinetic studies. The thermal analysis consisted of an isothermal DSC run to determine total reaction heat Q_i at that temperature and then followed by a dynamic ramp to a suitable high temperature to determine the residual heat of polymerization Q_r for all the samples. The conversion at a given time, $\alpha(t)$, was approximately calculated from:

$$\alpha(t) = Q_t / (Q_r + Q_i) \quad (4-1)$$

where Q_t is the heat produced by the reaction at the time t . These heats are a combination of the heats given off by all double bond reactions in the system, and thus represent an approximation of the extent of double bond conversion. However, since in this 80% dimethacrylate and 20% styrene mixture, the dimethacrylate and styrene react at the same rate, this approximation is quite accurate. Details of the reaction were reported previously.^{21,24}

4.2.3.2. Glass Transition (T_g) Measurements

During the 70°C isothermal cure, the reactant in DSC pan was quenched to -100°C after reacting for a period of time, then heated up to 70°C at 5°C/min to characterize the glass transition at different conversions using the inflexion point as determined by the TA instruments software.

4.2.4. Rheology

A TA instrument AR 1000 rheometer was used to measure the viscosity changes and detect the gelation during the isothermal cure: Forty millimeter diameter aluminum parallel plates separated with a sample thickness of 2mm were used in the measurements. Liquid monomers were loaded and housed inside an environmental test chamber. The storage modulus G' , loss modulus G'' and $\tan\delta$ were measured at regular intervals, from 0.1 Hz to 1 kHz, at zero normal force. The gel point was determined from the time at which $\tan\delta$ became independent of frequency.⁴² This is the point in time when the values of $\tan\delta$ measured at different frequencies become equal and crossover each other. The gel times are in agreement with previously reported values.²⁴

Dynamic mechanical measurements were performed in torsion mode with a pulsation of $6.28 \text{ rad}\cdot\text{s}^{-1}$. Samples were rectangular bars with 1.5mm thickness and an overall dimension of $20 \times 10 \text{ mm}^2$. G' , G'' and $\tan\delta$ were recorded as a function of temperature.

4.2.5. Transmission Electron Microscopy (TEM) Measurement

The heterogeneity of samples was examined with a Zeiss EM109 transmission electron microscope with an 80kV accelerating voltage. The sample is cut into thin pieces with ultramicrotome and examined under microscopy. Osmium tetroxide (OsO_4) staining was done in the liquid phases (1% pH 7.2-7.4 buffered solution) for 48 hours at room temperature.

4.3. Results and Discussion

4.3.1. D121/St system

4.3.1.1. Dielectric Measurements during Isothermal Cure

Dielectric measurements were performed on the free radical copolymerization of D121/St at 60°C , 70°C and 80°C . Figures 4.1a-c show the loss component ϵ'' of the permittivity scaled by the frequency versus time during the isothermal cures. The ionic mobility contribution to the dielectric loss is determined by the overlapping lines at the low frequencies. The contribution of rotational mobility of bound charge to the dielectric loss is observed by the peaks in the spectrum at high frequencies.

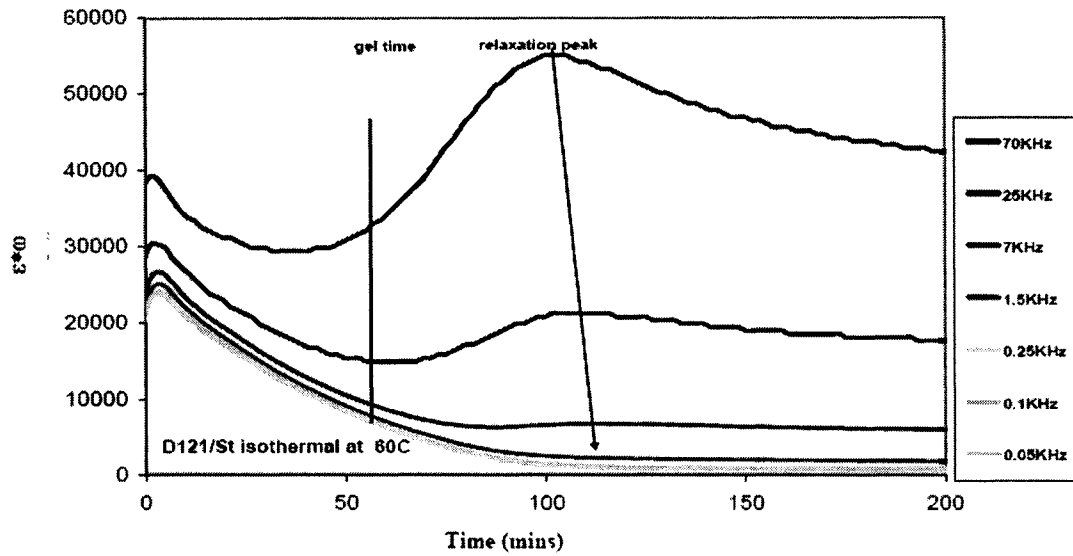


Figure 4.1a. $\epsilon''*\omega$ versus time during 60°C isothermal cure of D121/St

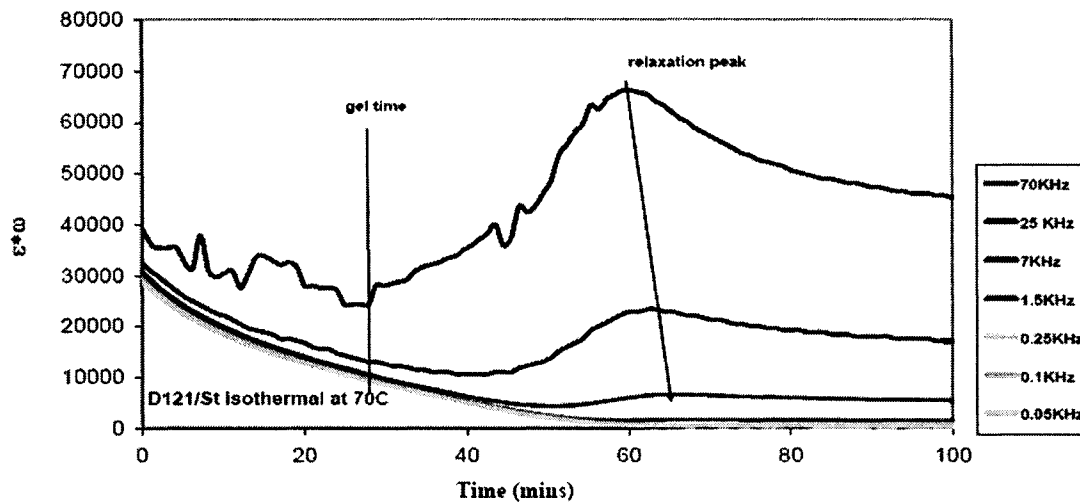


Figure 4.1b. $\epsilon''*\omega$ versus time during 70°C isothermal cure of D121/St

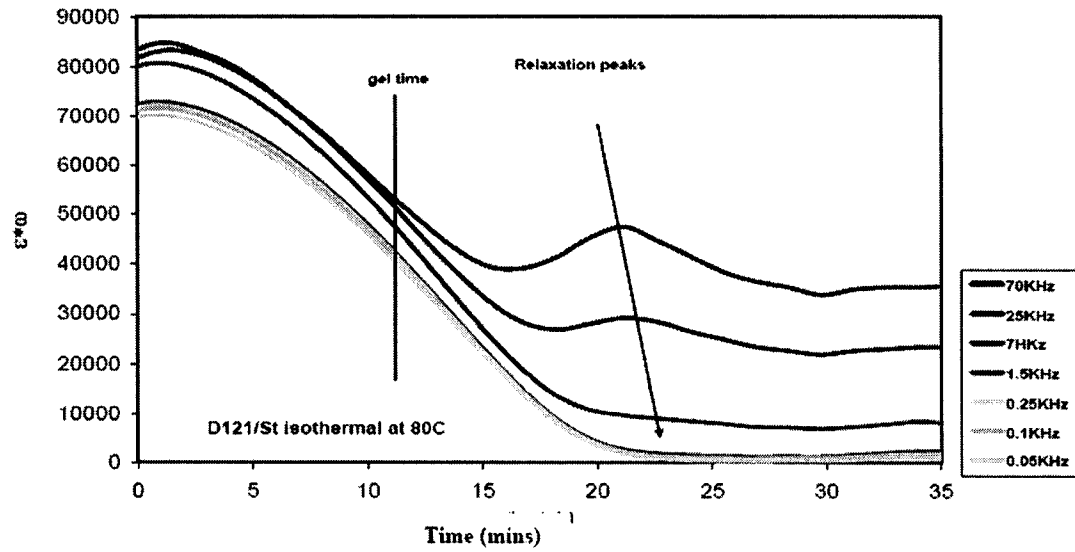


Figure 4.1c. $\epsilon''\omega$ versus time during 80°C isothermal cure of D121/St

As seen in Figure 4.1, the low frequency dielectric loss ϵ'' shows overlapping values up to 200 minutes at 60°C in Figure 1a and up to 100 minutes in Figure 1b. These values can be used to determine a frequency independent conductivity using Equation 4-2

$$\sigma(\text{ohm}^{-1}\text{cm}^{-1}) = \epsilon_0 \omega \epsilon_i'' \quad (4-2)$$

The dielectric loss ϵ'' at high frequencies in Figure 4.1a-c shows distinct peaks during the isothermal curing. These peaks are due to the dipolar mobility being close at that time and temperature to the frequency or time scale of the oscillating electric field. This dipolar contribution to ϵ'' can be determined more accurately by subtracting the ionic component.

$$\epsilon_d'' = \epsilon'' - \frac{\sigma}{\epsilon_0 \omega} \quad (4-3)$$

The gel time measured by dynamic rheological tests agrees with the results in Rey et al.'s paper.²⁴ At 70°C, gelation occurs at a total conversion of 14% after 28 minutes.

The results for all three temperatures are shown in able 4.2.

Table 4.2. Gel times (min) in the dielectric loss spectra (at 0.1KHz) during isothermal cure for D121/St

Temp(°C)	60	70	80
Gel Time (min)	64	28	13

Figures 4.1a-c show that the molecular gelation has no corresponding event in the ionic mobility as measured by the dielectric loss for this system. This strongly supports the view that fundamentally the dielectric spectrum is not associated with the gelation event. This is because ionic conductivity at low frequencies monitors in general the motions on a much smaller scale than those being affected by macroscopic gelation. Thus, the gelation process should not, and clearly in this case, is not observed through dielectric spectroscopy as previously suggested in some articles.^{51,52}

The peaks in $\varepsilon''_{dipolar}$ (which are usually close to the peak in ε'') can be used to determine the time or point in the cure process when the “mean” dipolar relaxation time has attained a specific value comparable to the time scale of the frequency of the applied force. At the time of a peak, a relaxation time characterizing molecular dipolar mobility can be calculated from $\tau = 1/\omega$. These relaxation times monitor the α relaxation process associated with vitrification. The peaks at different frequencies represent the time during conversion at which the materials appear to behave as a glass at that frequency and corresponding time scale. Thus these peaks can be used to probe the build up in time of T_g during the isothermal cure.

4.3.1.2. Dielectric Relaxation and the DSC profile during a Temperature Ramp

As seen in Figure 4.1 a-c, the relaxation time of the α relaxation process changes with the increase in the glass transition temperature as the reaction advances producing a series of $\epsilon''_{dipolar}$ peaks for D121/St system during the isothermal cure. But even with the modulated DSC, it is hard to determine the calorimetric glass transition during the isothermal cure. This is because the amount of heat created during the polymerization conceals the glass transition's thermal event during cure and particularly because the temperature width of the glass transition is large. Thus, another temperature-time reaction procedure shown in Figure 4.2 was used to investigate and compare the changes in both the dielectric-dynamic and the calorimetric glass transitions during the polymerization.

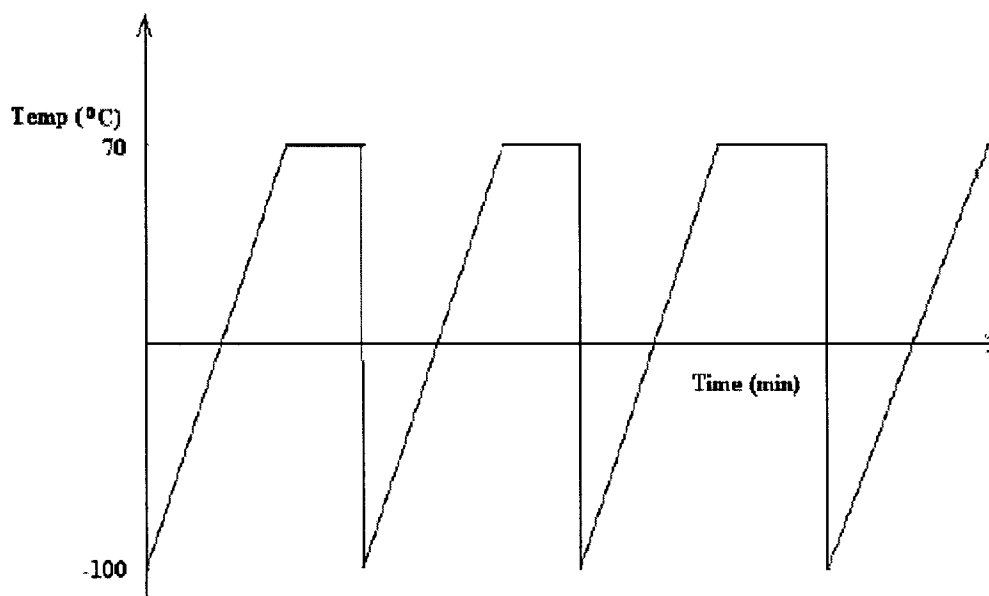


Figure 4.2. Temperature –time procedure used to measure dielectric properties and Tgs at different degrees of cure

In this procedure, the unreacted monomer mixture was cooled to -100°C and heated back to the curing temperature at a constant rate. Then, it was held at the curing temperature for a period of time. After the reactant was partially reacted, it was quenched again to -100°C and heated back to curing temperature at a constant rate. The quenching and heating steps are repeated several times until the system is cured. Table 4.3 shows the extent of conversion of the styrene and methacrylate double bonds after each cycle as measured by DSC.

First we examine the information in the cure sequence shown in Figure 4.2 using dielectric sensing. Figures 4.3a-e display the dielectric results for the temperature ramp steps during the cure. Only the α -relaxation peak for the monomers in the unreacted mixture was observed at the beginning of the reaction. As the extent of conversion increases, two distinct relaxation peaks are observed. We believe they are both α -relaxations for the D121/St system. We associate the higher temperature peak with vitrification of the microgel D121/St network. A much faster α relaxation peak at a lower temperature remains throughout most of the cure reaction. This peak was associated initially by Bowman to the pools of monomer's T_g and then to short oligomeric structures as the reaction advances.¹⁵ We agree and associate this peak with the monomer-oligomer region. Table 4.3 reports the values of the temperatures of the α -relaxation peaks observed as the reaction progresses at a frequency-time scale of 2.5kHz.

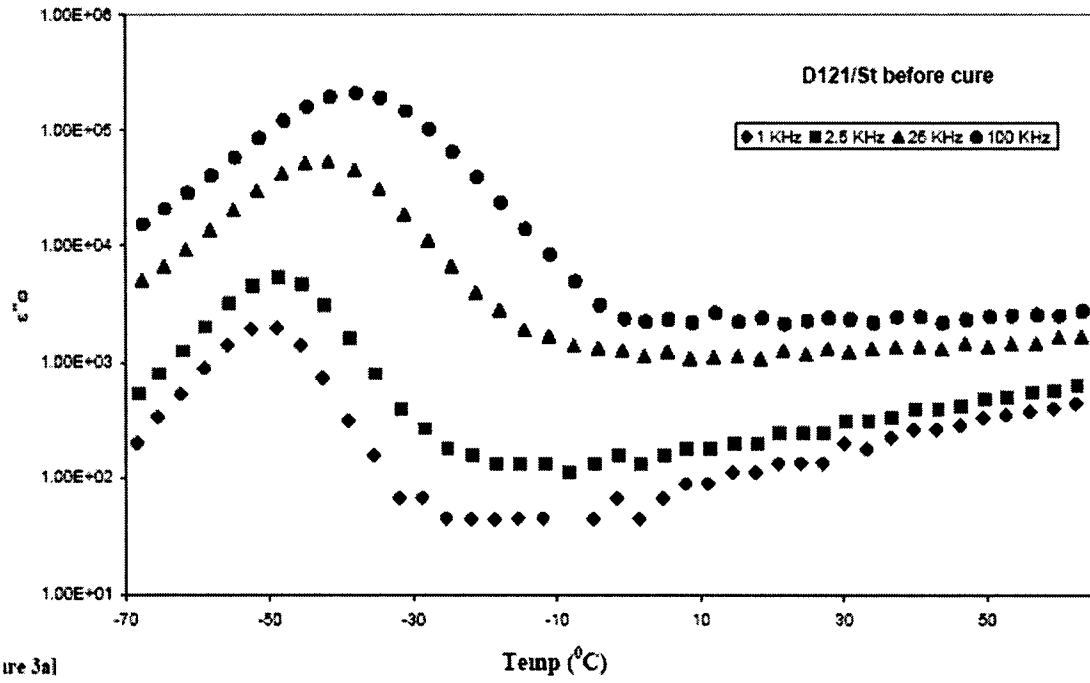


Figure 4.3a. $\epsilon'' \cdot \omega$ versus temperature before cure

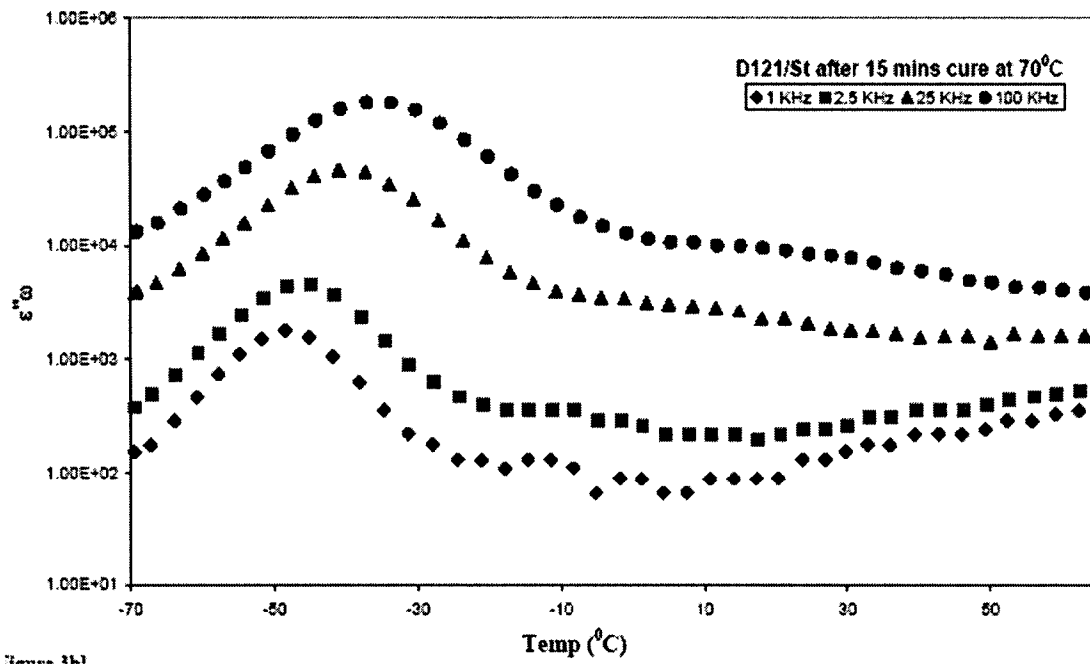


Figure 4.3b. $\epsilon'' \cdot \omega$ versus temperature after 15 mins cure at 70°C

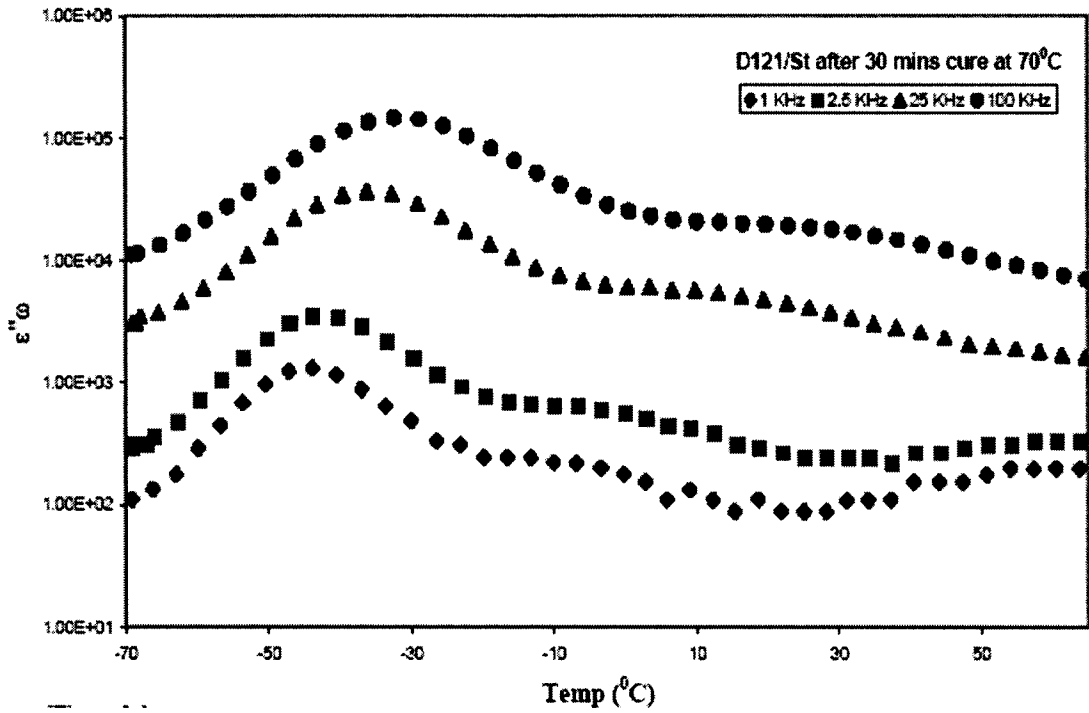


Figure 4.3c. $\epsilon'' \cdot \omega$ versus temperature after 30 mins cure at 70°C

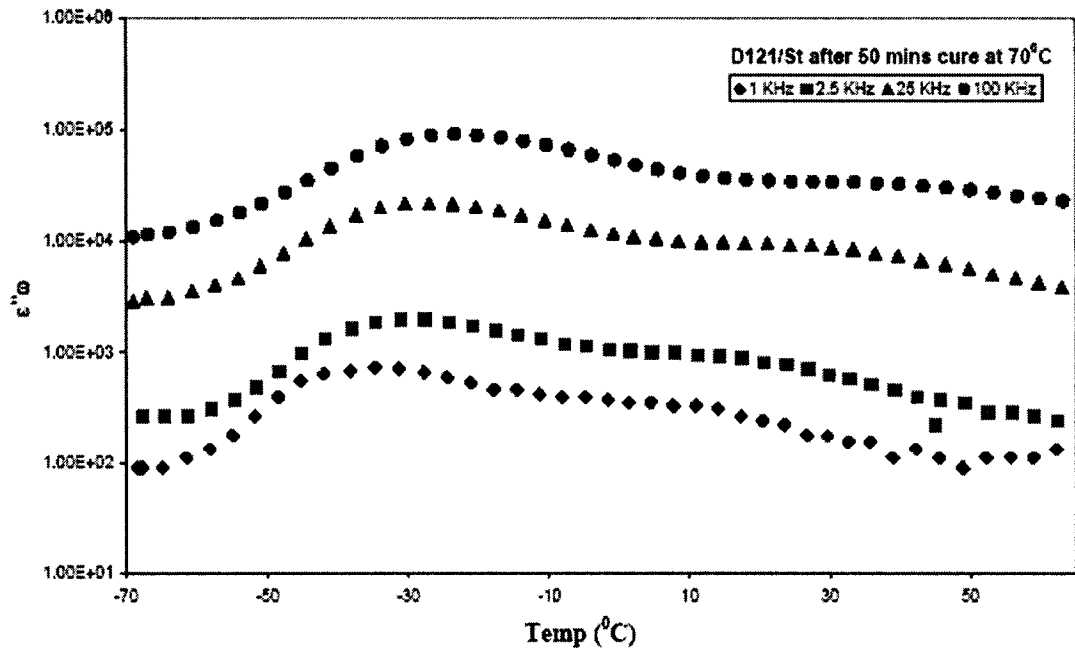


Figure 4.3d. $\epsilon'' \cdot \omega$ versus temperature after 50 mins cure at 70°C

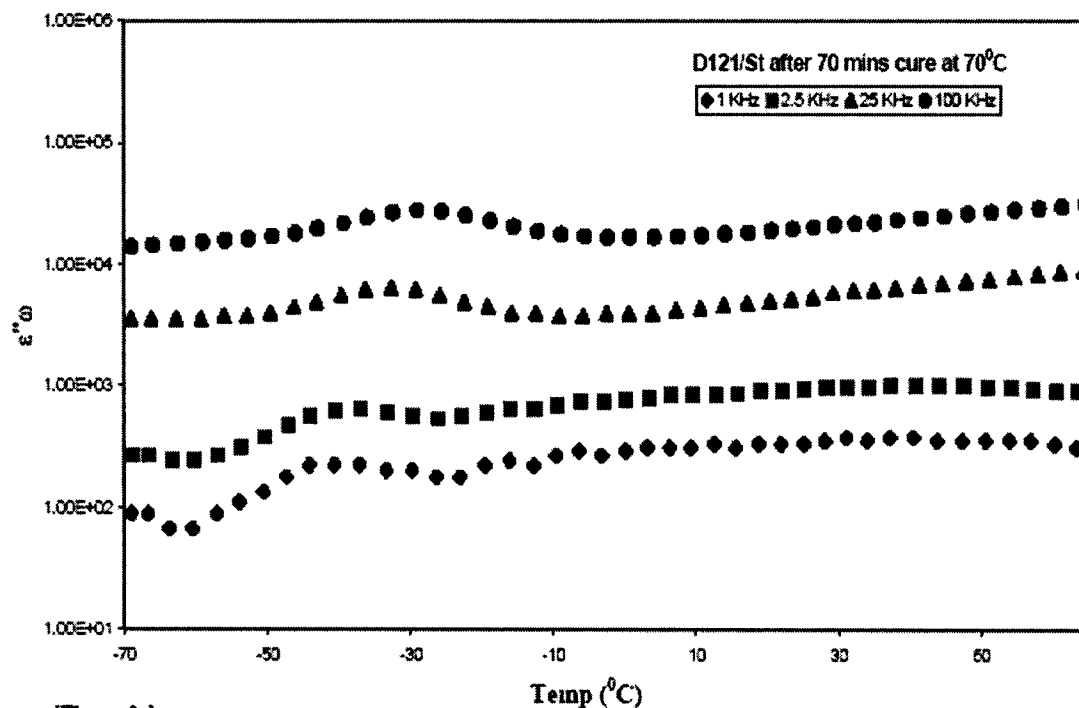


Figure 4.3e. $\epsilon'' \cdot \omega$ versus temperature after 70 mins cure at 70°C

Next we report the results of this cure sequence using DSC. Figure 4.4 shows the DSC profiles during the temperature ramp for D121/St at different degrees of conversion. The monomer/oligomer glass transition is observed at -64°C . As the conversion increases, a second Tg transition is observed at a higher temperature in addition to the monomer-oligomer Tg transition for D121/St. The heat capacity change of the first transition is about 0.3J/g/K , which is close to an expected value of about 0.5J/g/K . The second transition is much smaller as the fraction of mass in the network state is also small. Table 4.3 reports values of the Tg's observed in the DSC spectra. The glass transition of the 88% conversion sample is very broad and the $T_g = 10^{\circ}\text{C}$ for this sample is a calorimetric software determined value, which conflicts with the visual appearance of a glass at room temperature.

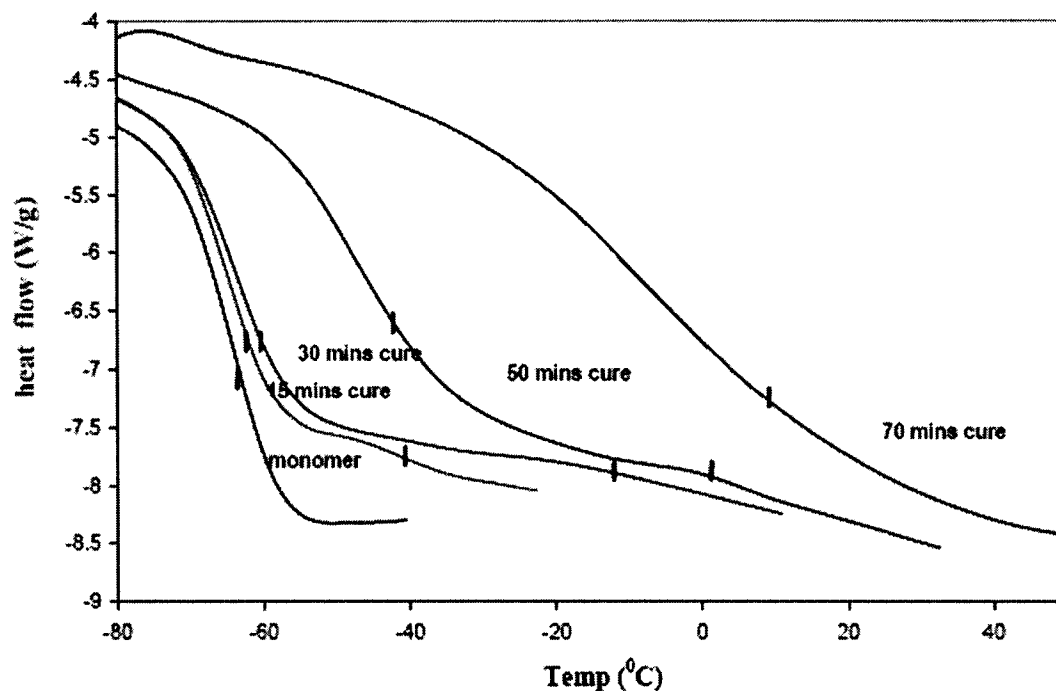


Figure 4.4. Tg evolution during 70°C isothermal polymerization of D121/St (The Tg mark (|) is determined by TA instrument software)

Table 4.3. Total conversion, Tg temperatures determined by DSC and Tg temperatures determined by dielectric measurement (2.5 KHz) at different curing cycles for D121/St shown in Figure 4.2

Time (min)	Total Conversion* (%)	Tg(1) °C	Tg(2) °C	T _{a1} (2.5KHz) °C	T _{a2} (2.5KHz) °C
0	0	-64	-	-46	-
15	5	-62	-41	-45	-18
30	19	-56	-15	-41	-7
50	41	-44	0	-32	6
70	88	-	10	-34	too broad

* Acrylic and styrene monomers

For the monomer mixture, the system is homogeneous and only one relaxation process exists. As the polymerization proceeds, the environment becomes more and more restricted for radical diffusion. As K. Dusek et al. suggested¹⁰⁻¹² the radicals trapped in polymer rich regions produce the growth in the microgel structure. This in turn results in the system becoming heterogeneous and another relaxation response in the dielectric spectra is generated in addition to the monomer-oligomer relaxation response. As seen in Table 4.3, the results show that the Tg's and the α -relaxation temperatures for the two relaxation peaks reflect the change in Tg in each region. In the dielectric spectra, especially at low conversion, the monomer/oligomer α -relaxation is dominant. The α -relaxation of the microgel polymer network at low conversions is hidden by the tail of the strong monomer/oligomer α -relaxation peak. Thus the temperatures reported in Table 4.3 for the microgel α -relaxation peak at the lowest degrees of conversion are approximate.

The dielectric α -relaxation peaks correspond to the temperature at which the time scale of dipolar mobility is comparable to the applied frequency. The increasing cooperativity of the dynamics increases these relaxation times with the extent of reaction. The calorimetric glass transition measured by MDSC monitors the chain's segmental motions effect on the heat capacity. Empirically it has been reported that the calorimetric glass transition temperature corresponds to an approximate relaxation rate which corresponds to a much lower frequency of 10^{-3} to 10^{-2} Hz⁵³.

The formation of spatial heterogeneity during the cure for D121/St was also observed in atomic force microscopy (AFM), dynamic light scattering (DLS) and positron annihilation lifetime spectroscopy (PALS) measurements.²¹⁻²⁴ Three

distributions of particles, which related to oligomer, single microgel and microgel clusters, were observed in DLS analysis. Further, a nodular structure was observed in AFM graphs²⁴. This nodular structure is a consequence of the network buildup through the formation of microgels and their growth into clusters.

4.3.1.3. WLF Equation Fitting for the Relaxation Peaks

The temperature dependence of the relaxation rate of the α -relaxation can be parameterized by the Williams-Landel-Ferry (WLF) equation near the glass transition temperature:⁵⁴

$$\log(\tau/\tau_0) = -C_1(T-T_0)/(C_2+T-T_0) \quad (4-4)$$

Where τ is the relaxation time for molecules, T_0 is a reference temperature. C_1 and C_2 are constants related to the fractional free volume (v_0) and thermal expansion coefficient (α_f) of the free volume at T_0 .

The monomer /oligomer relaxation peaks at different frequencies are quite obvious in the dielectric spectra (Figures 4.3a-e). The relaxation rate τ and corresponding temperature T at different conversions are determined from the dielectric spectra and fitted with the WLF equation (Equation 4-4), which can be written in the form:

$$-(T-T_0)/\log(\tau/\tau_0) = (T-T_0)/C_1 + C_2/C_1 \quad (4-5)$$

The following procedure is used to determine the constants C_1 and C_2 : First, the calorimetric glass transition temperature T_g was chosen as the reference temperature at different conversions. $\tau = 100s$ was chosen due to the relation between the relaxation rate

and T_g .⁵³ Then, $-(T-T_0)/\log(\tau/\tau_0)$ and $T-T_0$ were calculated at different relaxation rates. The constants C_1 and C_2 were calculated from the slope and intercept using Equation 4-5. The resulting WLF parameters C_1 and C_2 at different conversions are listed in Table 4.4.

The WLF fitting results indicate that the WLF parameters C_1 and C_2 are increasing functions of conversion for monomer/oligomer α -relaxation processes. C_1 is inversely proportional to the fractional free volume (v_0) in the material at the temperature of interest. The increase of C_1 indicates the movement of the molecules becomes restricted with the advancement of the reaction as the free volume decreases. This result is consistent with the free volume study conducted by L. Rey et al. for D121/St system.²³ C_2 equals the fractional free volume (v_0) divided by the thermal expansion coefficient (α_f). Normally, the thermal expansion coefficient decreases with the crosslinking density of the materials.⁵⁵⁻⁵⁷ The slight increase of C_2 suggests the thermal expansion coefficient decreases faster than the free volume during the polymerization. The thermal expansion coefficient (α_f), which is inversely related to the product of C_1 and C_2 , is observed to decrease with the advancement of the reaction. Another observation for C_1 and C_2 is that the values of C_1 and C_2 approach to 17.44 and 51.5, which are the universal values for the WLF equation for a polymer with $T_0=T_g$. This means that the monomer/oligomer region is shifting toward polymer region values slowly with the advancement of cure.

Accurate fitting of the microgel α relaxation peaks with WLF function was not possible due to the tail of monomer/oligomer peaks.

Table 4.4. D121/St monomer/oligomer WLF fitting parameters

conversion(%)	T _g (°C)	C ₁	C ₂ (K)	R ²
0	-64	12.04	19.81	0.996
5	-62	13.19	23.73	0.975
19	-56	13.98	24.41	0.998
41	-44	15.24	26.50	0.919

4.3.1.4. Width of the Relaxation Peaks

In general, the relaxation peaks when observed at a fixed temperature move from a high frequency to a low frequency as the reaction advances. The width of the ϵ'' versus frequency (f) plot at half height, $\Delta\log(f^{1/2})$, increases and the strength of the relaxation peaks decreases with reaction advancement. For the unreacted mixture, the α relaxation response is narrow because the molecules and domains of cooperative interaction are smaller and of similar size. As the reaction progresses, with the build-up of the microgel network regions, many molecules remain as an oligomer/monomer in other regions. The increasing distribution in the size and regions of the monomer/oligomer molecules in the resin causes a broadening of the relaxation spectrum as be measured by $\Delta\log(f^{1/2})$ in the monomer/oligomer regions.

The half width ($\Delta\log(f^{1/2})$) value at different conversions can be used to estimate the parameter (β) of the stretched exponential relaxation decay function $\phi(t)$ for the monomer/oligomer glass transition regions, where⁵⁸⁻⁶¹

$$\phi(t) = \exp(-t/t_0)^\beta \quad (4-6)$$

β indicates the distribution in the dipolar mobilities, or relaxation times, in the system.

The β values calculated from half widths ($\Delta\log(f^{1/2})$) for the monomer-oligomer

relaxation spectrum are listed in Table 4.5. The parameter β varies between 0 and 1. A value close to zero implies a very broad distribution of relaxation times, and a value close to 1 implies a narrow distribution of relaxation times. Generally, a polymer's high frequency β -relaxation spectrum displays a broad dielectric loss peak with half widths of 4-6 decades.^{53,62} The half width ($\Delta \log(f^{1/2})$) values in Table 4.5 are all less than 4 decades. This is consistent with these low temperature peaks being associated with the α relaxation of the monomer-oligomer region.

Table 4.5. Shape parameter (β) determined by half height width of relaxation peak (Δ) of D121/St monomer-oligomer region

Time (min)	Conversion (%)	$\Delta \log f_{1/2}$	β
0	0	1.96	0.58
15	5	2.79	0.41
30	19	3.34	0.32
50	41	-	-
70	88	-	-
Fully cured*		-	0.11

* Fully cured data is measured by dynamic mechanic rheometer (cited from reference 21)

As seen in Table 4.5, the value of β for the monomer-oligomer α -relaxation region decreases from 0.58 to 0.32 during the initial 30 minutes of the polymerization as the conversion increases to 19%. At 50 minutes and a conversion of 41%, the breadth of the monomer-oligomer α -relaxation overlaps the already broad α -relaxation spectrum of the microgel regions. At this point in the reaction as already discussed, microgel networks are extending into the monomer-oligomer regions. As the reaction progresses beyond this point, the overlap of the α -relaxation processes of these two regions continues to increase. This is observed in Figures 4.3d and 4.3e at 50 minutes and 70 minutes. At this point, a very broad α -relaxation process is observed which extends over more than

100°C. Evidence of two relaxation regions remains, as seen by the apparent maxima in the loss around -30°C and +30°C.

The breadth of the combined α -relaxation processes of these two regions has been characterized also by dynamic mechanical measurements of the fully cured resin as reported in Table 4.5.²¹ The value of β as determined from the total width of the dynamic mechanical measurements decreased to 0.11 and the total width of the α -relaxation processes of both regions as characterized by the dynamical mechanical measurements extended from -50°C to 200°C.²¹

Overall, these results are in good agreement with a number of observations and conclusions made by Christopher Bowman based on dielectric and mechanical measurements on cured dimethylacrylate networks.¹³⁻¹⁵ In their studies, they observed two distinct relaxation regions. The higher mobility relaxation spectrum was attributed to “monomer pools” of unreacted double bonds. This relaxation process was separate and in addition to a “primary” peak at low frequencies. The high temperature relaxation spectrum was attributed to the glass transition. Taken together, these two peaks implied a “very high degree of structural heterogeneity.” They are indeed similar to the spectra observed here as our dimethacrylate system approaches full cure. What is now clear is that the secondary high mobility peak is the dominant peak throughout the initial stages of the reaction and that the microgel, lower mobility peak occurs very early on in the course of the reaction. This low frequency, high temperature relaxation is observed here after only 15 minutes at 5% conversion, before “macroscopic gel”, by both our dielectric and differential scanning calorimetric measurements.

4.3.1.5. Network, monomer heterogeneity

In summary, in the very early stages of the reaction, a polymer microgel region builds up. The increasing molecular connectivity forms polymer domains with different size from the monomer/oligomer domains²⁴. Due to the existence of the microgel domain, a new lower frequency, higher temperature α -relaxation process appears in the dielectric spectra. The polymer microgel relaxation peak appears as a shoulder on the monomer/oligomer relaxation peak after only 15 minutes of cure (Figure 4.3b). Formation of the microgel region as detected by the dielectric technique is observed much earlier than the gel time (28 minutes) measured by rheometer. With the advancement of the reaction, these two α relaxation peaks begin to separate and form two distinct peaks as seen in Figure 4.3d. During the initial 30 minutes, Figures 4.3b-d indicate the formation in molecular mobility of the polymer clusters decreases more rapidly, while the dipolar mobility in the monomer/oligomer region changes less as the conversion increases.

In the early stages of the reaction, the related glass transition build-up in the polymer microgel region can be observed in DSC spectra (Figure 4.4). At the beginning of the reaction, no microgel region existed in D121/St system. As reported with the advancement of the reaction at 15 minutes, $\alpha = 5\%$, two thermal glass transitions are observed in Figure 4.4. This figure shows that during the initial 30 minutes, the glass transition of the microgel region shifts from low temperature to high temperature as does the monomer oligomer region's glass transition. As in the dielectric spectra, the change in T_g in the monomer-oligomer region is at a slower rate than in the microgel region.

During the later stages of the reaction, the monomer-oligomer glass transition, as observed by DSC, merges with the microgel glass transition due to the now interconnected network between microgels and oligomers in the resin. During the later step, peaks of the microgel region show the same overall behavior as α relaxation time. The peaks shift to a higher temperature and the distribution becomes wider as the conversion increases. This produces one very broad glass transition event and a very broad α -relaxation spectrum at 70 minutes (88% conversion) as is observed in the DSC spectra.

4.3.2. Influence of the comonomer structure on the network buildup

Compared with D121/St system, the use of DVB as comonomer will increase the cross-linking density of the network because of the increasing meaning functionality of the monomer mixture. In this part, we compare the development of spatial heterogeneity during the network formation in D121/St and D121/DVB systems. The objective for this work is to understand how the chemical structures and cross-linking density affect microgel formation and its spatial distribution.

4.3.2.1. Isothermal Polymerization

Figures 4.5a and 4.5b show the loss component ϵ'' of the permittivity scaled by the frequency versus time during the 70°C isothermal cures for both two systems. As discussed previously, a plot of $\omega*\epsilon''$ is a particularly informative representation of the ion and dipole mobility changes during cure. The overlapping of $\omega*\epsilon''$ indicates the transnational diffusion of charge is the dominant physical process at low frequency.

Similarly, the peaks of $\omega \cdot \epsilon''$ at high frequency indicates the contribution of dipolar α relaxation rotational diffusion process with the buildup in T_g .

The gel time and the change in the dipolar loss due to changes in charge translational diffusion of ions are shown in Figure 4.5. For both systems, the gel point is not related to an inflexion point in the changing conductivity. Furthermore, the gel point does not appear to relate to any dielectric event in the dielectric spectra. This phenomenon is undoubtedly because as the gel develops the viscoelastic properties of the resin involve the cooperative motion of many chains while the translational diffusion of the ions continues to involve motions over much smaller molecular dimensions and within the monomer/oligomer region.

The broadness of peaks in the dielectric loss $\omega \cdot \epsilon''$ plot relates to the length scales of the cooperative relaxation region. The broader relaxation peak in D121/DVB system indicates a much larger range of cooperativity length scales during cure compared to D121/St.

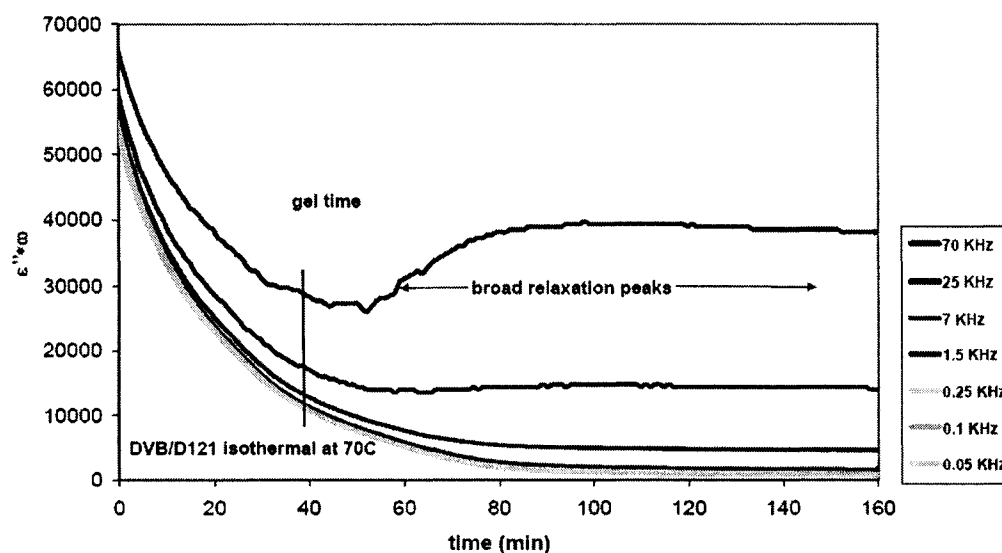


Figure 4.5a. $\epsilon'' \cdot \omega$ versus time during isothermal polymerization of D121/DVB at 70°C

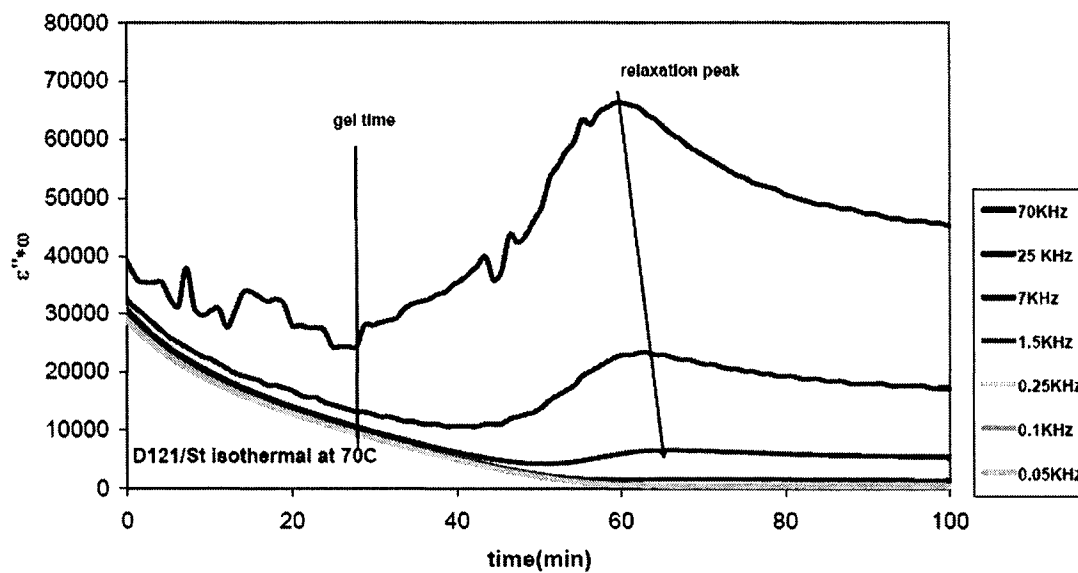


Figure 4.5b. $\epsilon'' \cdot \omega$ versus time during isothermal polymerization of D121/St at 70°C

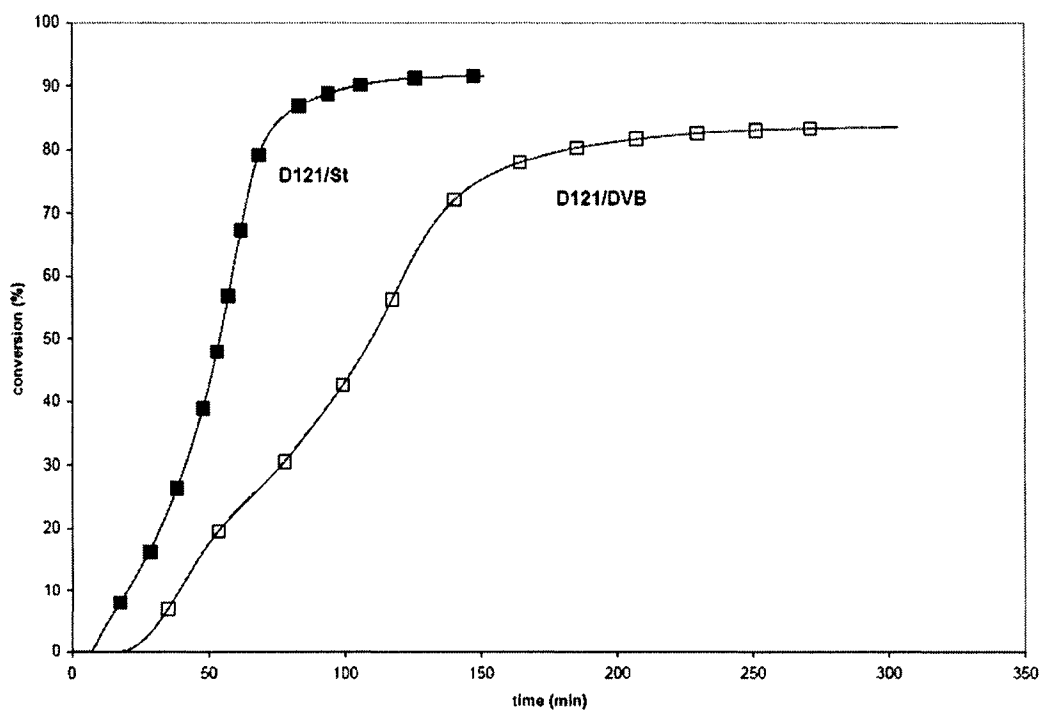


Figure 4.6. Monomers conversion during cure for D121/DVB and D121/St

Compared to the D121/St system, the D121/DVB has much broader dynamic relaxation peaks (Figure 4.5). It also has a much slower polymerization rate (Figure 4.6), although the unit number of double bonds is higher. The presence of DVB has a complex influence on the polymerization. On one hand, the additional cross-linking facilitates the gel formation leading to an auto acceleration effect. On the other hand, the propagation rate is influenced by the diffusion rate of the reactive species. Because the D121/DVB system generates a higher cross-linked structure, the diffusion rate and thereby the polymerization rate is reduced and lower than in the D121/St system.

4.3.2.2. Structural evolution and network heterogeneity during cure

The dielectric, thermal and mechanical properties of each resin at different conversions are important to understanding the chemical structural and the molecular dynamics during network formation and growth. Thus, another temperature-time reaction procedure shown in Figure 4.2 was used to investigate the properties of each system at differing extents of reaction. Table 4.6 shows the extent of conversion for each cycle.

Table 4.6. Total conversions at different curing cycles for D121/St and D121/DVB

D121/St		D121/DVB	
Time (min)	Total Conversion* (%)	Time (min)	Total Conversion* (%)
0	0	0	0
15	5	35	5
30	19	60	21
50	41	100	42
70	88	150	77

4.3.2.2.1. Dielectric spectroscopy

First we examine the information in the cure sequence shown in Figure 4.2 using dielectric sensing.

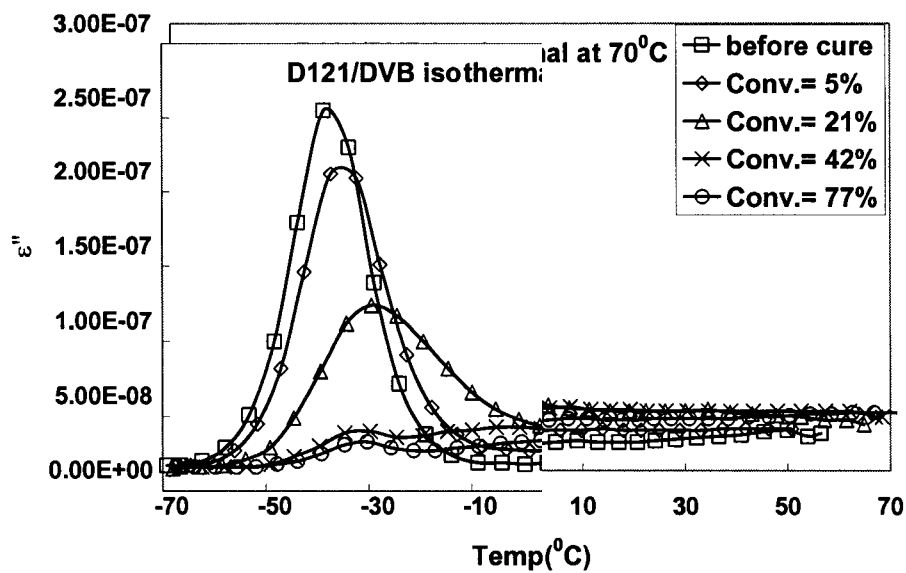


Figure 4.7a. ϵ'' versus temperature at different degrees of conversion for D121/DVB

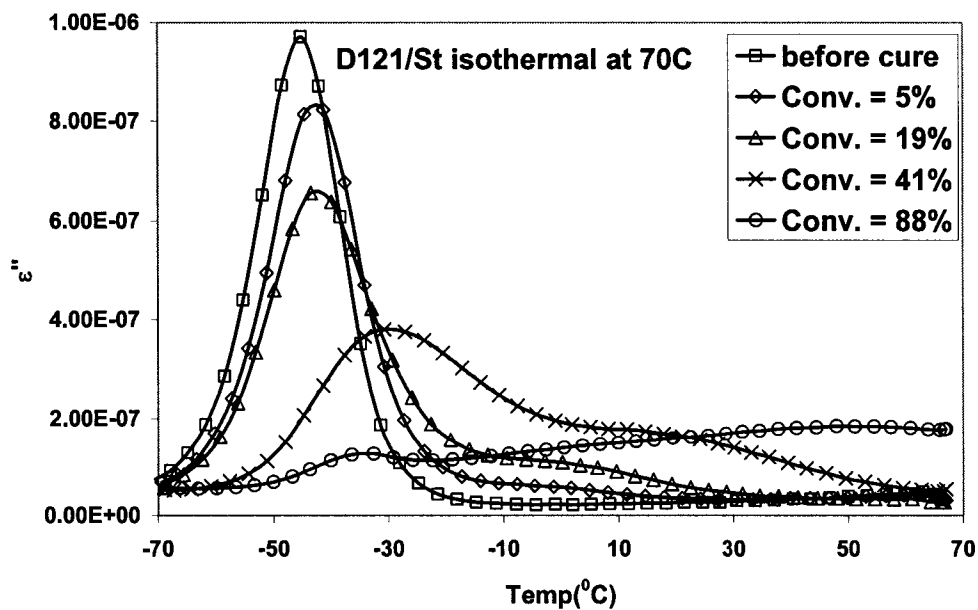


Figure 4.7b. ϵ'' versus temperature at different degrees of conversion for D121/St

Figures 4.7a and b display the evolution of α -relaxations with the advancement of the reaction. In the D121/DVB (Figure 4.7a) and in the D121/St system (Figure 4.7b), only the α -relaxation peak associated with the T_g for the monomer is observed before the reaction. As the conversion increases, the magnitude of monomer/oligomer α -relaxation peak decreases, and the shape of this peak becomes broader. These changes can be explained by the decrease of monomer concentration and formation of oligomers.

During the cure of the D121/DVB and the D121/St, another distinct relaxation peak associated with microgel/microgel clusters is formed in dielectric spectra. For D121/St, this occurs at the early stage of the reaction ($\alpha = 0.05$). This peak advances to a higher temperature and becomes broader with the increase of conversion (Figure 4.7b). The strength and shape changes of the microgel/microgel cluster relaxation peaks reflect the evolution of network formation and the existence of the spatial heterogeneity in the D121/St system.

Compared with the D121/St system, the changes in the D121/DVB monomer/oligomer α -relaxation peak show the same tendency but with a larger broadening effect as the reaction advances (Figure 4.7a). For example, at $\alpha = 0.21$, the D121/DVB monomer/oligomer relaxation peak spreads from -50°C to 10°C . However, at the same conversion, the relaxation peak for D121/St monomer/oligomer only extends from -50°C to -10°C . In contrast to the D121/St system, a less distinct relaxation peak associated with microgel/microgel clusters is observed at different degrees of cure for D121/DVB. Rather in D121/DVB, the microgel/microgel clusters particles appear to create a flat, very broad relaxation peak which is less easily discerned in the dielectric

spectra (Figure 4.7a). The relaxation of the microgels with small particle size overlaps into the monomer/oligomer relaxation and it extends to a high temperature. This peak in the relaxation spectrum is highly skewed toward a broad, flat spectrum with increasing high temperature which encompasses the relaxation properties of the microgel and microgel clusters.

The diameter distribution of the microgels in the D121/St and D121/DVB systems has been investigated with Dynamic Light Scattering (DLS) during the early stages of the reaction²⁴. The D121/DVB system has a much broader distribution in particle size (3-355nm) with a high percentage (49%) of relatively small particles (3-14 nm). In contrast, the D121/St system forms more uniform, large particles (75-158nm) at low conversion along with small particles (3-40nm). As a result, the D121/St system has two distinct relaxation peaks in the dielectric spectra. The broad distribution in size of the microgels in D121/DVB and overall the very broad overlapping relaxation of these two regions supports the much broader distribution in size and suggests a higher heterogeneous nature of D121/DVB. The differing sizes of the microgels in each system provide direct evidence for the difference in their dielectric relaxation response.

At the final stage of cure of the D121/DVB reaction, the very broad dynamic relaxation peak extends from a very low temperature (down to -45°C) to a very high temperature (higher than the reaction temperature 70°C) as the magnitude of ϵ'' is still increasing. These observations concerning the distribution of relaxation times in the final stages of cure also suggest that the breadth of the heterogeneity of the D121/DVB network structure is much larger than in D121/St. As will be discussed in section 3.2.2.3

and previously reported²¹, dynamic mechanical measurements exhibit similar differences in relaxation properties for a cured D121/DVB resin versus the D121/St resin.

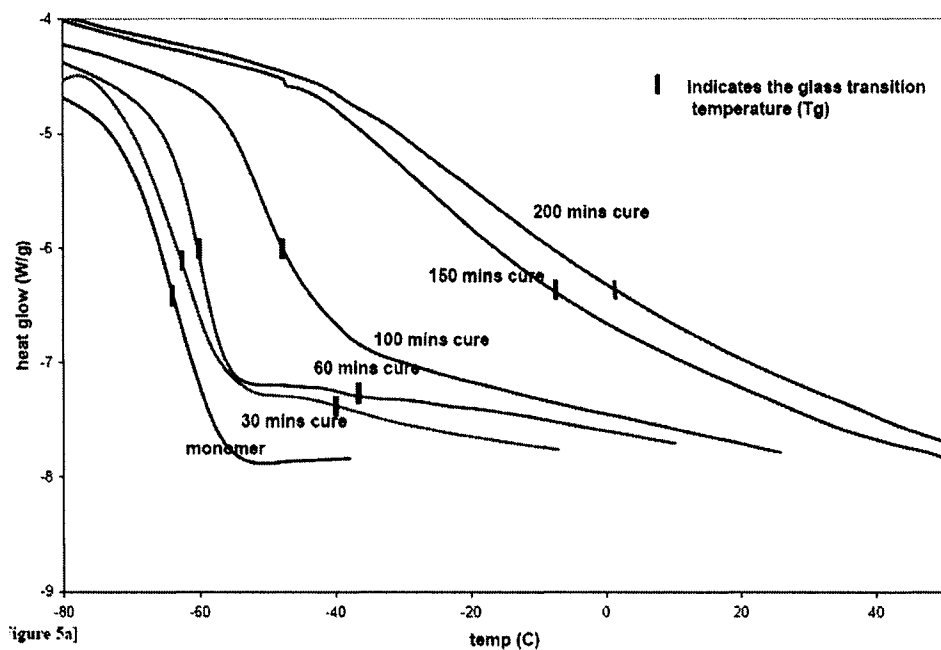


Figure 4.8a. Tg evolution during 70°C isothermal polymerization of D121/DVB

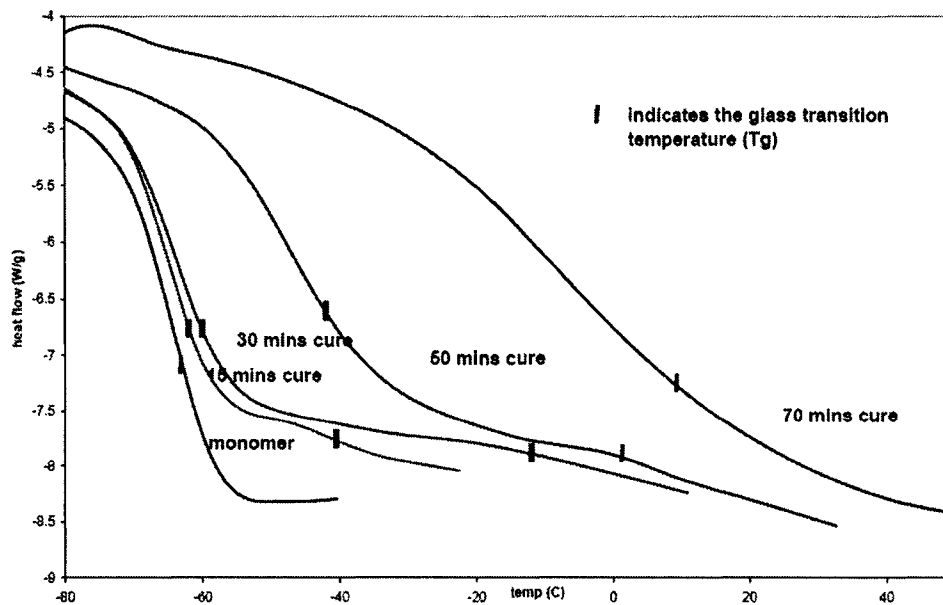


Figure 4.8b. Tg evolution during 70°C isothermal polymerization of D121/St

4.3.2.2.2. DSC profile

DSC profiles during the temperature ramp for both systems at different degrees of conversion were shown in Figures 4.8a and 4.8b. The D121/DVB monomer glass transition is observed at -65°C . As the conversion increases, the glass transition temperature for monomer/oligomer region shifts to higher temperatures, and another weak transition appears at low conversions (0.05 and 0.21). After that, the monomer/oligomer glass transition emerges with the broad glass transition of microgel/microgel clusters to form a broad transition.

The same trends are observed in D121/St system (Figure 4.8b), but the emergence of two glass transitions happens at higher conversion (after 50 minutes cure, 44% conversion). Comparing the fully cured samples for both systems, the D121/DVB has a much broader glass transition than D121/St. It also indicates a broader distribution of relaxation times involving cooperative segmental motions and more heterogeneous network formation during D121/DVB cure. One needs to stress that the D121/St has indeed a broad relaxation spectrum and that the D121/DVB system is even broader. It apparently involves a longer length scale of the boundary and interpenetration of these two regions.

4.3.2.2.3. Dynamic mechanical properties

. Viscoelastic properties of D121/St and D121/DVB systems at different conversions have been characterized in the torsion mode. Figures 4.9a-d show the evolution of the shear modulus, G' and $\tan\delta$ as a function of temperature. The dynamic

mechanical α -transition is characterized with the decrease of the shear modulus and the peak of $\tan\delta$ in the dynamic mechanical profiles. As in the dielectric relaxation measurement, the width of the transition reflects the distribution of relaxation times and the existence of two α -relaxation regions supports the existence of a spatial heterogeneity.

As seen in Figures 4.9a and 4.9b, at around 20% conversion, two α -transition peaks in $\tan\delta$ versus plot are consistent with the existence of the monomer/oligomer region and microgel/polymer region during the reaction. The dynamic mechanical measurement was made at a frequency of 2 Hz. Based on the frequency dependence of the α -transition temperature, the transition temperature measured by DMA should be lower than the FDEMS measurement (2.5 kHz) and higher than the calorimetric transition temperature measured by DSC. The results are shown in Table 3 and support the conclusion that all three measurement techniques are sensing the α -transition of both the monomer/oligomer and the microgel/polymer regions.

With the advancement of the reaction, the α -transition of monomer/oligomer region and microgel/polymer region merges and extends to a higher temperature. As seen in Figure 4.9a and 4.9b, a distinct monomer/oligomer α -transition peak is no longer observed. Rather a very broad peak which includes the monomer/oligomer and the microgel/polymer α -relaxation has increased in width at around 50% conversion for both systems in the dynamic mechanical as well as in the dielectric response. At this point, the relaxation spectrum extends from -45°C to about 80°C for the D121/St system and to even higher temperature for the D121/DVB.

In comparing the D121/St and D121/DVB systems, the structure and the functionality of the vinyl comonomer has a stronger influence on the microgel/polymer α -transition than on the monomer/oligomer region. For D121/St network at 22% conversion (Figure 4.9c), the microgel/polymer α -transition begins near -40°C and extends to 40°C . The corresponding α -transition is much flatter and broader when DVB is used as comonomer and begins at -40°C and extends to 70°C at this rather low conversion.

For D121/St network with 55% monomer conversion (Figure 4.9d), a weak broad α -transition starts around -40°C and the stronger microgel cluster α -transition has a peak at 60°C again reflecting the spatial heterogeneity and breadth of the chain mobility in the network.

For the D121/DVB network with 54% monomer conversion, only one extremely broad α -transition which extends from the monomer/oligomer α -relaxation region through the microgel cluster α -relaxation region can be observed. This is a result of the more tightly crosslinked network and the larger length scale of the boundary where the two regions interpenetrate each other in the D121/DVB system. The α -transition of the monomer/oligomer region and microgel/polymer regions have grown into each other and extend to a higher temperature than the curing temperature (70°C). The magnitude of $\tan\delta$ is still increasing with temperature as observed in D121/DVB dielectric spectroscopy at this final stage of reaction.

This DMA result supports more spatial heterogeneity in the D121/DVB system as is also indicated by dielectric spectroscopy and DSC profile. This difference is undoubtedly due to the higher functionality of the DVB.

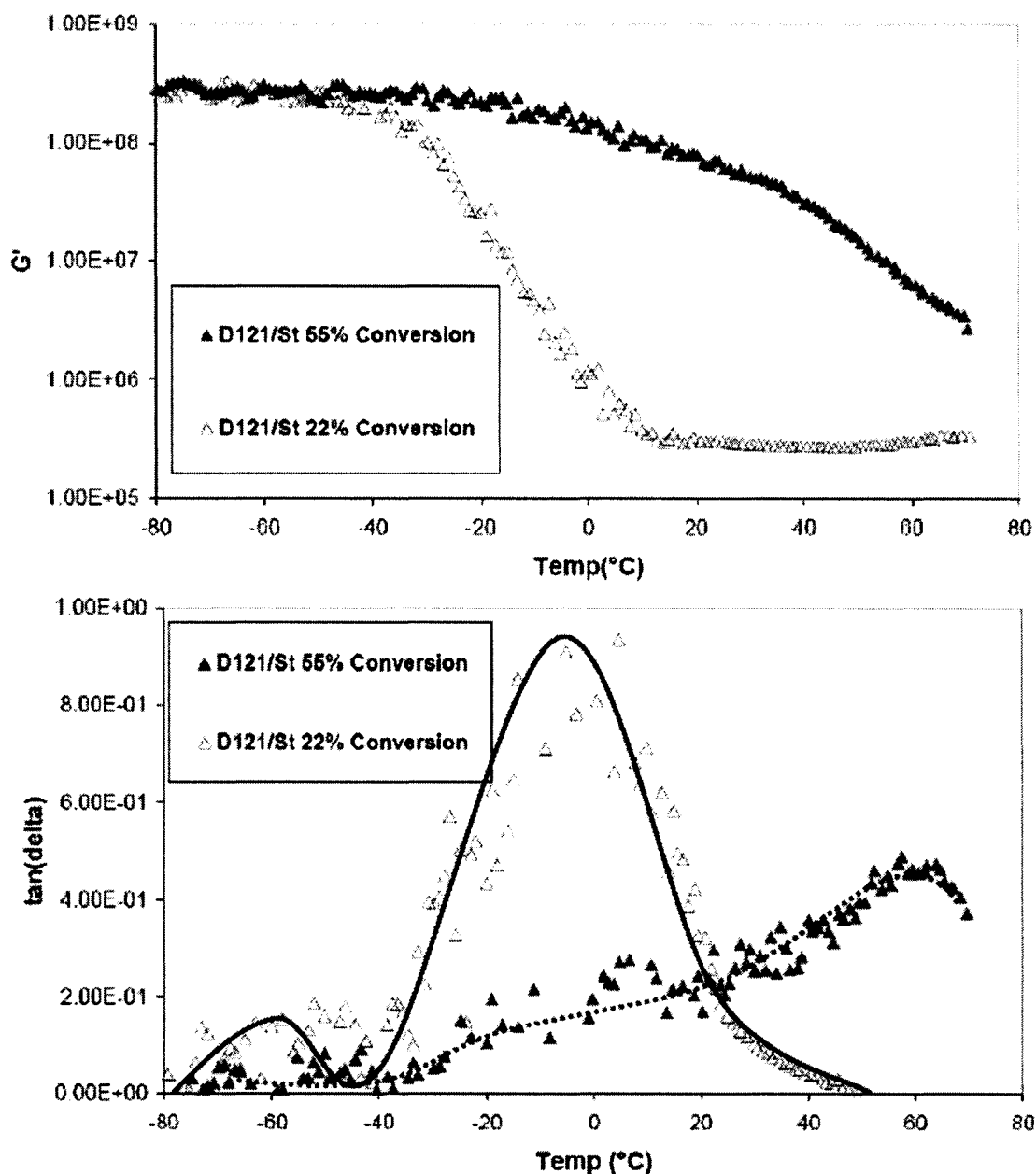


Figure 4.9a. Evolution of the storage modulus G' and $\tan\delta$ as a function of temperature for D121/St

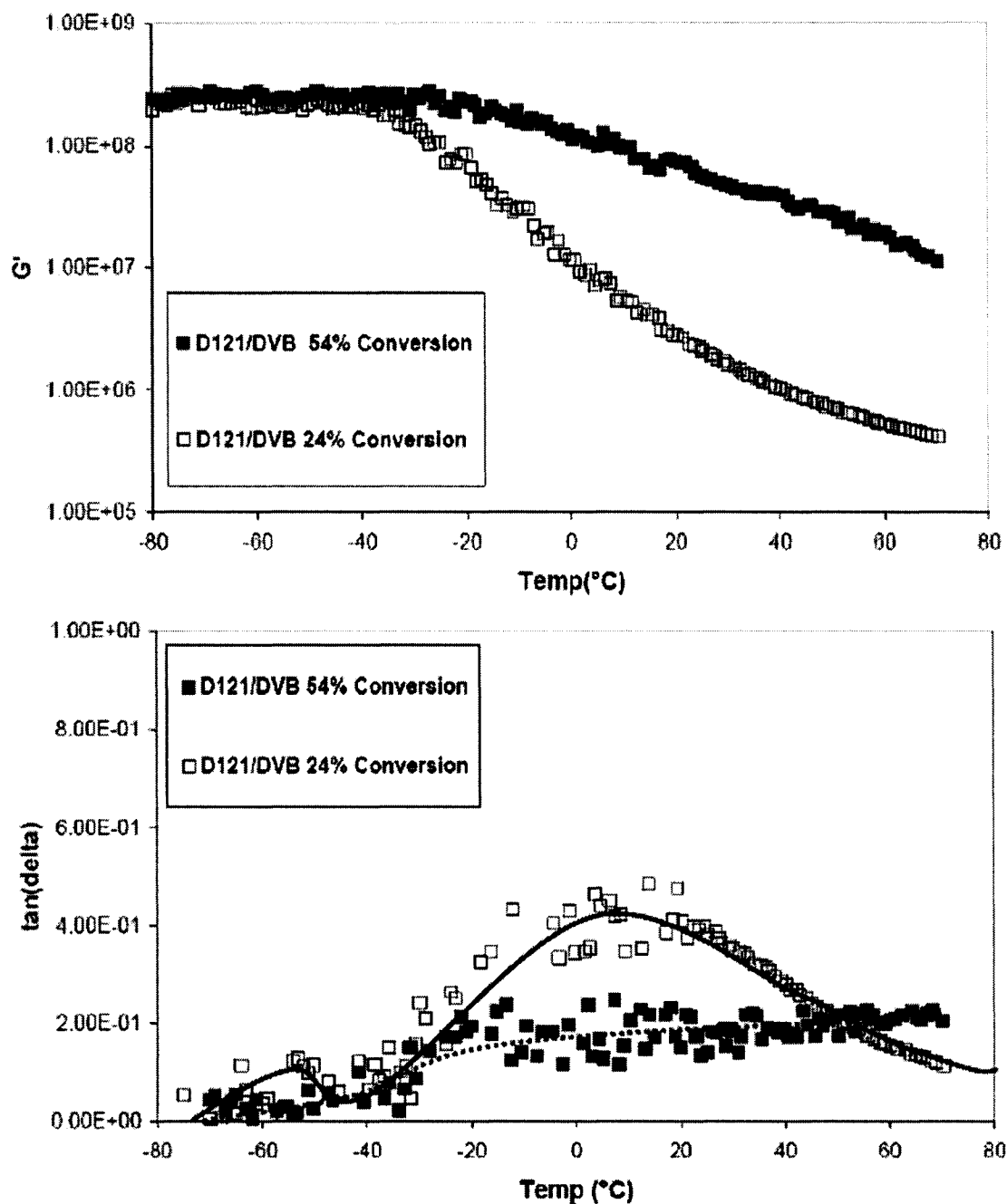


Figure 4.9b. Evolution of the storage modulus G' and $\tan\delta$ as a function of temperature for D121/DVB

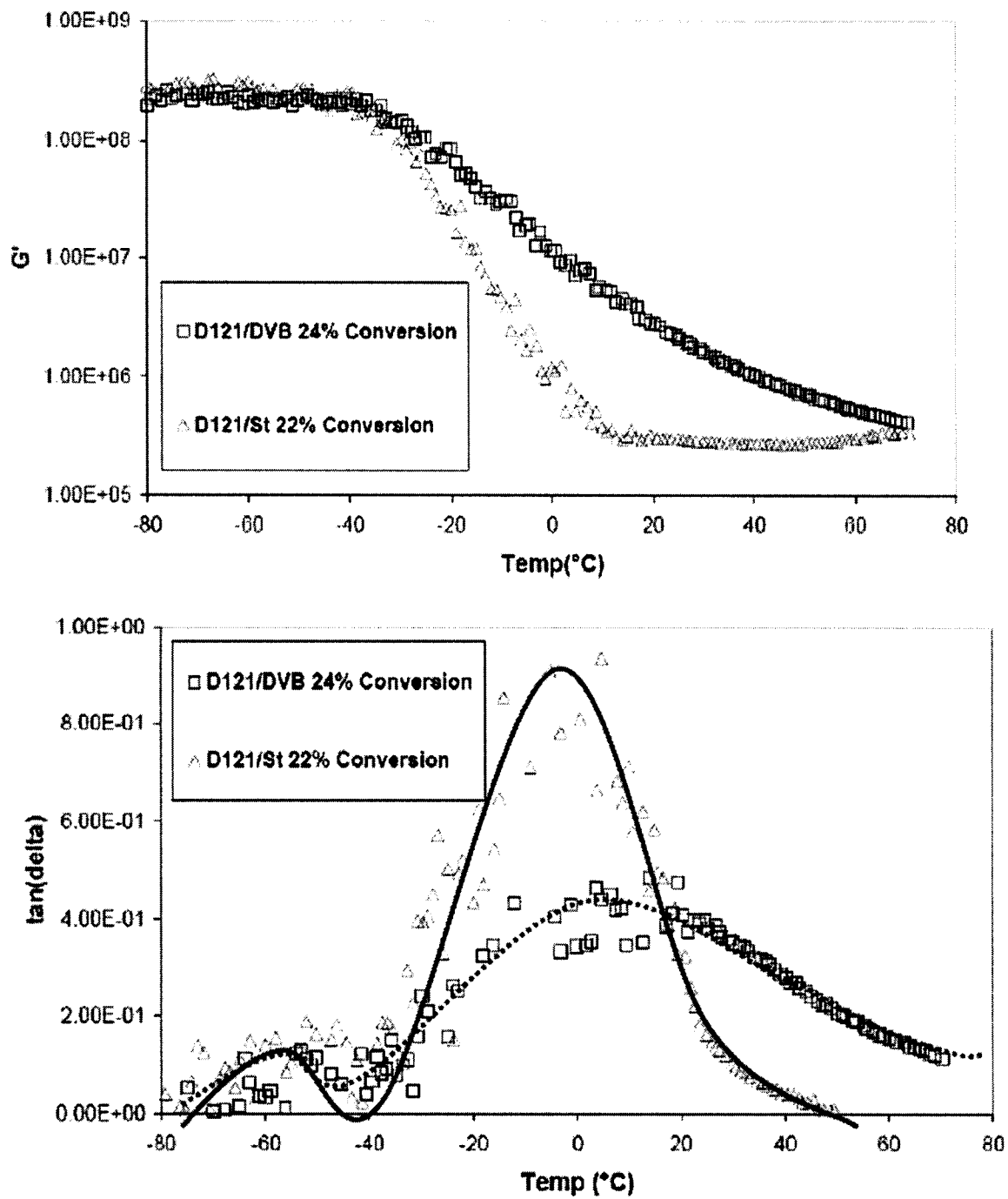


Figure 4.9b. Evolution of the storage modulus G' and $\tan\delta$ as a function of temperature for D121/St and D121/DVB at low conversion

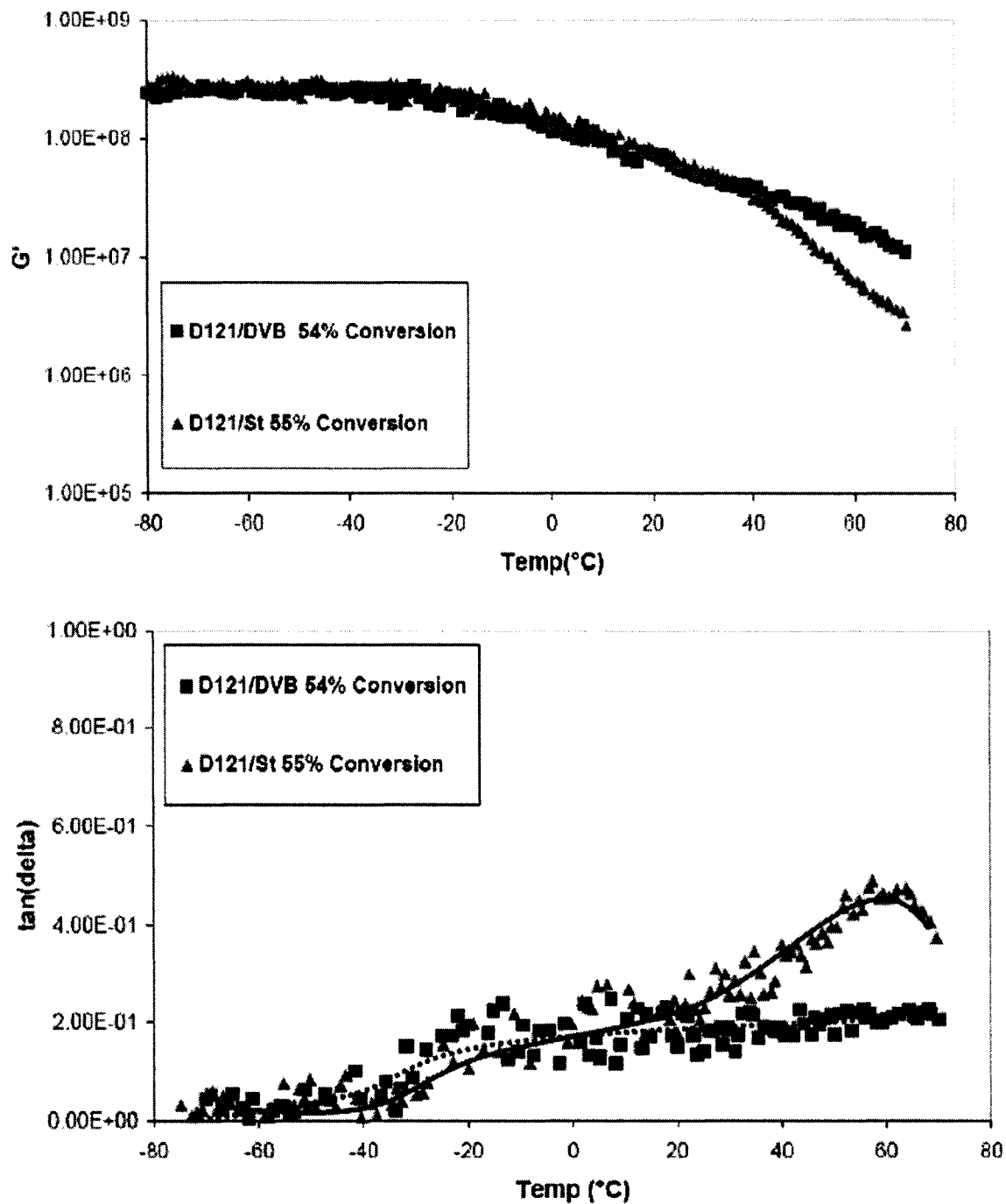


Figure 4.9d. Evolution of the storage modulus G' and $\tan\delta$ as a function of temperature for D121/St and D121/DVB at high conversion

4.3.2.2.4. Morphology from TEM images

Figure 4.10a and 4.10b show the TEM pictures for the D121/St at 54% and D121/DVB at 55% conversion. OsO₄ was used to stain the sample to give a contrast for the monomer/oligomer regions and microgel regions. The monomer/oligomer regions should have higher double bond concentration than the microgel regions during the network formation for both systems. Since the OsO₄ reacted with the double bonds to stain the polymer sample, more OsO₄ was bonded to the monomer/oligomer regions, which is supposed to give a bright region in the TEM picture. But in the TEM pictures, we can hardly observe the contrast between monomer/oligomer regions and microgel regions. This is caused by two facts: 1) The transition between monomer/oligomer region and microgel region is not sharp. There is no distinct interface between them. 2) The large amount of benzene ring in dimethacrylate and vinyl monomers would bond with OsO₄ during the staining. It creates a strong background in TEM pictures and largely decreases the contrast between the monomer/oligomer region and microgel region.

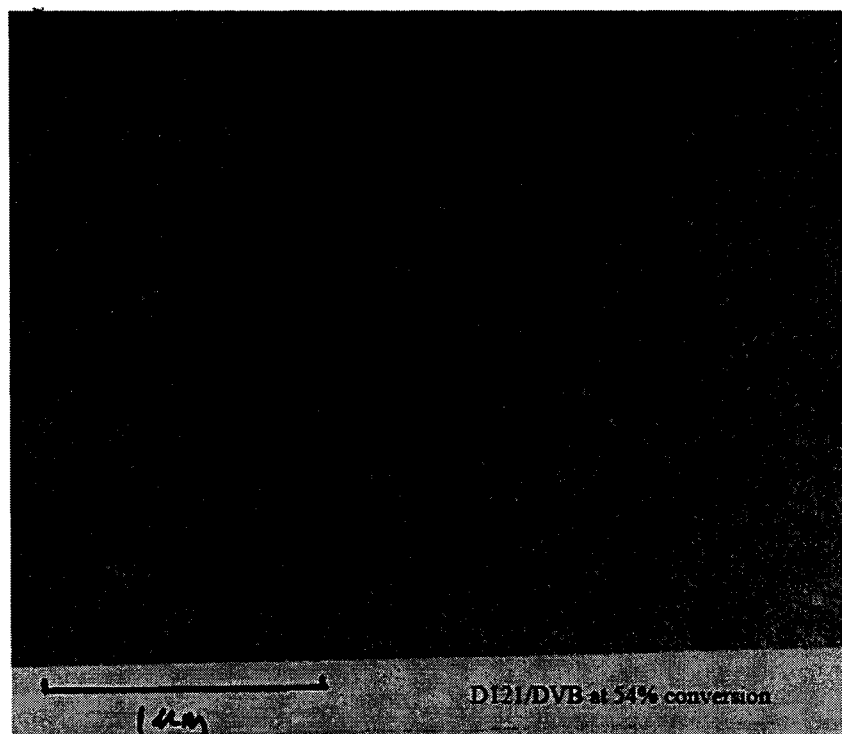


Figure 4.10a. TEM morphology for 54% conversion D121/DVB

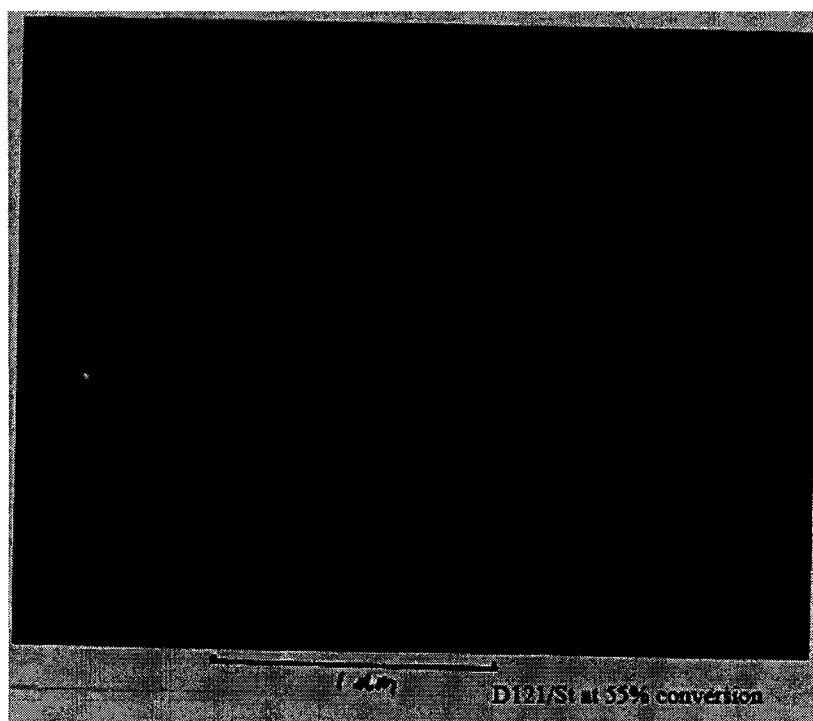


Figure 4.10b. TEM morphology for 55% conversion D121/St

4.3.2.3. Summary of the influence of the comonomer structure on the network buildup

The comonomer structures have influence on the polymerization rate, network buildup and the system heterogeneity. The use of DVB instead of St increases the mean functionality of the monomer blend and increases the cross-linking density of the microgel network formed. A significant difference between those two systems is that DVB acts as a cross-linking agent while St acts as a chain extender. This change in comonomer functionality decreases the polymerization rate and increases the heterogeneity of the network structure. It increases the breadth and decreases the sharpness of the boundary between the monomer-oligomer and microgel regions.

4.4. Conclusion

It is evident from the dielectric, rheometer and DSC results that a spatial heterogeneity develops very early during the polymerization of the dimethacrylate (D121) with both the styrene and the divinylbenzene comonomers. The spatial heterogeneity exists throughout the polymerization but the overlap or interpenetration of each region (monomer/oligomer and the microgel/microgel clusters) into the other increases as the reaction advances. At full cure, an extremely broad frequency-temperature range of relaxation times is created. It represents a very wide range of dynamics extending from the mobility of the short oligomers to the tightly crosslinked microgel clusters

It is often accepted in the polymer community that the existence of two glass transitions indicates phase separation. Thus, the question becomes “does phase separation occur in these systems early during the polymerization?” No, not in the conventional

sense in which two well defined different compositions exist with the same chemical potential. In that case, a sharp interfacial boundary separates the two chemical compositions. In this chemical homogeneous single phase system, there exists a spatial heterogeneity. This produces a dynamic heterogeneity observed in the dielectric, mechanical and DSC experiments. There are two distinct regions of differing structure, oligomers and microgels, a point confirmed by dynamic light scattering. There is not a distinct interface between them, rather there is a gradient of interpenetration of one into the other, which is why there is only one phase. What is of particular note is that in the D121/St and the D121/DVB systems, the oligomer and microgel regions are of sufficient size to exhibit distinctly different glass transitions as detected by DSC. With reaction advancement, the interpenetration of the two regions into each other increases. This creates a spatial heterogeneity encompassing oligomer regions, tightly crosslinked microgel clusters and a very large length scale of overlap and interpenetration of each into the other. Finally, we note this result provides additional evidence that the existence of two Tg's does not by itself indicate a two phase system.

REFERENCES

- (1) Alloin, F.; Sanchez, J. Y.; Armand, M. *Journal of the Electrochemical Society* **1994**, *141*, 1915.
- (2) Anseth, K. S.; Newman, S. M.; Bowman, C. N. *Advances in Polymer Science* **1995**, *122*, 177.
- (3) Koo, J.-S.; Smith, P. G. R.; Williams, R. B.; Grossel, M. C.; Whitcombe, M. J. *Chemistry of Materials* **2002**, *14*, 5030.
- (4) Leung, S. H. S.; Robinson, J. R. *Journal of Controlled Release* **1988**, *5*, 223.
- (5) Shah, J.; Ryntz, R. A.; Gunn, V. E.; Xiao, H. X.; Frisch, K. C.; Feldpausch, A.; Kordomenos, P. I. *Journal of Coatings Technology* **1989**, *61*, 61.
- (6) Stansbury, J. W. *Journal of Dental Research* **1992**, *71*, 1408.
- (7) Yukawa, Y.; Yabuta, M.; Tominaga, A. *Progress in Organic Coatings* **1994**, *24*, 359.
- (8) Roice, M.; Kumar, K. S.; Pillai, V. N. R. *Macromolecules* **1999**, *32*, 8807.
- (9) Dullens, R. P. A.; Claesson, E. M.; Kegel, W. K. *Langmuir* **2004**, *20*, 658.
- (10) Dusek, K. *Polymer Gels and Networks* **1996**, *4*, 383.
- (11) Dusek, K. *Angewandte Makromolekulare Chemie* **1996**, *240*, 1.
- (12) Dusek, K.; Matejka, L.; Spacek, P.; Winter, H. *Polymer* **1996**, *37*, 2233.
- (13) Kannurpatti, A. R.; Anderson, K. J.; Anseth, J. W.; Bowman, C. N. *Journal of Polymer Science, Part B: Polymer Physics* **1997**, *35*, 2297.
- (14) Kannurpatti, A. R.; Anseth, J. W.; Bowman, C. N. *Polymer* **1998**, *39*, 2507.
- (15) Kannurpatti, A. R.; Bowman, C. N. *Macromolecules* **1998**, *31*, 3311.
- (16) Simon, G. P.; Allen, P. E. M.; Bennett, D. J.; Williams, D. R. G.; Williams, E. H. *Macromolecules* **1989**, *22*, 3555.
- (17) Simon, G. P.; Allen, P. E. M.; Williams, D. R. G. *Polymer* **1991**, *32*, 2577.
- (18) Wilson, T. W. *Journal of Applied Polymer Science* **1990**, *40*, 1195.

- (19) Allen, P. E. M.; Simon, G. P.; Williams, D. R. G.; Williams, E. H. *Macromolecules* **1989**, *22*, 809.
- (20) Anseth, K. S.; Wang, C. M.; Bowman, C. N. *Macromolecules* **1994**, *27*, 650.
- (21) Rey, L.; Duchet, J.; Galy, J.; Sautereau, H.; Vouagner, D.; Carrion, L. *Polymer* **2002**, *43*, 4375.
- (22) Rey, L.; Galy, J.; Sautereau, H.; Lachenal, G.; Henry, D.; Vial, J. *Applied Spectroscopy* **2000**, *54*, 39.
- (23) Rey, L.; Galy, J.; Sautereau, H.; Simon, G. P.; Cook, W. D. *Polymer International* **2004**, *53*, 557.
- (24) Rey, L.; Galy, J.; Sautereau, H. *Macromolecules* **2000**, *33*, 6780.
- (25) Bonnet, A.; Pascault, J. P.; Sautereau, H.; Rogozinski, J.; Kranbuehl, D. *Macromolecules* **2000**, *33*, 3833.
- (26) Baillif, P.; Tabellout, M.; Emery, J. R. *Polymer* **2000**, *41*, 5305.
- (27) Boyd, R. H.; Devereaux, R. W.; Thayer, R. B. *Polymer Preprints (American Chemical Society, Division of Polymer Chemistry)* **1990**, *31*, 279.
- (28) Se, K.; Takayanagi, O.; Adachi, K. *Macromolecules* **1997**, *30*, 4877.
- (29) Ngai, K. L.; Mashimo, S.; Fytas, G. *Macromolecules* **1988**, *21*, 3030.
- (30) Fournier, J.; Williams, G.; Holmes, P. A. *Macromolecules* **1997**, *30*, 2042.
- (31) Espadero Berzosa, A.; Gomez Ribelles, J. L.; Kripotou, S.; Pissis, P. *Macromolecules* **2004**, *37*, 6472.
- (32) Dudognon, E.; Bernes, A.; Lacabanne, C. *Macromolecules* **2001**, *34*, 3988.
- (33) Dudognon, E.; Bernes, A.; Lacabanne, C. *Macromolecules* **2002**, *35*, 5927.
- (34) Schroeter, K.; Unger, R.; Reissig, S.; Garwe, F.; Kahle, S.; Beiner, M.; Donth, E. *Macromolecules* **1998**, *31*, 8966.
- (35) Theobald, S.; Pechhold, W.; Stoll, B. *Polymer* **2000**, *42*, 289.
- (36) Bedekar, B. A.; Tsuji, Y.; Ide, N.; Kita, Y.; Fukuda, T.; Miyamoto, T. *Polymer* **1995**, *36*, 4735.

- (37) Calleja, R. D.; Garcia-Bernabe, A.; Sanchez-Martinez, E.; Hormazabal, A.; Gargallo, L.; Gonzalez-Nilo, F.; Radic, D. *Macromolecules* **2001**, *34*, 6312.
- (38) Mijovic, J.; Sy, J.-W.; Kwei, T. K. *Macromolecules* **1997**, *30*, 3042.
- (39) Sy, J. W.; Mijovic, J. *Macromolecules* **2000**, *33*, 933.
- (40) Zhang, S.; Jin, X.; Painter, P. C.; Runt, J. *Macromolecules* **2002**, *35*, 3636.
- (41) Aihara, T.; Saito, H.; Inoue, T.; Wolff, H.-P.; Stuhn, B. *Polymer* **1997**, *39*, 129.
- (42) Pascault, J. P.; Sautereau, H.; Verdu, J.; Williams, R. J. J.; Marcel Dekker, 2002.
- (43) Landin, D. T.; Macosko, C. W. *Macromolecules* **1988**, *21*, 846.
- (44) Zhu, S.; Tian, Y.; Hamielec, A. E.; Eaton, D. R. *Macromolecules* **1990**, *23*, 1144.
- (45) Zhu, S.; Tian, Y.; Hamielec, A. E.; Eaton, D. R. *Polymer* **1990**, *31*, 154.
- (46) Zhu, S.; Tian, Y.; Hamielec, A. E.; Eaton, D. R. *Polymer* **1990**, *31*, 1726.
- (47) Kloosterboer, J. G.; Lijten, G. F. C. M.; Greidanus, F. J. A. M. *Polym. comm.* **1986**, *27*, 268.
- (48) Kloosterboer, J. G.; van de Hei, G. M. M.; Boots, H. M. J. *Polym. comm.* **1984**, *25*, 354.
- (49) Kloosterboer, J. G.; van de Hei, G. M. M.; Gossink, R. G.; Dortant, G. C. M. *Polym. comm.* **1984**, *25*, 322.
- (50) Kloosterboer, J. G.; van de Hei, G. M. M.; Boots, H. M. J. *Polym. comm.* **1984**, *25*, 354-357.
- (51) Parthun, M. G.; Johari, G. P. *Macromolecules* **1992**, *25*, 3254.
- (52) Parthun, M. G.; Johari, G. P. *Macromolecules* **1993**, *26*, 2392.
- (53) Schonhals, A. In *Dielectric Spectroscopy of polymeric materials*; Runt, J. P.; Fitzgerald, J. J., Eds.; American Chemical Society, 1997; pp 81-106.
- (54) Ferry, J. D. *viscoelastic properties of polymers*, 3th Edition ed.; John Wiley & Sons, Inc., 1980.
- (55) Wang, B.; Wang, Z. F.; Zhang, M.; Liu, W. H.; Wang, S. J. *Macromolecules* **2002**, *35*, 3993.

- (56) Meijerink, J. I.; Eguchi, S.; Ogata, M.; Ishii, T.; Amagi, S.; Numata, S.; Sashima, H. *Polymer* **1994**, *35*, 179.
- (57) Salgueiro, W.; Marzocca, A.; Somoza, A.; Consolati, G.; Cervený, S.; Quasso, F.; Goyanes, S. *Polymer* **2004**, *45*, 6037.
- (58) Moynihan, C. T.; Boesch, L. P.; Laberge, N. L. *physics and chemistry of glasses* **1973**, *14*, 122.
- (59) Bartolomeo, P.; Chailan, J. F.; Vernet, J. L. *Polymer* **2001**, *42*, 4385.
- (60) Williams, G. In *Dielectric Spectroscopy of Polymeric Materials*; American Chemical Society: Washington D.C., 1997; pp 3-66.
- (61) Williams, G.; Watts, D. C. *Trans. Faraday Soc.* **1970**, *66*, 80.
- (62) A. Schonhals, F. K. In *Broadband Dielectric Spectroscopy*; Friederich Kremer, A. S., Ed.; Springer-Verlag, 2002; pp 349-384.

CHAPTER 5. DYE DIFFUSION – A VISUALLY COLOR CHANGING (VCP) SYSTEM

5.1. Introduction

Visually Changing Paper (VCP) is a new type of printing technology that makes words and images visually appear at different times from several minutes to several weeks. It performs as an image ‘time-releasing’ device. It works by placing a self-adhesive frontpart on top of a backpart, which contains the image to be revealed. As soon as the two parts are adhered together, the VCP is “activated”, the image appearing process begins and the image becomes visible after the time specified by the design of the “front part”. The timing control is dependent only on the materials and construction of the frontpart and backpart, which makes VCP an easy-to-use, disposable and ‘label-like’ product that requires no hardware, no electronics or other accessories of any kind to function.

The image appears by means of a dye migration technology; dyes migrate out of the printed ink on the backpart into the layers on the frontpart. As long as two parts are kept separate, no migration occurs. But when the adhesive frontpart comes into contact with the printed backpart, the timing begins for the appearance of the images as a result of the initiation of a physical/chemical process.

VCP products offer solutions to various security concerns faced by all types of businesses. By helping identify visitors and alerting staff when a visitor's badge is expired, VCP products increase security and enhance access control to better protect people, facilities, and information. It can be used for the following applications:

- Visitor management
- Expiring ID badges
- Aging time of products such as foods and drugs which degrade
- Security tapes and seals

5.2. Dye Migration Mechanism

Immediately after the visually color changing paper is activated by attaching the frontpart to the backpart substrate, the image is not yet revealed. Physical and chemical processes are designed to control the ink migration. The image is hidden, covered or blocked to make it invisible at the beginning; generally, there are two ways to create a latent image with a controlled time.

5.2.1. Simple diffusion process

The basis of this technique is using an opaque adhesive layer with a certain thickness to hide the migrating ink and create a timing effect. When one looks at the adhesive layer, the image cannot be observed by the eye. Upon contact, dye flows slowly into the opaque adhesive layer. As the dye goes through the opaque adhesive layer, the migrating ink begins to be seen by the viewer. At first the color is faint, and will eventually turn dark as more ink migrates through the opaque adhesive layer. Figure 5.1 is the design for the VCP system described above.

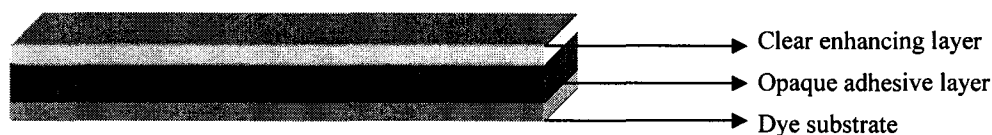


Figure 5.1. Simple diffusion system

The dye concentrates in the enhancing layer above the opaque adhesive layer to produce an intense color.

In this design, the thickness of the opaque adhesive layer controls the color-changing timing by a diffusion process. A thicker adhesive layer creates a longer timing effect, but also make it hard to determine the exact start time of the color change. It takes a long time for the color change from an off-white, faint color to an intensive color. With a thick opaque adhesive layer, the color change time would always be ambiguous for the long-term color changing system. The envisioned time period for expiration would be several weeks or several months.

5.2.2. Chemical reaction controlled timing process

In order to develop a quick-triggered, longer-term timing process, the mechanism for the color change should not be controlled only by the dye diffusion process. Ideally, the dye should remain immobilized until it is activated by another event or process. After the activation, the dye should be able to migrate very rapidly though the opaque layer to show the color in the enhancing layer. One approach is to use chemical reactions to control the initiation of the ink or dye diffusion process. A pH triggered dye structure conversion is sensitive, and convenient to meet this requirement. A small change of pH in

the environment around the neutralization point can change the dye structure from a polar non-migration to a non-polar migration state. A long-term VCP system is possible to be achieved with the transformation of a non-migrating dye to a migrating dye triggered by a change in the pH environment.

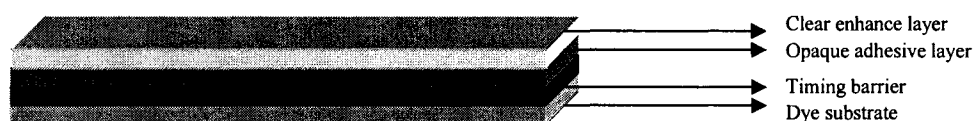


Figure 5.2. Design of long-term VCP system

In the long-term VCP system (Figure 5.2), a timing barrier with an acid-base neutralization reaction is designed to activate the transformation of a non-migrating dye to a migrating dye. The opaque adhesive layer for diffusion is thin to obtain a sharp color change in a short time.

It is reported¹ that the reaction product of amine and aldehyde bisulfite, which is called an ionamine, is a water-soluble polar salt compound that cannot be dissolved in a non-polar organic solvent. In the base environment, this ionamines readily decompose to the corresponding non-polar structure. Cellulose acetate or poly(vinylacetate) films can be used as a selectively permeable barrier, allowing the diffusion of a non-polar compound, but rejecting a highly polar one. This feature of ionamine makes it a promising candidate for our VCP system

Thus, research needs to solve the following problems for this new approach to the long-term, quick triggered VCP:

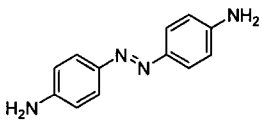
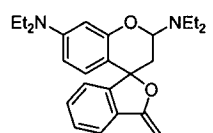
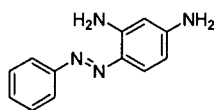
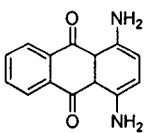
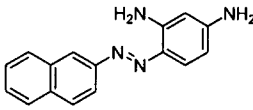
- Prepare the polar state of dyes (ionamines) from non-polar dyes

- select a vehicle or resin substrate in which the polar state of the dyes could be dispersed and is immobile
- Select an activator to transform the dye from a polar, non-migrating structure to a non-polar, migrating structure
- Find the most effective way to deliver the activator into the polar dye substrate
- Test and modify this new VCP system to optimize the results

5.3. Stability and migration tests

Five non-polar dyes (Table 5.1) were investigated in our research. All these dyes are commercially available.

Table 5.1. Structures of unmodified non-polar dyes

Banana Yellow (BY) $C_{12}H_{12}N_4$ Mol. Wt.: 212.25	
Neptun Red (NR) $C_{25}H_{32}N_2O_2$ Mol. Wt.: 392.53	
Neptun Orange (NO) $C_{12}H_{12}N_4$ Mol. Wt.: 212.25	
Keyplast Violet PF (KV) $C_{14}H_{12}N_2O_2$ Mol. Wt.: 240.26	
Fat Brown (FB) $C_{16}H_{14}N_4$ Mol. Wt.: 262.31	

These dyes need to be converted to a polar state to keep them from migrating through the non-polar films. Ionamines were synthesized according to the standard procedure described in following text (Chapter 5.4). Ionamine formation involves the reaction of a bisulfite salt of an aldehyde with an existing primary amine. Bisulfite analogs of propionaldehyde, butyraldehyde and benzaldehyde were synthesized by addition of sodium bisulfite to the corresponding aldehyde. The sodium bisulfite adduct of formaldehyde was purchased from Aldrich Chemical Corporation.

Table 5.2. Structures of modified polar state dyes (ionamines)

BY Formaldehyde Bisulfite product (BY-FBP)	
BY Butyraldehyde Bisulfite product (BY-BAB)	
BY Benzaldehyde Bisulfite product (BY-BZB)	
NO Formaldehyde Bisulfite product (NO-FBP)	
NO Butyraldehyde Bisulfite product (NO-BAB)	
NO Benzaldehyde Bisulfite product (NO-BZB)	
FB Formaldehyde Bisulfite product (FB-FBP)	

We examined the reaction products from different starting materials, and found that not all dyes form the corresponding ionamines as expected.

Neptun-Red (NR) does not react with aldehyde sodium bisulfite to get the corresponding ionamines derivatives due to solubility and lack of a primary amine group.

Although we obtained a very dark violet-colored material for Keyplast-Violet (KV), the product readily migrated through a one-hour sticker as did the starting-unreacted dyes. Examination of this solid by infrared spectroscopy showed that the adduct was devoid of aromatic groups present in the starting material and only sulfite stretching absorptions were recorded. Consequently, we believed that the solid obtained was formaldehyde bisulfite contaminated with KV to impart a significant color. Most likely, the presence of ketone on the side of the primary amine would not favor the equilibrium to form the ionamine product.

According to elemental analysis, only one primary amine of Fat Brown (FB) and Neptun Orange (NO) reacted with formaldehyde sodium bisulfate, the secondary amine does not favor the ionamine product due to the spatial limitation. Only Banana Yellow (BY) reacted with aldehyde sodium bisulfite quantitatively in a 1:2 mole ratio.

The reaction products obtained are listed in Table 5.2. We tested the stability of these ionamines with a hourly sticker. In table 5.3, we generally found that for NO, the formaldehyde bisulfate ionamine product was the least stable adduct whereas the benzaldehyde adduct was the most stable. For BY, the opposite trends hold true, the formaldehyde product was the most stable and benzaldehyde adduct was the least stable. Overall, the NO products were more variable in stability than those of BY. As shown in Table 5.3, FB and BY formaldehyde bisulfite adducts are the most stable ionamines in

the test. No obvious migration was detected during the observation period of more than 5 months.

Base (NaOH) was investigated as a decomposition initiator on the formaldehyde bisulfite ionamine BY-FBP, FB-FBP as well as NO-FBP. It appears that hydroxide caused all products tested to migrate through hourly stickers.

Table 5.3. Ionamines and their stability

Dye	Migration environment*	Time of migration
BY	-	2 hours
	w/ water	2 hours
	w/ <i>p</i> -TSA and water	2 hours
BY-FBP	-	No migration
	w/ <i>p</i> -TSA and water	No migration
	w/ dried NaOH	1 day
	w/ NaOH and water	2.5 hours
BY-BAB	-	4 days
BY-BZB	-	5.5 hours
NR	-	1.5 hours
NO	-	1 hour
NO-FBP	-	4 hours
	w/ <i>p</i> -TSA	4 hours
	w/ NaOH	2 hours
NO-BAB	-	1 day
NO-BZB	-	3 days
KV	-	1 hour
FB	-	2 hours
FB-FBP	-	No migration
	w/ <i>p</i> -TSA	No migration
	w/ NaOH	3 hours

*Standard migration test method: all dyes, dye/base and dye/acid mixtures were tested with Temtec hourly sticker at room temperature and lab humidity

p-TSA = *para*-toluenesulfonic acid

NaOH = crushed sodium hydroxide pellets

The effect of acid (*para*-toluene sulfonic acid (pTSA)) was examined on all dyes and ionamines. Generally, this did not lead to consistent affects on migration rates of any

of the ionamines studied and the migration of free dyes (i.e., unmodified BY and NO). The pTSA had no noticeable effect on the migration of unmodified or modified dyes. By testing the base, acid effects on ionamines separately, we tried to formulate a combination of base and acid such that it would decompose the ionamines in a controlled way.

5.4. Dye synthesis and modification

Banana Yellow (BY)

Banana Yellow (4,4'-diaminoazobenzene) was synthesized according to the procedure described in the reference²:

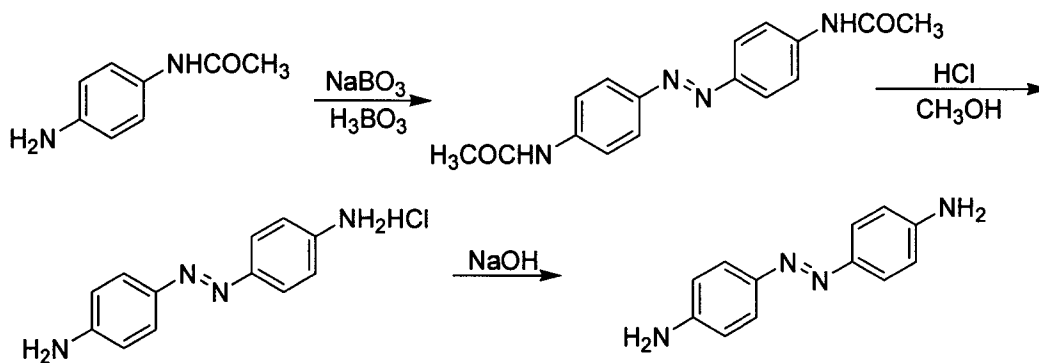


Figure 5.3. Scheme of Banana Yellow preparation

Chloride substituted BY

Since BY-FBP has good performance in stability and in migration tests, we wanted to add some electron withdrawing groups on BY's aromatic ring, which will shift its vis-light absorbency to a longer wavelength, to get a red or violet color.

Although we synthesized the compound 2,2'-dichloro-4,4'-diaminoazobenzene, but it was not red as reported in the literature³. Actually, it was also yellow, albeit a bit darker than the Banana Yellow had been using.

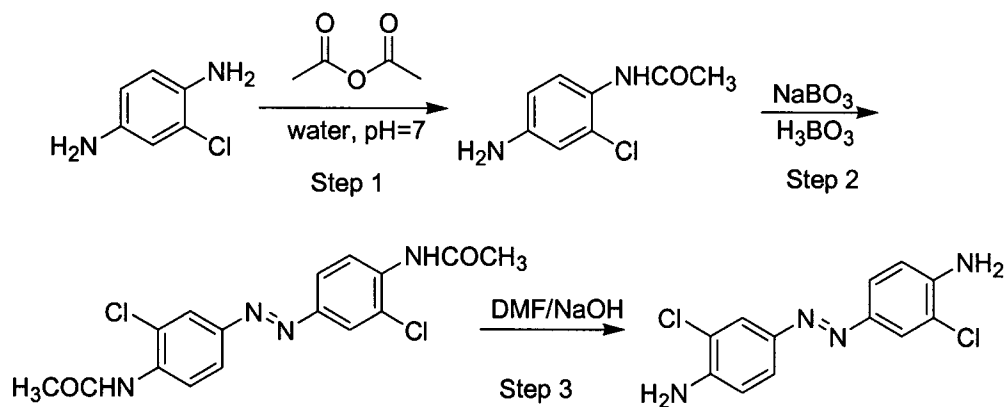


Figure 5.4. Scheme of Chloride substituted Banana Yellow preparation

Procedure to synthesize the compound 2,2'-dichloro-4,4'-diaminoazobenzene.

Dissolve 10 gram (0.07mol) of 1,4-diaminobenzene in 150 mL water at 0-2 °C. Simultaneously and uniformly add 5.9g 50% NaOH (0.074 mol) and 6.3 g acetic acid anhydride (0.063mol) drop by drop. Keep the pH at 7. After completing the addition, adjust the pH to 7, heat to 95 °C and react for 3 h with active carbon as decolorizing agent, then filter it to get solution, add Na_2SO_4 to the clear solution as a stabilizing agent. Cool the solution to 10 °C and collect the solid. Dry in the oven to obtain 2-chloro-*p*-aminoacetanilide.

In a 250 mL three-necked round-bottomed flask equipped with an efficient stirrer, a reflux condenser, and a thermometer is placed 125 mL of glacial acetic acid, 8.4 g 2-chloro-*p*-aminoacetanilide, 10 g sodium perborate tetrahydrate, and 2.5 g of boric acid. The mixture is heated with stirring to 50-60°C and held at this temperature for 6 hours.

Initially the solids dissolve but, after heating for approximately 40 min, the product begins to separate. At the end of the reaction period, the mixture is cooled to room temperature and the yellow product is collect. It is washed with water until the washings are neutral and then dried in an oven at 110 °C to afford 3,3'-bis(chloro)-4,4'-bis(acetamido)azobenzene.

In a 250 mL round-bottomed flask equipped with an efficient stirrer and a reflux condenser is placed 150 mL of *N,N'*-dimethylformamide, 6.5g NaOH and 5.6g 3,3'-bis(chloro)-4,4'-bis(acetamido)azobenzene. Heat the solution to reflux, and the color turns into bright red. Reflux for 2 hours, cool the solution to room temperature, and pour it into 500 ml of water in a 1-L beaker equipped with a stirrer, the yellow solid product separates in water. The 3,3'-bis(chloro)-4,4'-diaminoazobenzene was washed with water, and dried under reduced pressure.

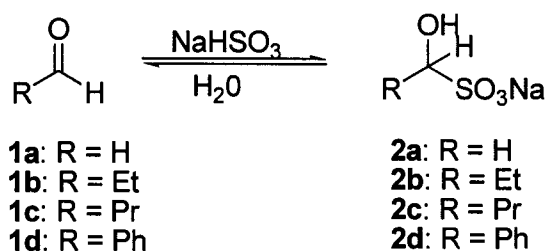


Figure 5.5. Scheme of aldehyde bisulfite salts preparation

Standard procedure for aldehyde bisulfite salts synthesis

Mix 25 mL of supersaturated sodium bisulfite in a 1:2 molar ratio with aldehyde addition in 50mL round bottom flask. Stir for 5 minutes then filter the precipitate with a Buchner funnel. Wash twice with 5mL 100% ethanol and diethyl ether and dry the solid at room temperature for several minutes. Recrystallize the solid from ethanol, collect the crystalline and dry it in the air.

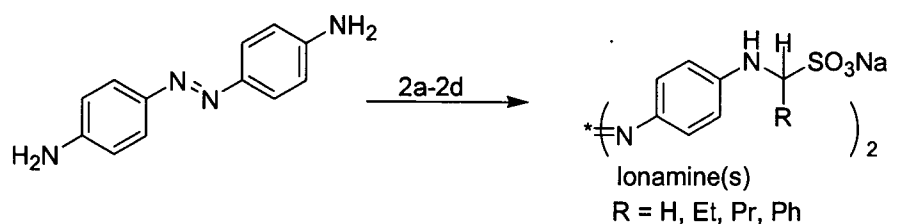


Figure 5.6. Scheme of ionamines preparation

Standard procedure for ionamine synthesis

In a two neck round bottom flask, with a magnetic stirrer, reflux condenser, thermometer, heating plate, stirring mantle, mix in a 2:1 molar ratio, aldehyde bisulfite addition, and dye starting material. Add 200 mL of 50/50 solution of ethanol-methanol mixture, 20 mL of 2-propanol, and 2 mL of methyl isobutyl ketone. Stir and heat the mixture for approximately 6 hours, leaving to cool overnight. Filter the reddish brown precipitate using a Buchner funnel and vacuum. Let air dry overnight, and then dry for several hours on filter paper in 105°C oven to remove solvents

5.5. Experimental Tests on the VCP System

5.5.1. System design

As described above, acids can stabilize the ionamines, and base can decompose them to form non-polar migrating state. This structure conversion is very sensitive to pH changes. So a base/acid neutralization reaction was applied to trigger the mobility of the dye. We put ionamines into an acid substrate and controlled the base diffusion into this substrate to neutralize the acid, which changes the pH of the environment slowly. When all the acid is neutralized, a small amount of additional base diffusing into the substrate

will decompose the ionamine and trigger the migration of the dye. The following design (Figure 5.7) is applied in our research.

In order to develop such a system, various factors should be considered and optimized to get the best result. The first step is to find the suitable materials (such as acid, base, plasticizer and resin for polymer films). After identifying the materials meeting the requirements, we varied the experimental conditions (base acid ratio, film thickness etc.) to optimize the results.

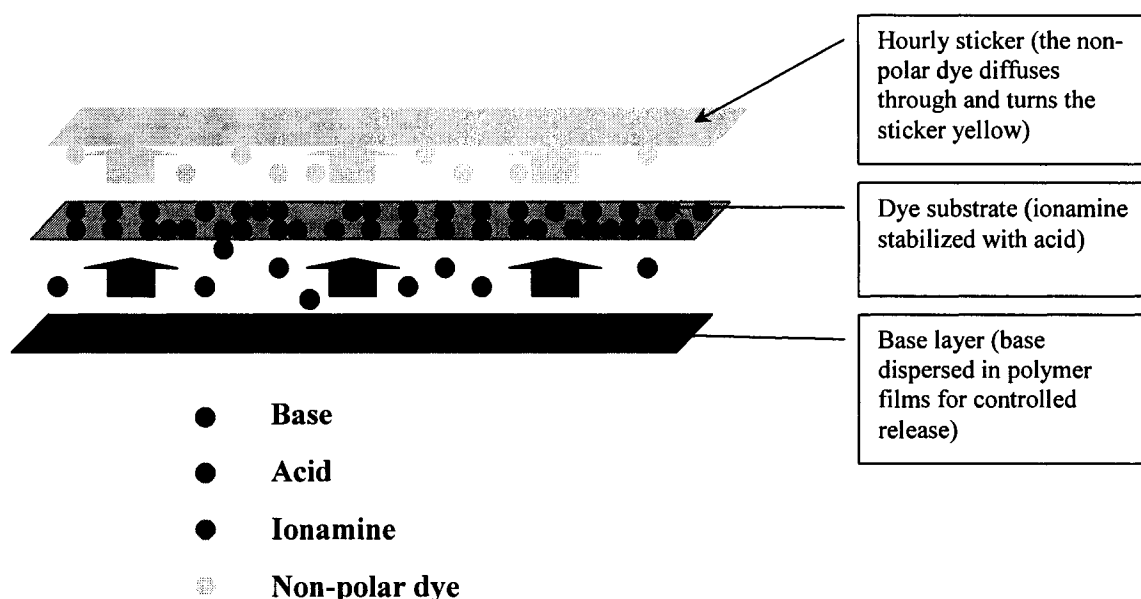


Figure 5.7. Fast triggered, long-term VCP system

5.5.2. Polymer film

As mentioned above, the cellulose acetate or poly(vinylacetate) films can be used as a selectively permeable barrier, allowing the diffusion of non-polar compound, but

rejecting polar compounds. We dispersed ionamines in a polymer film, which can hold the polar dye and release it after the dye is decomposed. We also put base into the same film to get a good compatibility between the base layer and dye substrate. A small amount of glycol was added into the base layer to help the base releasing and act as plasticizer.

In our experiments, we used two materials to cast poly(vinylacetate) films. One was poly(methyl methacrylate) (PMMA) with a molecular weight around 120,000, the other was DURO-TAK 80-1100 adhesive (composed of vinyl acetate polymers and oligomers) purchased from National Starch Corp. The PMMA film is rigid and needed some plastizer to make it flexible. The following is the procedures to cast these two films

PMMA films casting

Mix the PMMA particles with plasticizer and other components, then the mixture was dissolved in ethyl acetate by heating it to get a uniform, low viscosity, flowing liquid, Cast the film on a hot glass plate using a casting rod before it cooled down. The solvent was evaporated in the hood overnight. Peel the film off the glass.

DURO-TAK 80-1100 adhesive film casting

Dissolved the components in a certain amount of ethyl acetate. After all solids were dissolved, added adhesive into the solution. Ultrasonic wave was used to mix them and obtained a viscous liquid solution. The solution was spread onto a waxed paper and left in the hood for 1-2 days to evaporate the ethyl acetate. The film was heated in a 150°C convection oven for 3 minutes to create a gel-like film which was cut into small pieces for migration experiments.

5.5.3. Acid

Eleven acids (Table 5.4) were tested. The acid films were made by Brady Corp. with varied wt% concentration (10%, 20% and 30%) in a DURO-TAK 80-1100 adhesive film.

Table 5.4. Structures of acids

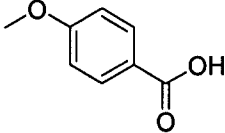
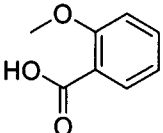
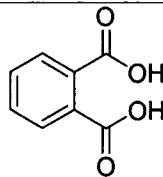
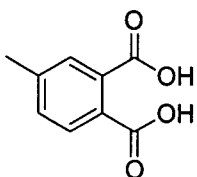
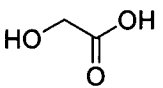
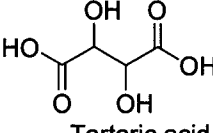
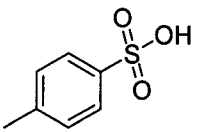
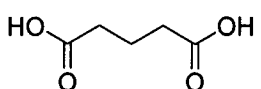
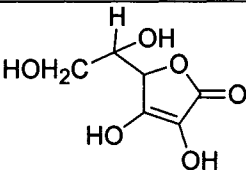
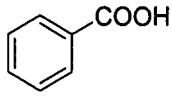
 p-Anisic	 o-Anisic	 phthalic
 methyl phthalic	 glycolic acid	 Tartaric acid
 p-toluenesulfonic acid	 Glutaric	$C_{76}H_{52}O_{46}$ Tannic
 Ascorbic acid	 benzoic acid	

Table 5.5 lists the experiment results with different acid/base ratio. It shows that at constant acid concentration, increasing the base concentration speeds up the diffusion time (the color comes through faster). It also seems that varying the acid concentration

has no obvious effect on the total color-changing time for benzoic acid. Perhaps benzoic acid is not strong enough to react with 2-amino-2-ethyl-1,3-propanediol (AEPD) efficiently.

Table 5.5. Acid (benzoic acid) and Base (AEPD)* ratio effects

Acid/Base Ratio (mol).	Time for Faint Color (Day)	Time for Final Strong Color (Day)
1 : 1	6	**
1 : 2	3	26
1 : 5	2	5
2 : 1	8	-
2 : 5	2	5
3 : 1	6	-
3 : 2	2	-
3 : 5	2	5

* Acid and base are dispersed in DURO-TAK 80-1100 adhesive film, the thickness of all adhesive films is around 0.3mm.

** - indicates the color never turns to strong in the observation period

Table 5.6 reports results for the color-changing tests with different acids. AEPD DURO-TAK 80-1100 adhesive base film is used to set up all these tests. The variation of color-changing time is related to the acidity of the acid for the same base film. It seems that strong acids can create a better timing effect due to a more efficient neutralization reaction.

From the experimental data, *p*-TSA, tartaric and glutaric acid work the best among all these acids. Most of the acids have a constant timing effect, such as methyl phthalic, *p*-anisic. *p*-TSA, tartaric and glutaric acid have a significant difference in the timing effect for various acid concentrations.

Table 5.6. Color-changing test with different acids*

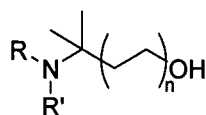
Acid	Acid/Base Ratio (mol).	Time for Faint Color (Day)	Time for Final Strong Color (Day)
Phthalic	1 : 1	8	-**
	1 : 3	8	11
	1 : 5	5	8
	2 : 3	8	13
	2 : 5	5	8
	3 : 5	5	8
Glycolic	1 : 5	4	7
	2 : 5	4	7
Ascorbic	1 : 5	7	13
	2 : 5	7	15
	3 : 5	7	-
Glutaric	1 : 5	7	10
	2 : 5	9	21
	3 : 5	-	-
Tannic	2 : 5	7	9
	3 : 5	7	9
Tartaric	1 : 5	3	5
	2 : 5	3	7
	3 : 5	6	13
<i>o</i> -Anisic	3 : 5	6	9
<i>p</i> -Anisic	2 : 5	7	9
	3 : 5	7	9
	1 : 5	7	9
Methylphthalic	1 : 5	7	9
	2 : 5	7	9
	3 : 5	7	9
<i>p</i> -TSA	1 : 5	1	2
	4 : 5	7	15
	1 : 1	10	21

* Acids and base (AEPD) are dispersed in DURO-TAK 80-1100 adhesive film, the thickness of all adhesive films is around 0.3mm.

** - indicates the color never turns to strong in the observation period

5.5.4. Base

A base with both amine and hydroxide groups in its structure shows a good potential for diffusion out of PMMA, DURO-TAK 80-1100 adhesive films and neutralization of the acid.



We chose five bases that have these functional groups in their structures (Table 5.7). First, we mixed them with PMMA to produce rigid PMMA base films with same base concentration (2×10^{-3} mmol/mg). We tested their performance for the dye migration process with BY-FBP/*p*-TSA adhesive film (Table 5.8, 5.9). Small amounts of glycol and glycerol were added into base layers as a base-releasing agent.

Table 5.7. Structures of bases

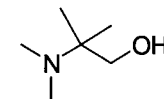
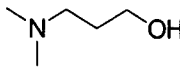
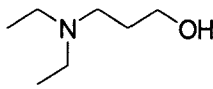
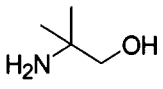
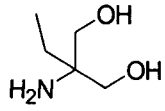
DMAMP-80:	 80% and 20% of water 2-Dimethylamino-2-methyl-1-propanol
DMAP:	 3-Dimethylamino-1-propanol
DEAP:	 3-Diethylamino-1-propanol
AMP-95:	 95% and 5% of water 2-Amino-2-methyl-1-propanol
AEDP:	 little water 2-Amino-2-ethyl-1,3-propanediol

Table 5.8. Color-changing test with base in PMMA films, glycol as releasing agent*

Base	Acid/Base Ratio (mol).	Time for Faint Color (Day)	Time for Final Strong Color (Day)
DMAMP-80	3 : 10	1.5	3
	3 : 5	2	6
DMAP	3 : 10	3	10
	3 : 5	5	**
DEAP	3 : 10	1	7
	3 : 5	8	-
AMP-95	3 : 10	1	4
	3 : 5	2	13
AEPD	3 : 10	7	17
	3 : 5	11	-

* *p*-TSA is dispersed in DURO-TAK 80-1100 adhesive for acid film, the thickness of acid adhesive films is around 0.3mm.

** - indicates the color never turns to strong in the observation period

Table 5.9. Color-changing test with base in PMMA films, glycerol as releasing agent*

Base	Acid/Base Ratio (mol).	Time for Faint Color (Day)	Time for Final Strong Color (Day)
DMAMP-80	3 : 5	20	-**
DMAP	3 : 5	-	-
DEAP	3 : 5	-	-
AMP-95	3 : 5	12	-
AEPD	3 : 5	-	-

* *p*-TSA is dispersed in DURO-TAK 80-1100 adhesive for acid film, the thickness of acid adhesive films is around 0.3mm.

** - indicates the color never turns to strong in the observation period

From Table 5.8, we see that the AEPD has a long-term releasing property, because the dye diffusion test with AEPD has a longer white time compared with the other base tests. Another observation is that the glycerol delays the base release from the PMMA film to a greater extent than glycol does and cannot leach out all base in the base film for neutralization.

From these experiments, we also found that the base release from the PMMA film is not very efficient. It appears that only the base on the PMMA film surface in contact with adhesive layer can diffuse into the adhesive acid layer for the neutralization reaction. For the experiment that changes the color, the base/acid ratio is very high and the color change is relatively fast (several days).

In an attempt to address this problem, A new approach was investigated. We used the standard adhesive in both acid and base layers, which provides better compatibility at the interface between the layers and a more uniform rate of diffusion with these soft adhesive films. All bases in the adhesive layer can diffuse into the acid layer for neutralization.

We cast a series of acid and base films with DURO-TAK 80-1100 adhesive. Their compositions are shown in Table 5.10. The dye diffusion tests were performed with different combination of these films. The results are shown in Table 5.11.

Table 5.10. The composition of acid and base films*

Film No.	Acid or base	Concentration (mmol/mg)
B-1	AEPD	8.5×10^{-3}
B-2	AEPD	1.7×10^{-2}
B-3	AEPD	2.6×10^{-2}
B-4	AEPD	3.4×10^{-2}
B-5	AEPD	4.3×10^{-2}
A-1	Glutaric	1.5×10^{-2}
A-2	Glutaric	3.0×10^{-2}
A-3	Glutaric	4.5×10^{-2}
A-4	Tartaric	1.3×10^{-2}
A-5	Tartaric	2.7×10^{-2}
A-6	Tartaric	4.0×10^{-2}
A-7	<i>p</i> -TSA	5.3×10^{-3}
A-8	<i>p</i> -TSA	1.1×10^{-2}
A-9	<i>p</i> -TSA	1.6×10^{-2}

* Acids and base are dispersed in DURO-TAK 80-1100 adhesive film; the thickness of all adhesive films is around 0.3mm.

Compared to the old PMMA system, the advantage of this new system is that it is more reliable and predictable in the color change time. Due to the increased compatibility and diffusion rate of the base, the base film did not hold the base for a long time and it was not possible to achieve a very long-term color changing time (several months) with this system.

Table 5.11. Color-changing test with acid and base films*

Acid film No.	Base film No.	Acid/Base ratio** (mol)	Time for Faint Color (Day)	Time for Final Color (Day)
A1	B5	1 : 2.9	4	10
A2	B5	1 : 1.4	14	20
A3	B5	1 : 1.0	15	***
A2	B1	1 : 0.3	-	-
A2	B2	1 : 0.6	17	-
A2	B3	1 : 0.9	15	-
A2	B4	1 : 1.1	8	-
A4	B5	1 : 3.3	9	18
A5	B5	1 : 1.6	17	-
A6	B5	1 : 1.1	-	-
A5	B1	1 : 0.3	-	-
A5	B2	1 : 0.6	-	-
A5	B3	1 : 1.0	12	-
A5	B4	1 : 1.3	10	-
A7	B5	1 : 8.1	1	2
A8	B5	1 : 3.9	1	2
A9	B5	1 : 2.7	2	4
A8	B1	1 : 0.8	13	21
A8	B2	1 : 1.5	6	14
A8	B3	1 : 2.3	2	3
A8	B4	1 : 3	1	2

* Acids and base are dispersed in DURO-TAK 80-1100 adhesive film, the thickness of all adhesive films is around 0.3mm.

** approximate acid/base ratio

***- indicates the color never turns to strong in the observation period

5.6. Issues to be examined

5.6.1. *New ionamine synthesis*

Developing a new ionamine structure non-migration dye is one key point in this project. So far, we have two colors: yellow and dark yellow. If we can find a blue and a red dye, then we can get all other colors with different combination of these three primary colors. Theoretically, all non-polar dyes with a primary amine group can be used to synthesize the corresponding ionamine. In practice, the solubility, spatial block and the side group effect will not favor the reaction to the final product. The modification of the current ionamines with electron donation or electron withdrawing groups may be an approach to create dyes with different colors.

5.6.2. *Good dispersion for the dye*

So far we did not find a good dispersion method for the ionamine in to the acid adhesive films. The ionamine is not soluble in all organic solvents, so it forms a suspended solution. For some organic solvents (methanol, ethanol), the solvent is not compatible with DURO-TAK 80-1100 adhesive, and cannot be used to cast uniform adhesive films. We used ethyl acetate to dilute DURO-TAK 80-1100 adhesive and put ionamine powder into the low viscosity mixture. After it is cured at a high temperature, there is still some phase separation in the gel like films. The ionamine particles tend to congregate to form high-density regions in the films. The non-uniform dispersion of ionamine in the substrate causes the variable color-changing time on the same timing test badge.

The best solution to this problem is using a powder deposition method to form a very thin ionamine layer on the acid adhesive substrate. With a thin ionamine layer instead of mixing in the adhesive, the color changing is expected to be sharper and the color should be more extensive.

5.6.3. Migration issues

The constant base releasing from the base layer, which is used to activate the structure conversion of ionamine in the acid layer, is a key point for the long-term timing effect. The compatibility between different layers affects molecule transportation and migrations between the interfaces. In our experiment, the base may diffuse into the acid layer and the corresponding acid may also migrate into the base layer to create a reaction. We need to find a method to monitor the acidity related to the base diffusion process. It will help us to design the color-changing badge with the knowledge of the pH change in the dye substrate.

REFERENCES

- (1) Green; Saunders. *Journal of the Society of Dyers and Colourists* **1923**, *39*, 11-16.
- (2) Santurri, P.; Robbins, F.; Stubbings, R. *Organic Synthesis, Coll. 5*, 341-343.
- (3) Rajendran, V.; Nanjan, M. J. *J. Polym. Sci.: Part A* **1987**, *25*, 829-838.

CHAPTER 6. SUMMARY AND CONCLUSIONS

The investigations in the previous three chapters focus on:

- The mobility of charge carriers in an epoxy-amine polymerization system to characterize the physical and chemical property changes during cure.
- The dipolar mobility in styrene and divinylbenzene/dimethacrylate systems to characterize the structural evolution and development of a spatial heterogeneity during cure.
- The mobility of dye molecules in polymer films to obtain a long term color changing paper system.

Specific conclusions of the three studies include:

1. The ITOF technique, coupled with dielectric measurements of conductivity can be used to monitor separately the number of charge carriers and their mobility. In a DGEBA/MCDEA system, the intermolecular hydrogen bonding is the primary source of the charge carriers. The changes in the charge carrier concentration monitored by ITOF with conductivity characterize the changes in the hydrogen bonding structure with temperature and reaction advancement. There is a significant increase in the

number of mobile charge carriers during the buildup in the crosslink density. Hence the conductivity changes during the epoxy amine polymerization are due to both an increase in viscosity which affects mobility and changes in the number and type of proton transfer groups produced as a result of the elementary epoxy-amine reactions, which occur in this complex polymerization.

2. FDEMS can be used to characterize the heterogeneous formation of a monomer/oligomer region and a microgel region during the polymerization reaction. In the both D121/St and D121/DVB systems, two distinct T_g , α relaxation responses are observed very early and prior to macroscopic gel during polymerization in both the dielectric and DSC spectra. They correspond to two spatially distinct regions: a glass transition in monomer/oligomer regions and a glass transition in the polymer microgel regions. The comonomer structure influences the polymerization rate, network build-up, spatial heterogeneity evolution, dynamic mechanical properties and morphology. The use of DVB instead of St increases the spatial heterogeneity of the network, and creates a very broad relaxation spectrum in dielectric spectroscopy, a glass transition extending over than 100 degrees in DSC profile and wide α transition in the dynamic mechanical plot.
3. The mobility of dye molecules in polyvinyl films can be controlled by the acidity of the environment. Ionamine derivatives of Banana Yellow, Fat Brown are stable when mixed with acid. Their diffusion through polymer films can be quickly triggered with acid/base neutralization reaction. The type of base, acid and the compatibility of polymer films affect the diffusion rate.

APPENDIX

Publications:

1. Isolating the mobility of charge carriers during an epoxy-amine reaction, **Z. Guo**, D. Kranbuehl *Polymer Preprints* **2004** 45(2), 795
2. Ion Mobility Time-of-Flight Measurements: Isolating the Mobility of Charge Carriers During an Epoxy-Amine Reaction **Z. Guo**, J. Warner, P. Christy, D.E. Kranbuehl, G. Boiteux, G. Seytre, *Polymer* **2004** 45, 8825
3. Monitoring structural evolution during vinyl/dimethacrylate copolymerization with frequency dependent dielectric sensing, Guo, Z.; Best, P.; Kranbuehl, D. E.; Sautereau, H, *Polymer Preprints* **2005** 46(1), 692-693
4. Isolating the Mobility and Characterizing the Effect of Crosslink Structure versus the Monomer State using Ion Time of Flight, D. Krouse, **Z. Guo**, D.E. Kranbuehl, *J. Non-Cry. Solid* (in press)
5. Structural Evolution and Heterogeneities Studied by Frequency Dependent Dielectric Sensing in a Styrene/Dimethacrylate network, **Z. Guo**, H. Sautereau, D. Kranbuehl, *Macromolecules* (accepted)
6. Evidence for Spatial Heterogeneities Observed by Frequency Dependent Dielectric Measurement in Vinyl Dimethacrylate Systems, **Z. Guo**, H. Sautereau, D. Kranbuehl, *Polymer* (to be submitted)

Activities:

1. **Presentation** “Monitoring structural evolution during vinyl/dimethacrylate copolymerization with frequency dependent dielectric sensing.” 229th ACS National Meeting, San Diego, CA, United States, March 13-17, 2005
2. **Poster** “Ion mobility time-of-flight measurements: Isolating the mobility of charge carriers during an epoxy-amine reaction.” 228th ACS National Meeting, Philadelphia, PA, United States, August 22-26, 2004

VITA**Zhenrong Guo**

Zhenrong Guo was born in Jiangyin, Jiangsu province, P. R. China on October 14, 1976. He received his B.S. at Fudan University in 1998 with a degree in Chemistry. He received his M.S. at Fudan University in 2001 with a concentration in Polymer Science.

In September 2001, the author entered the College of William and Mary as a graduate student. He received his M.S. in 2003 with a degree in Chemistry. Zhenrong defended his dissertation in July of 2005 and will receive his Ph.D. in Applied Science.

Upon graduation the author will embark on a career as a Senior Research Chemist in Sawgrass Technology Inc. in South Carolina.